Physics – Uspekhi **58** (12) 1159 – 1205 (2015)

REVIEWS OF TOPICAL PROBLEMS

PACS numbers: **03.70.+k**, 05.60.Gg, 11.10.Wx, 72.10.Bg

On the nonequilibrium diagram technique: derivation, some features, and applications

P I Arseev

DOI: 10.3367/UFNe.0185.201512b.1271

Contents

Abstract. We review the succession of ideas underlying the emergence of the nonequilibrium diagram technique (Keldysh diagram technique). Simple examples are used to illustrate the implementation of the technique and to demonstrate possible difficulties and the ways to overcome them. Together with well-known facts, some lesser-discussed details are considered, in particular, whether the so-called three-component technique is necessary. Several applications of the nonequilibrium diagram technique are discussed including, notably, tunneling systems and linear response problems. We hope that some parts of the review can be useful even for the reader familiar with the nonequilibrium diagram technique.

Keywords: diagram technique, nonequilibrium diagram technique, Keldysh diagram technique, nonequilibrium processes, quantum kinetics

---

P I Arseev Lebedev Physical Institute, Russian Academy of Sciences, Leninskii prosp. 53, 119991 Moscow, Russian Federation
E-mail: ars@lpi.ru

Received 4 August 2015, revised 11 October 2015
Uspekhi Fizicheskikh Nauk **185** (12) 1271 – 1321 (2015)
DOI: 10.3367/UFNr.0185.201512b.1271
Translated by K B Alkalaev; edited by A M Semikhatov

1. Introduction

The history of the nonequilibrium diagram technique (NDT) began 50 years ago with the work by Keldysh [1] published in 1964 in Russian in the *Journal of Theoretical and Experimental Physics* (*JETP*), and in 1965 in the English version of *JETP* (*Soviet Physics – JETP*). Although, of course, there was work that paved the way for the appearance of this article, it was [1] where simple rules that are the cornerstone of the diagram technique for nonequilibrium processes were formulated for the first time. In that paper, moreover, such rules were first shown to exist, which had not been obvious previously.

Article [1] has an unusual history. On the one hand, the article attracted attention and it was generally appreciated. On the other hand, the habit of using the temperature diagram technique in condensed matter physics was so embedded that many problems that could be solved much more easily and in a more natural way by the NDT continued (and continue) to be considered in the temperature technique. To make the temperature technique efficient, great ingenuity was often required, for example, in the case of the analytic continuation procedure proposed by Eliashberg [2]. Somehow, the doubling of variables in the NDT was considered an unnecessary complication, but in fact calculations using the NDT are often simpler and clearer.

In some cases, the temperature technique was used for systems (for example, tunnel junctions) where it cannot work correctly in principle. (We should not be misled by the fact that the temperature technique gives correct results in simple cases.) We note that as early as 1971, Caroli, Combescot, Nozieres, and Saint-James, in a series of superb papers [3–5], systematically applied the NDT to the problem of tunneling through an intermediate system with a phonon interaction within the tight-binding approximation. However, later, the temperature technique language was very often used in spite of being unsuitable for describing interacting systems with nonequilibrium current. It was only after the appearance of paper [6] (taking almost 30 years to recognize that the NDT is a natural language for this area!) that the NDT began to be widely used in such problems. Presently, the Keldysh technique is commonly used in the theory of solid-state heterostructures.

The NDT was also applied to a wide range of problems related to the interaction of high-intensity light with superconductors, the description of lasing in semiconductor structures, and the development of the cascade laser theory (many results are collected in book [7] and a number of references are given in Section 10). The incoming high-intensity wave creates a large density of nonequilibrium electrons and holes, which are scattered by impurities, interact with each other and with phonons, and recombine with emission of light. The NDT turns out to be a suitable tool for describing nonstationary and strongly nonequilibrium states in such systems.

In recent years, the technique has also been increasingly used in areas such as cosmology, heavy-ion collisions, and some other problems of elementary particle physics (nuclear physics).

Historically, the first diagram technique was the Feynman–Dyson technique [8, 9], which was remarkably clear and simple (for pioneering papers, see [10]). However, this 'quantum field theory' technique was based on averaging all observables over a vacuum (it was later generalized in solid state theory to the case of zero temperature and averaging over the many-body ground state). In 1955, Matsubara proposed his version of the diagram technique for many-body systems in thermodynamic equilibrium [11]. Due to the efforts of many theorists (see, e.g., [2, 12–15]), technical methods were developed that allowed applying the temperature technique more efficiently. But this technique is not suitable for directly finding propagators in real time (Green's functions). The first steps to real-time calculations were made in the first paper by Mills [16], where time propagators were considered, albeit for thermodynamic equilibrium only. The thermodynamic equilibrium condition allowed using the spectral decomposition and analytic continuation methods to construct a scheme for calculating time propagators.

However, the problem of describing real-time systems in other (nonequilibrium) states seemed to be very complicated. This view was based on the fact that any technique for calculating the retarded correlators underlying the description of the nonequilibrium response was complicated and cumbersome.

The main achievement of paper [1], which appeared 50 years ago, is that it showed that things were much simpler than most theorists thought at that time. This is how its author explains his motivation (a talk at the interdisciplinary seminar "Progress in nonequilibrium Green's functions," 19 August 2002, Dresden, Germany [17]): "The Feynman diagram technique seemed so logical and natural to me that I could not believe that its validity was limited to very particular, though important, classes of states — the ground state or the thermodynamic equilibrium state. So the program was simple and straightforward: to repeat the original Feynman–Dyson derivation step by step, looking for a step that fails for any state, and then try to circumvent the difficulties following the original formulation as closely as possible."

In the same talk, Keldysh explains how much had already been done (in particular, in the Soviet Union) for extending field-theoretical concepts and methods, including the Green's functions, to many-body problems by the time the NDT was formulated [18–21]. In a sense, the NDT arose as a necessary generalization of field theory methods. In what follows, we mention some of the work that was conducive to the creation of the NDT.

The temperature diagram technique is often preferred in applications because at first glance it appears to be simpler than the NDT. However, this simplicity of formulation has its price: calculations become rather complicated in all nontrivial cases. Moreover, the temperature technique is applicable only to the thermodynamic equilibrium and response theory. Although the NDT is a two-component theory and looks more complicated, it leads to much simpler and clearer calculations for complex systems and allows considering both nonequilibrium and nonstationary cases. We show in what follows that both the derivation and the operational rules of the NDT are in fact no more difficult than those in the temperature technique. After a brief derivation of the original NDT equations, we use some simple examples to discuss principles and subtleties of the NDT that are usually not mentioned in the reviews. To show how the NDT works, we consider several problems in solid state physics. Finally, we briefly discuss some other applications of the Keldysh technique.

2. Basic concepts of the nonequilibrium diagram technique

In this section, we briefly review quite elementary facts from quantum mechanics (statistics). In this way, we show the logic underlying the approach used by Keldysh in his paper. We first note that a nonequilibrium diagram technique aims to calculate time variations in a system under the action of external fields. Hence, to build the NDT, we begin with a general description of time evolution in quantum mechanics. As always, the starting point here is the Schrödinger equation, giving rise to the well-known formula for calculating any observable I at a time t,

$$I(t) = \langle \Psi(t)|\hat{I}|\Psi(t)\rangle = \langle 0|S(t_0, t)\hat{I}S(t, t_0)|0\rangle\,, \tag{1}$$

where the evolution (matrix) operator is defined by the Schrödinger equation

$$\mathrm{i}\,\frac{\partial}{\partial t}\,S(t, t_0) = HS(t, t_0)\,, \qquad S(t_0, t_0) = 1\,. \tag{2}$$

In the many-body case, we deal with quantum statistics, and hence the evolution is described by a density matrix. Any observable can be calculated if the density matrix is known at a time t:

$$I(t) = \langle\hat{I}\rangle \equiv \mathrm{Sp}\left[\hat{\rho}(t)\hat{I}\right]. \tag{3}$$

The time evolution of the density matrix itself is defined by the same evolution operator,

$$\rho(t) = S(t, t_0)\, \rho(t_0)\, S^+(t, t_0)\,. \tag{4}$$

A diagram technique arises when the evolution operators cannot be found explicitly, and have to be calculated as perturbative series. The Hamiltonian is then assumed to be split into an initial unperturbed Hamiltonian and a perturbation operator,

$$H = H_0 + V\,. \tag{5}$$

It is important that all solutions of the unperturbed system be known. We note that the Hamiltonian H_0 can contain a number of external fields as long as we can explicitly calculate expectation values with respect to the unperturbed density matrix. The perturbation operator can contain external fields as well as interactions between various particles in the system. It is convenient to formulate such a perturbation theory using the Heisenberg picture, because we are interested in both observables at a given time and their temporal correlation functions. In the case of a single operator, we have

$$\begin{aligned}\langle \hat{I} \rangle &= \mathrm{Sp}\left[S(t, t_0)\rho(t_0)S^+(t, t_0)\hat{I}\right] \\ &= \mathrm{Sp}\left[\rho(t_0)S^+(t, t_0)\hat{I}S(t, t_0)\right], \end{aligned}\tag{6}$$

$$\begin{aligned}\mathrm{Sp}\left[\hat{\rho}(t)\hat{I}\right] &= \mathrm{Sp}\left[\rho_0 S^+(t, t_0)\hat{I}S(t, t_0)\right] \\ &= \mathrm{Sp}\left[\rho_0 U^+(t, t_0)\hat{I}(t)U(t, t_0)\right], \end{aligned}\tag{7}$$

where

$$\hat{I}(t) = \exp\,(\mathrm{i}H_0 t)\hat{I}\exp\,(-\mathrm{i}H_0 t)\,, \tag{8}$$

$$U(t, t_0) = \exp\,(\mathrm{i}H_0 t)\, S(t, t_0)\,. \tag{9}$$

If the perturbation operator commutes with the initial Hamiltonian H_0, then the evolution operator in the interaction picture can be found simply as

$$U(t, t_0) = \exp\left[-\mathrm{i}V(t - t_0)\right]. \tag{10}$$

However, this is not usually the case. To find the operator U, we use the equation

$$\mathrm{i}\,\frac{\partial}{\partial t}\, U(t, t_0) = \hat{V}(t)U(t, t_0)\,, \tag{11}$$

where all operators are given in the interaction picture:

$$\hat{V}(t) = \exp\,(\mathrm{i}H_0 t)\, \hat{V}\exp\,(-\mathrm{i}H_0 t)\,. \tag{12}$$

Because the operators $\hat{V}$ and H_0 do not commute with each other, solutions of (11) are represented in terms of the so-called T-ordered exponential

$$U(t, t_0) = T\exp\left[-\mathrm{i}\int_{t_0}^{t} \hat{V}(t')\,\mathrm{d}t'\right]. \tag{13}$$

The time-ordering (T-ordering) operator arranges a set of operators (in the Heisenberg or the interaction picture) from left to right as the time argument increases:

$$T\hat{A}(t)\hat{B}(t') = \theta(t - t')\hat{A}(t)\hat{B}(t') \mp \theta(t' - t)\hat{B}(t')\hat{A}(t)\,. \tag{14}$$

We note that interchanging two fermion operators leads to a sign change (the upper sign in the above relation). Operator (13) is represented as a series,

$$\begin{aligned}U(t, t_0) = 1 &- \mathrm{i}\int_{t_0}^{t} \hat{V}(t_1)\,\mathrm{d}t_1 \\ &+ \mathrm{i}^2 \int_{t_0}^{t} \hat{V}(t_1)\,\mathrm{d}t_1 \int_{t_0}^{t_1} \hat{V}(t_2)\,\mathrm{d}t_2 + \ldots, \end{aligned}\tag{15}$$

$$\int_{t_0}^{t} \hat{V}(t_1)\,\mathrm{d}t_1 \int_{t_0}^{t_1} \hat{V}(t_2)\,\mathrm{d}t_2 = \frac{1}{2}\, T\left[\int_{t_0}^{t} \hat{V}(t_1)\,\mathrm{d}t_1 \int_{t_0}^{t} \hat{V}(t_2)\,\mathrm{d}t_2\right]. \tag{16}$$

The inverse operator

$$-\mathrm{i}\,\frac{\partial}{\partial t}\, U^+(t, t_0) = U^+(t, t_0)\hat{V}(t) \tag{17}$$

is defined using the inverse time-ordering operation, which places operators with later times to the right of those at earlier times:

$$\begin{aligned}U^+(t, t_0) = 1 &+ \mathrm{i}\int_{t_0}^{t} \hat{V}(t_1)\,\mathrm{d}t_1 \\ &+ \mathrm{i}^2 \int_{t_0}^{t} \mathrm{d}t_2 \int_{t_0}^{t_2} \mathrm{d}t_1\, \hat{V}(t_1)\hat{V}(t_2) + \ldots, \end{aligned}\tag{18}$$

$$U^+(t, t_0) = \tilde{T}\exp\left[+\mathrm{i}\int_{t_0}^{t} \hat{V}(t')\,\mathrm{d}t'\right]. \tag{19}$$

In many cases, we are interested in correlators of some observables. Moreover, it is known that much physical information is contained in the Green's functions, which are also the simplest correlators. A simple correlator of two operators is given by

$$\left\langle \hat{A}_H(t)\hat{B}_H(t')\right\rangle = \mathrm{Sp}\left[\rho_0 S^+(t, t_0)\hat{A}S(t, t')\hat{B}S(t', t_0)\right]. \tag{20}$$

In turn, a correlator representing an average of two T-ordered operators can be written in a more concise manner using the following property of evolution operators:

$$S(t, t_0) = S(t, t_1)S(t_1, t_0)\,. \tag{21}$$

The evolution matrices and the averaged operators can then be placed under the same T-ordering:

$$\left\langle T\hat{A}_H(t)\hat{B}_H(t')\right\rangle = \mathrm{Sp}\left[\rho_0 U^+(t, t_0)T\left\{U(t, t_0)\hat{A}(t)\hat{B}(t')\right\}\right]. \tag{22}$$

Therefore, the expectation values always have the form

$$\begin{aligned}\mathrm{Sp}\Bigg[\rho_0\tilde{T}\exp&\left[+\mathrm{i}\int_{t_0}^{t} \hat{V}(t_2')\,\mathrm{d}t_2'\right] \\ &\times T\left\{\exp\left[-\mathrm{i}\int_{t_0}^{t} \hat{V}(t_1')\,\mathrm{d}t_1'\right]\hat{A}(t)\hat{B}(t')\right\}\Bigg]. \end{aligned}\tag{23}$$

Formulas of this type solve the following problem. It is known that a system at the initial instant t_0 is described by a density matrix ρ_0, which allows calculating expectation values of any observables. Then the interaction V starts to act, which changes the density matrix such that the expectation values can no longer be calculated explicitly. Equation (23) allows finding the time evolution of any observable using the perturbation theory if the exponentials are expanded into series.

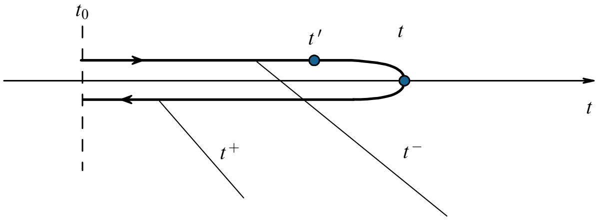

$$\mathrm{Sp}\left[\rho_0\tilde{T}\exp\left[+\mathrm{i}\int_{t_0}^{t}\hat{V}(t_2')\,\mathrm{d}t_2'\right]T\left\{\exp\left[-\mathrm{i}\int_{t_0}^{t}\hat{V}(t_1')\,\mathrm{d}t_1'\right]\hat{A}(t)\hat{B}(t')\right\}\right]$$

Figure 1. Keldysh contour.

In the usual 'field theory' technique (see Ref. [21] for applications in many-body problems), expectation values are evaluated over the ground state (the vacuum). The first factor in (23) then reduces to just a phase factor. Such a factorization is impossible for states described by an arbitrary density matrix, which for a long time had been considered the obstruction to simplifying real-time calculations. But it was shown in Ref. [1] that simple rules exist that allow building a perturbation series based on a formula like (23) in a simple and concise manner. These rules constitute the diagram technique for nonequilibrium systems.

The groups of operators in (23) are ordered in a certain way. In particular, any operator from the 'inverse' evolution matrix U^+ is always on the left ('after', if we track how the operators successively act from right to left) of all operators under the standard T-ordering.

All times in this operator can be assigned a '+' sign, while times in the conventionally T-ordered operators are assigned a '$-$' sign. It follows that arrangement rules for operators can be made more intuitive if we draw the contour depicted in Fig. 1. Here, we suppose that times with a '$-$' correspond to the upper branch of the contour, while those with a '+' are on the lower branch. Going around the contour starts at the initial instant t_0, then continues along the upper branch until the maximum time t of the averaged operators, and then returns to t_0 along the lower branch. Introducing the operation of T_C-ordering along the contour, we find that operators from U on the upper branch are T-ordered, while operators from U^+ on the lower branch are anti-T-ordered, because the direction of moving along this part of the contour from t to t_0 is reversed. We note that all operators from U^+ always follow those from U, as it must be in (23).

In this way, the notion of T_C-ordering along a contour allows representing Eqn (23) in a quite compact form

$$\mathrm{Sp}\left[\rho_0 T_C\left\{\exp\left[-\mathrm{i}\int_C \hat{V}(t_c)\,\mathrm{d}t_c\right]\hat{A}(t^-)\hat{B}(t'^-)\right\}\right], \tag{24}$$

taking into account that on the lower branch, we have

$$U^+(t,t_0)=\tilde{T}\exp\left[-\mathrm{i}\int_t^{t_0}\hat{V}(t')\,\mathrm{d}t'\right].$$

We note that the terms upper and lower referring to the branches of the contour are conventional. In fact, the integration along both branches of the contour goes strictly along the real time axis, and the contour is drawn as a loop for illustrative purposes only. There is no extension to the 'complex time-plane'. We discuss this point later in the context of the 'three-component' technique.

We traditionally started with a T-ordered product of two operators. Equation (24) can be easily generalized to the case of the usual correlator (called the Wightman function in field theory), where the ordering of operators is rigidly fixed. For example, we consider the correlator of two operators with the time t either less or greater than t':

$$\left\langle \hat{A}_H(t)\hat{B}_H(t')\right\rangle=\mathrm{Sp}\left[\rho_0 S^+(t,t_0)\hat{A}S(t,t')\hat{B}S(t',t_0)\right]. \tag{25}$$

It is sufficient to assign the index t^+ to the argument of A and the index t^- to the argument of B, such that the general T_C-operation always places B before A, and parts of the evolution matrix are properly arranged. For $t>t'$, we have

$$\begin{aligned}\left\langle \hat{A}_H(t)\hat{B}_H(t')\right\rangle&=\mathrm{Sp}\left[\rho_0 U^+(t,t_0)\hat{A}(t)U(t,t')\hat{B}(t')U(t',t_0)\right]\\&=\mathrm{Sp}\left[\rho_0\tilde{T}\exp\left[+\mathrm{i}\int_{t_0}^{t}\hat{V}(t_2')\,\mathrm{d}t_2'\right]\hat{A}(t)\right.\\&\quad\left.\times T\left\{\exp\left[-\mathrm{i}\int_{t_0}^{t}\hat{V}(t_1')\,\mathrm{d}t_1'\right]\hat{B}(t')\right\}\right],\end{aligned} \tag{26}$$

and for $t'>t$, we have

$$\begin{aligned}\left\langle \hat{A}_H(t)\hat{B}_H(t')\right\rangle&=\mathrm{Sp}\left[\rho_0 U^+(t,t_0)\hat{A}(t)U^+(t',t)\hat{B}(t')U(t',t_0)\right]\\&=\mathrm{Sp}\left[\rho_0\tilde{T}\exp\left[+\mathrm{i}\int_{t_0}^{t}\hat{V}(t_2')\,\mathrm{d}t_2'\right]\hat{A}(t)\tilde{T}\exp\left[+\mathrm{i}\int_{t}^{t'}\hat{V}(t_3')\,\mathrm{d}t_3'\right]\right.\\&\quad\left.\times T\left\{\exp\left[-\mathrm{i}\int_{t_0}^{t'}\hat{V}(t_1')\,\mathrm{d}t_1'\right]\hat{B}(t')\right\}\right].\end{aligned} \tag{27}$$

In both cases, the result again takes the general form

$$\mathrm{Sp}\left[\rho_0 T_C\left\{\exp\left[-\mathrm{i}\int_C \hat{V}(t_c)\,\mathrm{d}t_c\right]\hat{A}(t^+)\hat{B}(t'^-)\right\}\right]. \tag{28}$$

We note that the '+' and '$-$' signs assigned to the time arguments of the operators or to the operators themselves just indicate which (original or inverse) evolution operator these operators belong to and in which order they appear inside the averaging operation. It is at this point that two sets of variables are formed: one is from the forward evolution matrix, and the other from the 'backward' evolution matrix S^+. These variables are always mutually ordered in a certain way. We see that such a structure with two 'types' of operators naturally arises when calculating time variations of any quantum mechanical observable. It is not surprising that paper [22] by Schwinger, which is usually considered a predecessor of [1], already contained matrix evolution equations. Schwinger used equations of motion obtained by means of his functional differentiation technique to reveal the correct structure of the equations eventually rewritten in a 2×2 matrix form. The diagram technique was absent in Schwinger's papers, however.

The diagram technique cannot be built using Eqn (24) alone. The question now arises whether the calculation of expectation values of a product of many operators arising when expanding a T-exponential,

$$\begin{aligned}&\mathrm{Sp}\left\{\rho_0\tilde{T}\left[\frac{\mathrm{i}^n}{n!}\iiint\hat{V}(t_1)\ldots\hat{V}(t_n)\,\mathrm{d}t_1\,\mathrm{d}t_2\ldots\mathrm{d}t_n\right]\right.\\&\quad\left.\times T\left[\hat{A}(t)\hat{B}(t')\,\frac{(-\mathrm{i})^m}{m!}\iiint\hat{V}(t_1)\ldots\hat{V}(t_m)\,\mathrm{d}t_1\,\mathrm{d}t_2\ldots\mathrm{d}t_m\right]\right\}\end{aligned} \tag{29}$$

can be ‘automated’. Within the usual technique, Wick’s theorem allows proving that such T-products of a large number of creation and annihilation operators are reduced to pairwise expectation values. In our case, Wick’s theorem is not obvious.

It seems that one of the main achievements in [1] was the understanding that perturbative calculations of not only ordinary (T-ordered) Green’s functions but also any real-time correlators can be represented as a general T_C-ordering along a particular contour. Furthermore, such a generalized T-ordering does not break the general rules of the diagram technique.[1]

We emphasize the nontrivial fact that the modified Wick theorem is valid in the nonequilibrium case. This is stated in the first article [1], but the complete proof of this fact is not given there. Numerous review articles tend to discuss it as something taken for granted. The so-called proof of Wick’s theorem in the thermodynamic limit is just traditional stupidity (unfortunately, this can be found even in good textbooks on condensed matter theory). According to the ‘proof’, in any order of the perturbation theory, a pair of creation and annihilation operators for a particular state should appear only once, i.e., the averaging is trivial because pairs of operators in different states are averaged independently. Thus, for any perturbation, its impact on particles in any state is counted only once. Unfortunately, if Wick’s theorem were valid in many-body theory only in this sense, then it would be impossible to apply the diagram technique to any impurity problem (such as the Anderson model), the problem of polaritons with multiple re-emission of photons by an atom, and other problems in which the electron state is affected by multiple perturbations.

To streamline our presentation, we show in the Appendix that the T-ordering not only simplifies expressions like (24) but also allows generalizing Wick’s theorem to the nonequilibrium case. Moreover, this derivation immediately shows what happens if the system has initial correlations between particles in different states. The generalization of the nonequilibrium diagram technique for systems with initial correlations was done by Hall [25] and then significantly developed by Kukharenko and Tikhodeev [26].

Thus, the second step after the T_C-ordering leading to the appearance of the diagram technique is a generalization of Wick’s theorem: the expectation value of a T_C-ordered product of operators is equal to the sum of all possible partitions into pairwise T_C-ordered expectation values. For fermions, the standard rule is that the sign of each partition depends on the parity of the permutation of fermionic operators arranged in pairs.

3. Nonequilibrium diagram rules

Within the secondary quantization method, any perturbation Hamiltonian V consists of creation and annihilation operators for different particles. For bosons and fermions interacting with an external field (defined by a scalar potential), the perturbation operator then has the form

$$\hat V = \int \Psi^+(r)U(r,t)\Psi(r) = \sum_{p,q} a^+_{p+q}a_p U_q(t)\,. \tag{30}$$

We have

$$\hat V = \int \Psi^+(r_1)\Psi^+(r_2)U(r_1-r_2)\Psi(r_2)\Psi(r_1)\,\mathrm{d}r_1\,\mathrm{d}r_2$$
$$= \sum_{p,p',q} a^+_{p+q}a^+_{p'-q}U(q)a_{p'}a_p \tag{31}$$

for pair interaction, and

$$\hat V = \sum_{p,q} g_{p,q}a^+_{p+q}a_p(b^+_{-q}+b_q) \tag{32}$$

for electron–phonon interaction, where b_q is the phonon annihilation operator.

The basic elements of the diagram technique are pairwise averages of the creation and annihilation operators in perturbation operators. In what follows, we therefore discuss general expression (24) where arbitrary operators A and B are creation and annihilation operators of particles in a given state,

$$\hat A = a_p\,, \quad \hat B = a^+_{p'}\,. \tag{33}$$

The basic element of the conventional diagram technique is the usual T-ordered average of two operators in the interaction picture (one creation and one annihilation operator). Now, the situation is slightly more complicated, because the basic elements are the pairwise averages of all possible combinations of two T_C-ordered operators. We note that the general statement of Wick’s theorem [27] was originally formulated for all possible pairs of creation and annihilation operators; however, as in the usual case, only a pair of a and a^+ has a nonzero average value. (The superconductor case with anomalous averages of two creation or annihilation operators is discussed in Section 8.1.)

Because the time arguments of the operators can lie either on the upper or on the lower branch of the contour C, the general definition of the Green’s function as the mean value of the T_C-ordered pair of operators,

$$\hat G(r,t^\alpha;r't'^\beta) = -\mathrm{i}\left\langle T_C\Psi(\mathbf{r},t^\alpha)\Psi^+(\mathbf{r}',t'^\beta)\right\rangle = \hat G^{\alpha,\beta}(r,t;r',t')\,, \tag{34}$$

implies the appearance of four different functions of the real time variable $t-t'$ ($\alpha,\beta=+,-$). In the case of noninteracting particles, a straightforward calculation of the Green’s functions in momentum space shows that

$$\hat a^+_p(t) = \exp(\mathrm{i}\varepsilon_p t)\hat a^+_p\,, \qquad \hat a_p(t) = \exp(-\mathrm{i}\varepsilon_p t)\hat a_p\,, \tag{35}$$

$$\Psi(r,t) = \sum_p \hat a_p(t)\exp(\mathrm{i}pr)\,, \tag{36}$$

$$\hat G^{--}_p(t,t') = -\mathrm{i}\left\langle T_C\hat a_p(t^-)\hat a^+_p(t'^-)\right\rangle = -\mathrm{i}\left\langle T\hat a_p(t)\hat a^+_p(t')\right\rangle$$
$$= -\mathrm{i}\left[\theta(t-t')\pm n_p\right]\exp\left[-\mathrm{i}\varepsilon_p(t-t')\right]\,, \tag{37}$$

---

[1] We note that in Craig’s paper [23] published in 1968, four years after Keldysh’s paper, the diagram technique was reconsidered using a generalized concept of T-ordering along a contour around the real axis. In this article, the author notes that *some parts of the technique were obtained independently in* [1]. Surprisingly, the book by Mills in 1969 [24] already has a summary of this technique based on Craig’s work, but no reference to the pioneering work [1] is given. At the same time, both [23] and [24] describe the calculation of time propagators only in thermodynamic equilibrium. The possibility of using the technique to describe nonequilibrium and nonstationary states was not discussed (and, apparently, was not understood).

$$\hat{G}_p^{++}(t,t') = -\mathrm{i}\big\langle \tilde{T}\hat{a}_p(t)\hat{a}_p^+(t')\big\rangle$$
$$= -\mathrm{i}\big[\theta(t'-t) \pm n_p\big] \exp\big[-\mathrm{i}\varepsilon_p(t-t')\big]\,, \qquad (38)$$

$$\hat{G}_p^{+-}(t,t') = -\mathrm{i}\big\langle \hat{a}_p(t)\hat{a}_p^+(t')\big\rangle = -\mathrm{i}(1 \pm n_p) \exp\big[-\mathrm{i}\varepsilon_p(t-t')\big]\,, \qquad (39)$$

$$\hat{G}_p^{-+}(t,t') = \mp\mathrm{i}\big\langle \hat{a}_p^+(t')\hat{a}_p(t)\big\rangle = \mp\mathrm{i}n_p \exp\big[-\mathrm{i}\varepsilon_p(t-t')\big]\,, \quad (40)$$

where the upper (lower) sign refers to bosons (fermions).

It follows from definition (34) that the four Green's functions satisfy the equality

$$\hat{G}^{-+} + \hat{G}^{+-} = \hat{G}^{--} + \hat{G}^{++}\,. \qquad (41)$$

Clearly, Green's functions (37)–(40) for noninteracting particles also satisfy this relation.

We emphasize that the set of four functions can be defined without the T_C-ordering operation (as in the book by Landau, Lifshitz, and Pitaevskii [28]). However, it seems that using T_C-ordering leads to a more logical and uniform treatment and, in particular, allows considerably simplifying the proof of Wick's theorem. For example, a function such as

$$G^{+-}(rt, r't') = -\mathrm{i}\big\langle \hat{\Psi}(rt)\hat{\Psi}^+(r't')\big\rangle\,, \qquad (42)$$

whose definition involves no T-ordering, can be constructed according to the general definition of T_C-ordering,

$$G^{+-}(rt, r't') = -\mathrm{i}\big\langle T_C\hat{\Psi}(rt^+)\hat{\Psi}^+(r't'^-)\big\rangle\,. \qquad (43)$$

Here, the time t^+ on the contour C is always 'after' the time t^-, and hence the operator Ψ is always to the left of Ψ^+, irrespective of the relation between the times t and t' on the real axis.

The occupation numbers of states n_p in (37)–(40) are not necessarily Fermi or Bose distributions $n(\varepsilon_p)$. It is shown in the Appendix that the initial density matrix is only required not to contain correlations between different states. The Gibbs density matrix corresponding to the thermodynamic distribution for noninteracting particles satisfies this requirement, but the initial occupation numbers can in fact be *arbitrary*.

In many cases, we are interested in the time variation of occupation numbers (or concentration) in a given state. Such a variation is directly related to the function G^{-+}:

$$n(r,t) = -\mathrm{i}G^{-+}(rt, rt) = -\mathrm{i}\sum_p G_p^{-+}(t,t) = \sum_p n_p\,. \quad (44)$$

The simplest way to discuss nonequilibrium diagram rules is to consider corrections to the usual T-ordered Green's function

$$\hat{G}_{p,p'}^{--}(t,t') = -\mathrm{i}\big\langle T\hat{a}_p(t)\hat{a}_{p'}^+(t')\big\rangle \qquad (45)$$

in the case of particles in external fields:

$$\hat{V} = \sum_{p,q} a_{p+q}^+ a_p U_q(t)\,. \qquad (46)$$

In the first order of the perturbation theory, there are two terms arising in the decomposition of the evolution matrix S and S^+:

$$-\mathrm{i}\Big\langle T_C\Big[\Big((-\mathrm{i})\int_{t_0}^t \sum_{p_1,q} a_{p_1+q}^+(t_1^-)U_q(t_1)a_{p_1}(t_1^-)\,\mathrm{d}t_1$$
$$+ (+\mathrm{i})\int_{t_0}^t \sum_{p_1,q} a_{p_1+q}^+(t_1^+)U_q(t_1)a_{p_1}(t_1^+)\,\mathrm{d}t_1\Big)a_p(t^-)a_{p'}^+(t'^-)\Big]\Big\rangle\,. \qquad (47)$$

Figure 2. First-order diagrams in the case of an external field.

Splitting the expression into pairs of T_C-ordered operators, we obtain

$$G_{p+q,p}^{--(1)} = \int_{t_0}^t \mathrm{d}t_1\,\big[G_{p+q}^{--}(t-t_1)U_q(t_1)G_p^{--}(t_1-t')$$
$$- G_{p+q}^{-+}(t-t_1)U_q(t_1)G_p^{+-}(t_1-t')\big]\,. \qquad (48)$$

This equation corresponds to the two diagrams shown in Fig. 2.

The second term in (48) has a minus sign because the usual vertices arising from the evolution operator S have the prefactor $(-\mathrm{i})$, while vertices with the '+' sign arise from the inverse operator S^+ in (19) and have a different sign of the imaginary unit $(+\mathrm{i})$ [see Eqn (23)]. This rule is general: the '+' sign of a vertex is to be changed, in contrast to the conventional diagram technique.

Even this particular example shows that there is a sort of matrix structure, because the Green's functions for any interactions are always linked in chains of the form

$$G^{--} \propto G^{-\alpha}G^{\alpha,\beta}G^{\beta\gamma}\ldots G^{\delta-}\,, \qquad (49)$$

where the summation over all intermediate indices ranging over + and − is assumed.

By Wick's theorem, two more terms occur in (47) in the case of two paired external operators and mutually contracted operators from the evolution matrices. The terms described by the diagram in Fig. 3 correspond to the analytic expression

$$G_{pp'}^{--}(t-t')$$
$$\times\int_{t_0}^t \mathrm{d}t_1 \sum_{p_1}\big[G_{p_1,p_1+q}^{-+}(t_1,t_1)U_q(t_1) - G_{p_1,p_1+q}^{-+}(t_1,t_1)U_q(t_1)\big]\,. \qquad (50)$$

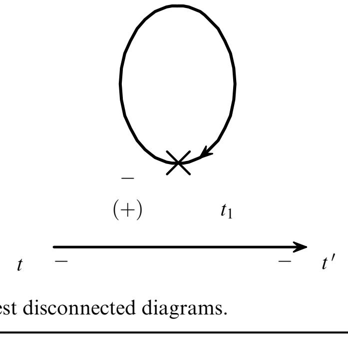

Figure 3. Simplest disconnected diagrams.

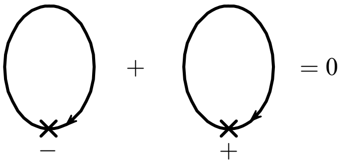

Figure 4. Vanishing sum of disconnected diagrams.

It follows that diagrams containing segments disconnected from the main line vanish: one closed loop is exactly canceled by the other one due to the change of the '+' sign of the vertex (Fig. 4).

A very important property of the NDT shown in the simplest example above is that the sum of all disconnected loops vanishes for any interaction. Any disconnected diagram, just like a sum of them, is a prefactor of all connected diagrams. We split each order in the perturbation theory into all possible connected and disconnected parts. Then, using standard combinatorics, it is easy to show that the sum of disconnected loops is given by a power series expansion where each term is calculated using Wick's theorem. It follows that the averaged product of the inverse and initial evolution matrix is given by

$$\mathrm{Sp}\left[\rho_0 U^{+}(t, t_0) U(t, t_0)\right] - 1 = \mathrm{Sp}\left[\rho_0\right] - 1 \equiv 0\,. \tag{51}$$

Therefore, the sum of all closed loops of the same order is exactly zero not only for an external field but also for any perturbation. This is completely analogous to calculating the series expansion, for example, of the following function:

$$\exp(x)\exp(-x) = 1\,, \quad (1+x)(1-x) = 1 + O(x^2)\,, \quad \text{etc}\,. \tag{52}$$

Thus, the diagram rules in the simple case of an external field are very simple:

— all connected topologically nonequivalent diagrams are drawn, just as in the conventional diagram technique;

— if we calculate corrections to the usual T-ordered function, then the endpoints are assigned the indices '$--$' or any other index for the corresponding correlators;

— there are two options for any vertex, '+' and '−', the lines with different signs at the endpoints correspond to different initial Green's functions, the potential U is in the '−' vertex, and the sign-reversed potential $-U$ is in the '+' vertex.

We consider the integration with respect to time in each vertex. While we follow the original scheme for calculating expectation values of several operators with a maximum time t, the integration domain is finite: from the initial time t_0, when the interaction is turned on, until the current time t. But when mutual positions of times on the time axis are not fixed, it is inconvenient to keep track of which of the 'outer' times is the biggest. For convenience, the integration domain can be extended to $+\infty$ by the same method as in the conventional diagram technique. In what follows, we also use the Fourier transformation. For this, it is also necessary to extend the integration with respect to intermediate times to infinity.

Because the evolution matrix has the property

$$\begin{aligned} S^{+}(+\infty, t) S(+\infty, t) &= S^{-1}(+\infty, t) S(+\infty, t) \\ &= S(t, +\infty) S(+\infty, t) = S(t, t) = 1\,, \end{aligned} \tag{53}$$

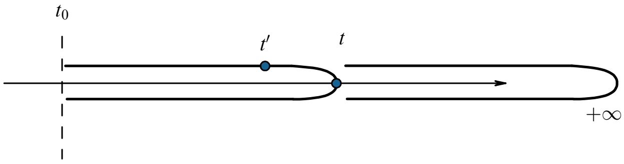

Figure 5. Contour in the steady-state case.

the unit operator can be inserted into the original equations

$$\begin{aligned} &\left\langle \hat{A}_H(t) \hat{B}_H(t') \right\rangle \\ &= \mathrm{Sp}\left[\rho_0 S^{+}(t, -\infty) S^{+}(+\infty, t) S(+\infty, t) \hat{A} S(t, t') \hat{B} S(t', -\infty)\right]. \end{aligned} \tag{54}$$

In the interaction picture, we find that

$$\begin{aligned} &\left\langle \hat{A}_H(t) \hat{B}_H(t') \right\rangle \\ &\quad = \mathrm{Sp}\left[\rho_0 U^{+}(+\infty, -\infty) T\left\{U(+\infty, -\infty) \hat{A}(t) \hat{B}(t')\right\}\right] \\ &\quad = \mathrm{Sp}\left[\rho_0 T_{C_\infty}\left\{\exp\left[-\mathrm{i}\int_{C_\infty} \hat{V}(t_c)\,\mathrm{d}t_c\right] \hat{A}(t^{-}) \hat{B}(t'^{-})\right\}\right]. \end{aligned} \tag{55}$$

This operation can be represented graphically as the original contour augmented by an 'empty' loop extending from the maximum time to $+\infty$ and back (Fig. 5).

Time integrals in the original expressions were restricted by the maximum time t, and now the integration domain is extended to infinity. This seems to change the value of each individual term in the perturbation series. However, there is no paradox because all terms of a given order are summed in such a way that the remaining integrals are taken over the original time domain. As we show in the next section, this can be explicitly demonstrated by writing the NDT equations in a different representation. If t is the maximum time in averaged operators, then integration with respect to the intermediate times from t to $+\infty$ is explicitly eliminated in each diagram.

4. Matrix Dyson equations. Various matrix formulations of the nonequilibrium diagram technique

In the presence of an external field, the summation over two possible signs in any vertex can be easily represented in matrix form by combining the perturbation series for all four Green's functions G^{--}, G^{-+}, G^{+-}, G^{++} into a single equation:

$$\hat{G}^{\alpha,\beta} = \hat{G}_0^{\alpha,\beta} + \hat{G}_0^{\alpha,\gamma} \Sigma^{\gamma,\delta} \hat{G}_0^{\delta,\beta} + \hat{G}_0^{\alpha,\gamma} \Sigma^{\gamma,\delta} \hat{G}_0^{\delta,\mu} \Sigma^{\mu,\nu} \hat{G}_0^{\nu,\beta} + \ldots\,, \tag{56}$$

$$\hat{G}^{\alpha,\beta} = \begin{pmatrix} G^{--} & G^{-+} \\ G^{+-} & G^{++} \end{pmatrix}, \tag{57}$$

$$\Sigma^{\alpha,\beta} = \begin{pmatrix} U & 0 \\ 0 & -U \end{pmatrix}. \tag{58}$$

This series can be conventionally represented as a Dyson equation in matrix form

$$\hat{G}^{\alpha,\beta} = \hat{G}_0^{\alpha,\beta} + \hat{G}_0^{\alpha,\gamma} \Sigma^{\gamma,\delta} \hat{G}^{\delta,\beta}\,. \tag{59}$$

We here assume that depending on the representation, we integrate in any vertex with respect to intermediate times and

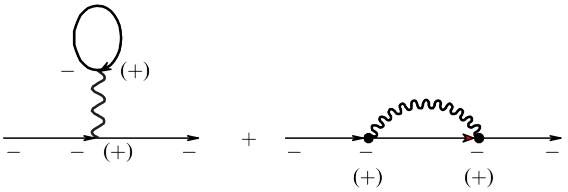

Figure 6. First-order diagrams for the pair interaction.

coordinates or sum over momenta:

$$G_0^{\alpha,\gamma}\Sigma^{\gamma,\delta}G^{\delta,\beta}$$
$$= \int \mathrm{d}t_1\,\mathrm{d}t_2 \sum_{p_1,p_2} G^{\alpha,\gamma}_{p,p_1}(t,t_1)\Sigma^{\gamma,\delta}_{p_1,p_2}(t_1,t_2)G^{\delta,\beta}_{p_2,p'}(t_2,t')\,. \quad (60)$$

In the presence of an external field, the irreducible matrix part turns out to be very simple: it is local in time and diagonal in the space of Keldysh indices '+, −'.

But the case of pair interactions between particles, Eqn (31), is more complicated. In the first order of the perturbation theory, the irreducible part is also diagonal in the indices '+, −'. But because any vertex has a sum over indices '+, −' there are two different connected diagrams corresponding to four contributions (Fig. 6). For example, the second graph in Fig. 6 corresponds to two terms:

$$G^{(1)--}(r,t;r',t')$$
$$= \int G^{--}(r-r_1)\left[\mathrm{i}G^{-+}(r_1-r_2)U(r_1-r_2)\right]G^{--}(r_2-r') \quad (61)$$
$$+\,G^{-+}(r-r_1)\left[-\mathrm{i}G^{-+}(r_1-r_2)U(r_1-r_2)\right]G^{+-}(r_2-r'). \quad (62)$$

The peculiarity of the rules in the case of pair interaction is that depending on the '+' and '−' signs, the line corresponding to the interaction potential corresponds to the expressions

$$U^{--} = -\mathrm{i}U(r_1-r_2)\,, \quad U^{++} = +\mathrm{i}U(r_1-r_2)\,, \quad (63)$$

containing not only a change of sign but also an additional imaginary unit.

Higher-order diagrams are more complicated. If we consider the Dyson equation in the usual way by extracting irreducible parts of the diagram series, then, in the pair interaction case, irreducible parts shown in Fig. 7 already appear in the second order. These parts are nondiagonal in the indices '+, −'. It follows that in all cases more complex than that of an external field, the irreducible part is a full-fledged matrix all of whose elements are nonzero. Hence, the NDT Dyson equation is more complicated. It becomes a system of four equations, which can always be written in matrix form (59). Because four Green's functions are related by (41), the four components of the irreducible part are not independent:

$$\Sigma^{--} + \Sigma^{++} + \Sigma^{-+} + \Sigma^{+-} = 0\,. \quad (64)$$

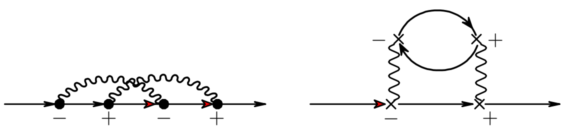

Figure 7. Irreducible parts off-diagonal in the indices '+−'.

Therefore, the matrix equations can be simplified by keeping only independent components. Usually, this can be done by choosing a linear transformation matrix such that one element of the Green's function (GF) matrix vanishes,

$$\hat{G} \Rightarrow L\hat{G}L^{-1} = \begin{pmatrix} 0 & G^{\mathrm{A}} \\ G^{\mathrm{R}} & G^{\mathrm{K}} \end{pmatrix}, \quad (65)$$

where the rotation matrix has the form

$$\hat{L} = \frac{1}{\sqrt{2}}\begin{pmatrix} 1 & -1 \\ 1 & 1 \end{pmatrix}. \quad (66)$$

The retarded and advanced Green's functions appear here as linear combinations of the NDT functions $G^{\alpha,\beta}$:

$$\hat{G}^{\mathrm{R}} = \hat{G}^{--} - \hat{G}^{-+} = \hat{G}^{+-} - \hat{G}^{++}\,, \quad (67)$$
$$\hat{G}^{\mathrm{A}} = \hat{G}^{--} - \hat{G}^{+-} = \hat{G}^{-+} - \hat{G}^{++}\,. \quad (68)$$

However, it is precisely these combinations that correspond to the definitions of the retarded and advanced functions:

$$\hat{G}^{\mathrm{R}}_p(t,t') = -\mathrm{i}\left\langle \hat{a}_p(t)\hat{a}^+_p(t') \pm \hat{a}^+_p(t')\hat{a}_p(t)\right\rangle\theta(t-t')$$
$$= -\mathrm{i}\exp\left[-\mathrm{i}\varepsilon_p(t-t')\right]\theta(t-t') \quad (69)$$

(the upper sign is for fermions and the lower sign is for bosons).

The advanced function is related to the retarded one as $G^{\mathrm{A}}(p,t,t') = [G^{\mathrm{R}}(p,t',t)]^*$.

The third new function, now commonly called the Keldysh function, is defined as

$$\hat{G}^{\mathrm{K}} = \hat{G}^{-+} + \hat{G}^{+-} \equiv \hat{G}^{<} + \hat{G}^{>}\,. \quad (70)$$

Because the retarded (advanced) function is defined by the anticommutator for fermions, the function G^{K} is the average of the commutator of the same operators (with the lower sign is for bosons):

$$\hat{G}^{\mathrm{K}}_p(t,t') = -\mathrm{i}\left\langle \hat{a}_p(t)\hat{a}^+_p(t') \mp \hat{a}^+_p(t')\hat{a}_p(t)\right\rangle$$
$$= -\mathrm{i}\exp\left[-\mathrm{i}\varepsilon_p(t-t')\right](1 \mp 2n_p)\,. \quad (71)$$

As we see below, this choice of 'independent variables' in the matrix Dyson equation leads to the correct 'ideology': the retarded and advanced functions are 'responsible' for a change in the system spectrum caused by external fields, interaction, etc., while the Keldysh function determines the nonequilibrium filling of the spectrum.

If we use (65) to put the matrix Green's functions into the triangular form, the transformed self-energy part also becomes a triangular matrix:

$$\hat{\Sigma} \Rightarrow L\hat{\Sigma}L^{-1} = \begin{pmatrix} \Sigma^{\mathrm{K}} & \Sigma^{\mathrm{R}} \\ \Sigma^{\mathrm{A}} & 0 \end{pmatrix}, \quad (72)$$

where

$$\Sigma^{\mathrm{K}} = -(\Sigma^{-+} + \Sigma^{+-})\,,$$
$$\Sigma^{\mathrm{R}} = \Sigma^{--} + \Sigma^{-+} = -(\Sigma^{++} + \Sigma^{+-})\,, \quad (73)$$
$$\Sigma^{\mathrm{A}} = \Sigma^{--} + \Sigma^{+-} = -(\Sigma^{++} + \Sigma^{-+})\,.$$

We write the matrix Dyson equations

$$\hat{G}^{\alpha,\beta} = \hat{G}^{\alpha,\beta}_0 + \hat{G}^{\alpha,\gamma}_0\Sigma^{\gamma,\delta}\hat{G}^{\delta,\beta} \quad (74)$$

and find the corresponding system of equations in the new representation. The (1,2) and (2,1) components give two conjugate equations for the retarded and advanced functions,

$$\hat{G}^{\mathrm{R}} = \hat{G}_0^{\mathrm{R}} + \hat{G}_0^{\mathrm{R}} \Sigma^{\mathrm{R}} \hat{G}^{\mathrm{R}} . \tag{75}$$

This equation contains the irreducible part of the retarded component only. It may seem that calculating the spectrum variations is independent of calculating the occupation numbers or concentration. But this is not true because calculating Σ^{R} typically requires knowledge of the functions G^{-+} and G^{+-} as well. In other words, the spectrum itself depends on the nonequilibrium occupation numbers.

The equation for the Keldysh function corresponds to the (2,2) component of the matrix Dyson equation and has a more complicated form:

$$\begin{aligned} \hat{G}^{\mathrm{K}} &= \hat{G}_0^{\mathrm{K}} + [\hat{G}_0 \Sigma \hat{G}]^{22} \\ &= \hat{G}_0^{\mathrm{K}} + \hat{G}_0^{\mathrm{K}} \Sigma^{\mathrm{A}} \hat{G}^{\mathrm{A}} + \hat{G}_0^{\mathrm{R}} \Sigma^{\mathrm{K}} \hat{G}^{\mathrm{A}} + \hat{G}_0^{\mathrm{R}} \Sigma^{\mathrm{R}} \hat{G}^{\mathrm{K}} . \end{aligned} \tag{76}$$

The matrix structure of the original equation manifests itself in three different types of integral terms in the right-hand side of (76).

We note that formulas for the irreducible parts Σ in (64) and (73) differ from those for the Green's functions by the sign (-1) at Σ^{-+} and Σ^{+-}. As already mentioned, this is because a vertex with the index '+' always corresponds to multiplying the whole expression by (-1) compared with the '−' vertices.

In (59), the sign change is part of the definition of Σ^{-+} and Σ^{+-} (in Σ^{++}, the sign is changed twice, and hence there is no such problem); hence, the occurrence of the (-1). Therefore, when calculating irreducible parts shown, for example, in Fig. 5, we should remember that expressions obtained by the general diagram rules are to be multiplied by (-1). This is due to the change of sign in one of the external vertices when substituting them in the Dyson equation. If Σ^{K} is defined as in (73), the irreducible part is calculated in accordance with the general rules as a standard diagram (ignoring signs in external vertices). Also, all equations like (76) contain the part with Σ^{K} on an equal footing with Σ^{R} and Σ^{A}. In the literature, another definition exists without the (-1) [see (73)], which is inconvenient, however, because the sign changes twice. First, the term Σ^{K} in Dyson equation (76) has a minus sign, in contrast to the other two terms, and second, when substituting the diagrammatically calculated Σ^{K} in the Dyson equation, we need to multiply by (-1).

Both the sign effect and the diagram rules in different matrix representations can be 'automated' by introducing a matrix (tensor) interaction and specifying how it changes when passing from one representation to another. In the original formulation, the indices of all Green's functions adjacent to a vertex are the same, and the sign is changed to (-1) for the '+' vertex. In other words, considering the vertex as a tensor quantity linking the matrix Green's function, we can say that any vertex is proportional to the matrix σ_z and the product of δ-functions. Hence, for electron–phonon interaction (32), the vertex can be represented as

$$\Gamma^{k}_{\alpha\beta} = g(\sigma_z)_{\alpha\beta} \delta_{\alpha k} , \tag{77}$$

where the indices k and α, β refer to the respective phonon and electron Green's functions. For pair interaction (31), the matrix structure is given by

$$\Gamma^{\alpha\beta}_{\gamma\delta} = \mathcal{U}(\sigma_z)_{\alpha\beta} \delta_{\alpha\gamma} \delta_{\alpha\delta} , \tag{78}$$

where the indices α, β and γ, δ correspond to the respective incoming and outgoing Green's functions (see Fig. 8).

All the NDT rules for diagram calculations are completely equivalent to the Feynman rules if we take lines to represent matrix Green's functions and associate vertices with tensors of a corresponding rank relating matrix Green's functions. All changes of sign following from changing the vertex index '−' to '+' are absorbed into the definition of the vertex tensor.

In this formalism, for example, the first-order self-energy for electron–phonon interaction is given by

$$\Sigma^{\alpha\beta} = \mathrm{i} g^2 \Gamma^{k}_{\alpha\beta_1} G^{\beta_1\gamma_1} D^{kq} \bar{\Gamma}^{q}_{\gamma_1\beta} . \tag{79}$$

In the new matrix representation, after transformation (65), the electron–phonon vertex with the emission of a phonon has a different form:

$$\tilde{\Gamma}^{k}_{\alpha\beta} = g \sum_{\alpha_1, \beta_1, k_1} \hat{L}_{\alpha\alpha_1} \Gamma^{k_1}_{\alpha_1\beta_1} \hat{L}^{(-1)}_{\beta_1\beta} L^{(-1)}_{k_1 k} . \tag{80}$$

Using explicit form (77), we obtain

$$\tilde{\Gamma}^{1}_{\alpha\beta} = g \frac{1}{\sqrt{2}} \delta_{\alpha\beta} , \qquad \tilde{\Gamma}^{2}_{\alpha\beta} = g \frac{1}{\sqrt{2}} (\sigma_x)_{\alpha\beta} . \tag{81}$$

This particular form of vertices yields the following structure of the simplest irreducible part (79):

$$\begin{aligned} \Sigma^{\mathrm{K}} &= \Sigma^{11} = \mathrm{i} g^2 \, \frac{1}{2} \, [G^{\mathrm{A}} D^{\mathrm{A}} + G^{\mathrm{R}} D^{\mathrm{R}} + G^{\mathrm{K}} D^{\mathrm{K}}] , \\ \Sigma^{\mathrm{R}} &= \Sigma^{12} = \mathrm{i} g^2 \, \frac{1}{2} \, [G^{\mathrm{K}} D^{\mathrm{R}} + G^{\mathrm{R}} D^{\mathrm{K}}] . \end{aligned} \tag{82}$$

Similar transformations in the case of pair interactions are considered below.

In the literature, there is also a slightly different matrix representation, which can be obtained from the one above if we further 'tune' the matrix Green's functions as follows:

$$\hat{G} \Rightarrow \begin{pmatrix} 0 & 1 \\ 1 & 0 \end{pmatrix} \hat{G} . \tag{83}$$

Then we also obtain the triangular representation

$$\hat{G} = \begin{pmatrix} G^{\mathrm{R}} & G^{\mathrm{K}} \\ 0 & G^{\mathrm{A}} \end{pmatrix} , \tag{84}$$

where the functions R and A are on the diagonal and the matrix of irreducible parts has the same form as the Green's function itself,

$$\hat{\Sigma} \Rightarrow L \hat{\Sigma} L^{-1} \begin{pmatrix} 0 & 1 \\ 1 & 0 \end{pmatrix} = \begin{pmatrix} \Sigma^{\mathrm{R}} & \Sigma^{\mathrm{K}} \\ 0 & \Sigma^{\mathrm{A}} \end{pmatrix} . \tag{85}$$

In this representation, of course, we obtain the same equations (75) and (76) for the functions G^{R} and G^{K}, but now they correspond to the (1,1) and (1,2) components of the matrix equation. The obvious advantage of transformations (65) is that they are unitary, while new transformation (83) and (84) is nonunitary. However, we show in what follows that the NDT rules can be 'automated' in the nonunitary case as well.

We note that in many cases we can use not the Keldysh function G^{K} but simply the function G^{-+}, which directly determines the concentration or the number of particles in a particular state. Inspection of the Green's functions G^{K} in (71) shows that

$$G^{\mathrm{K}} \propto (1 - 2n_p) \tag{86}$$

for fermions. This function has the particle–hole symmetry and is therefore commonly used in the theory of metals. On the other hand, a vast number of observables (including concentration of electrons in metals, currents in metal, and tunnel junctions) are expressed directly in terms of G^{-+}. For bosons (photons and phonons),

$$G^{\mathrm{K}} \propto 2\left(\frac{1}{2} + n_p\right), \tag{87}$$

and hence this function determines the energy in a given field mode. Of course, both G^{K} and G^{-+} contain exactly the same information. The use of a particular representation depends on the particular problem and, to a greater extent, is a matter of habit. Also, in the representation based on G^{-+}, this function is usually referred to as $G^{<}$, a notation that was introduced before [1], e.g., in [29]. The use of this notation often creates the illusion that some earlier work already described the basic NDT concepts. However, this is not true and no diagram technique had been proposed before the appearance of [1]. Nonetheless, the notation is convenient to use in our analysis.

The triangular representation with the function $G^{<} \equiv G^{-+}$

$$\hat{G} = \begin{pmatrix} G^{\mathrm{R}} & G^{<} \\ 0 & G^{\mathrm{A}} \end{pmatrix} \tag{88}$$

is obtained from the original matrix Green's functions by transformations similar to those used in deriving (84). Transformations (65), (83) reducing the matrix Green's functions to form (84) can be written as

$$\hat{G} \Rightarrow \hat{U}\hat{G}\hat{V} \tag{89}$$

with the matrices

$$\hat{U} = \frac{1}{\sqrt{2}}\begin{pmatrix} 1 & 1 \\ 1 & -1 \end{pmatrix}, \quad \hat{V} = \frac{1}{\sqrt{2}}\begin{pmatrix} 1 & 1 \\ -1 & 1 \end{pmatrix}. \tag{90}$$

To obtain triangular form (88), the matrices U and V must have the form

$$\begin{gathered} \hat{U} = \begin{pmatrix} 1 & 0 \\ 1 & -1 \end{pmatrix} = \hat{\sigma}_z + \sigma^{-}, \\ \hat{V} = \begin{pmatrix} 1 & 0 \\ -1 & 1 \end{pmatrix} = \hat{1} - \sigma^{-}, \quad \sigma^{-} = \begin{pmatrix} 0 & 0 \\ 1 & 0 \end{pmatrix}. \end{gathered} \tag{91}$$

The transformation of the irreducible part Σ is given by the inverse matrices,

$$\hat{\Sigma} \Rightarrow \hat{V}^{-1}\hat{\Sigma}\hat{U}^{-1}, \tag{92}$$

where $\hat{U}^{-1} = \hat{U}$ and $\hat{V}^{-1} = \hat{1} + \sigma^{-}$. This yields the same triangular form (85), but with Σ^{K} replaced by Σ^{-+}. After transformation (91), the (1,2) component of the matrix Dyson equation is quite similar to the equation for Keldysh function (76):

$$\hat{G}^{<} = G_0^{<} + G_0^{<}\Sigma^{\mathrm{A}}G^{\mathrm{A}} + G_0^{\mathrm{R}}\Sigma^{<}G^{\mathrm{A}} + G_0^{\mathrm{R}}\Sigma^{\mathrm{R}}G^{<}. \tag{93}$$

Similarly to Σ^{K} in (73), the quantity $\Sigma^{<}$ introduced in this equation contains an extra overall (-1) in front of Σ^{-+}:

$$\Sigma^{<} = -\Sigma^{-+}. \tag{94}$$

By analogy with the unitary transformation case in (65), finding any interaction vertex in the new representation can also be 'automated' for nonunitary transformations.

For example, for electron–phonon interaction [cf. (80)], the vertex with the emission of a phonon has the form

$$\tilde{\Gamma}^{k}_{\alpha\beta} = g \sum_{\alpha_1, \beta_1, k_1} \hat{V}^{-1}_{\alpha\alpha_1} \Gamma^{k_1}_{\alpha_1\beta_1} \hat{U}^{-1}_{\alpha_1\alpha} U^{-1}_{k_1 k}, \tag{95}$$

while the conjugate vertex corresponds to absorption:

$$\tilde{\Gamma}^{*k}_{\alpha\beta} = g \sum_{\alpha_1, \beta_1, k_1} \hat{V}^{-1}_{\alpha\alpha_1} \Gamma^{k_1}_{\alpha_1\beta_1} \hat{U}^{-1}_{\alpha_1\alpha} V^{-1}_{k k_1}. \tag{96}$$

Their explicit form is similar to (81) and is given by

$$\begin{gathered} \tilde{\Gamma}^{1}_{\alpha\beta} = g\delta_{\alpha\beta}, \quad \tilde{\Gamma}^{2}_{\alpha\beta} = g\begin{pmatrix} 0 & 0 \\ 1 & -1 \end{pmatrix}, \\ \tilde{\Gamma}^{*1}_{\alpha\beta} = g\begin{pmatrix} 1 & 0 \\ 1 & 0 \end{pmatrix}, \quad \tilde{\Gamma}^{*2}_{\alpha\beta} = g\delta_{\alpha\beta}. \end{gathered} \tag{97}$$

Accordingly, for the simplest irreducible part (79), instead of (82), we have

$$\begin{gathered} \Sigma^{<} = \Sigma^{12} = \mathrm{i}g^2 G^{<} D^{<}, \\ \Sigma^{\mathrm{R}} = \Sigma^{11} = \mathrm{i}g^2 (G^{<} D^{\mathrm{R}} + G^{\mathrm{R}} D^{<} + G^{\mathrm{R}} D^{\mathrm{R}}). \end{gathered} \tag{98}$$

In the case of pair interaction (31), this formal vertex transformation is more cumbersome, although the result is quite simple. In the triangular representation, instead of the original vertex (78), we arrive at the combination

$$\begin{aligned} \hat{\Gamma}^{\alpha_2\beta_2}_{\gamma_2\delta_2} &= \mathcal{U}(\hat{V}^{-1})^{\alpha_2\alpha}(\hat{V}^{-1})^{\beta_2\alpha}(\sigma_z)_{\alpha\alpha}(\hat{U}^{-1})^{\alpha\gamma_2}(\hat{U}^{-1})^{\alpha\delta_2} \\ &= \mathcal{U}\big[\delta_{\alpha_2 1}\delta_{\beta_2 1}\delta_{1\gamma_2}\delta_{1\delta_2} - \delta_{\alpha_2 2}\delta_{\beta_2 2}\delta_{2\gamma_2}\delta_{2\delta_2} \\ &\quad + (\delta_{\alpha_2 1}\delta_{\beta_2 2} + \delta_{\alpha_2 2}\delta_{\beta_2 1})\delta_{1\gamma_2}\delta_{1\delta_2} \\ &\quad + \delta_{\alpha_2 2}\delta_{\beta_2 2}(\delta_{2\gamma_2}\delta_{1\delta_2} + \delta_{1\gamma_2}\delta_{2\delta_2})\big]. \end{aligned} \tag{99}$$

In contrast to the original representation, there are now vertices with not necessarily equal indices α, β, γ, and δ. The same is true in the unitary transformation case (65), however, and hence the nonunitary transformation case can be considered along the same lines. Vertices for other interaction types can be transformed in a similar way.

To give an example, we show how the technique works when calculating the second-order irreducible part in the case of pair interaction (Fig. 8):

$$\hat{\Sigma}^{\alpha\gamma_1} = \hat{\Gamma}^{\alpha\beta}_{\gamma\delta} G_1^{\gamma\alpha_1} G_2^{\delta\beta_1} G_3^{\delta_1\beta} \Gamma^{\alpha_1\beta_1}_{\delta_1\gamma_1}. \tag{100}$$

Substituting the explicit form of vertex (99), we obtain

$$\begin{gathered} \Sigma^{<} = \Sigma^{12} = \mathcal{U}^2 G_1^{<} G_2^{<} G_3^{>}, \\ \Sigma^{\mathrm{R}} = \Sigma^{11} = \mathcal{U}^2 (G_1^{>} G_2^{\mathrm{R}} G_3^{<} + G_1^{\mathrm{R}} G_2^{<} G_3^{<} + G_1^{<} G_2^{>} G_3^{\mathrm{A}}). \end{gathered} \tag{101}$$

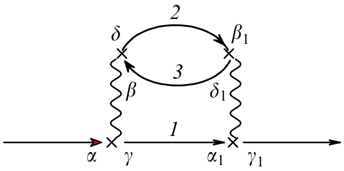

Figure 8. Matrix vertices of the second-order irreducible part for a pair interaction.

(Here, we use the compact form with the relation $G^> = G^< + G^{\mathrm{R}} - G^{\mathrm{A}}$ taken into account.)

Formal analysis of the simultaneous transformation of the matrix Green's functions and interaction vertices shows that in any NDT representation, we have clearly defined Feynman rules for finding analytic expressions for diagrams, where lines correspond to the matrix Green's function and vertices correspond to tensors of a given rank. We note that using relations between different Green's functions and irreducible parts (67), (68), and (73) in the original symmetric representation, we can directly (and often easily) find expressions corresponding to a particular diagram in a given representation. For example, using $\Sigma^< = -\Sigma^{-+}$ for the diagram in Fig. 8, we immediately obtain the expression $G_1^< G_2^< G_3^>$. To calculate Σ^{R}, we can use the relation $\Sigma^{\mathrm{R}} = \Sigma^{--} + \Sigma^{-+}$ and relations for incoming Green's functions (67) and (68), which also gives the result in (101).

Triangular representations (65), (84), and (88) are 'more efficient' not only because they contain only independent components of the Green's functions. For convenience, we have also extended the integration range with respect to intermediate times to $+\infty$ (to be able to use the Fourier transformation in time in what follows). On the other hand, we earlier noted that the integration from the latest time in external operators to $+\infty$ makes no contribution. In the original representation, every individual diagram contained a nonzero contribution from the added time domain, and only the sum of all contributions of a given order vanished.

In triangular representation (65), (84), (88), this fictitious region is absent from the very beginning, because the retarded and advanced functions explicitly depend on time as $\theta(t-t')$. All intermediate times in the equations for G^{R} or G^{A} are 'sandwiched' by θ-functions between time arguments of these functions. The functions R and A in each term of the equation for $G^<$ (or G^{K}), Eqn (93), are arranged such that integrals with respect to intermediate times are always bounded by the maximum time of 'external' averaged operators.

We now consider Eqn (76) or (93) in more detail. If the system is perturbed such that states of all particles are essentially changed, and if there are nonstationary transient processes, then it is clear that the filling of states can be very different from the initial (equilibrium) distribution. But the right-hand side of Eqn (76) or (93) involves the function G_0^{K} or $G_0^<$, which is determined by initial distribution (37), and it seems that the equation always depends on the initial state. However, already in the first article [1], it was shown that the presence of G_0^{K} ($G_0^<$) in this equation is in some sense 'fictitious'. The point is that matrix Dyson equation (59) can be converted into integro-differential equations using the inverse operator matrix

$$(\hat{G}_0)^{-1} = (G_0^{\mathrm{R}})^{-1}\sigma_z\,. \tag{102}$$

For noninteracting particles, the inverse of G_0^{R} in (69) is given by

$$(G_0^{\mathrm{R}})^{-1} = \mathrm{i}\,\frac{\partial}{\partial t} - \varepsilon_p\,. \tag{103}$$

Indeed,

$$\begin{aligned}(G_0^{\mathrm{R}})^{-1} G_p^{0\mathrm{R}} &= \left(\mathrm{i}\,\frac{\partial}{\partial t} - \varepsilon_p\right)\Big\{-\mathrm{i}\theta(t-t')\exp\left[-\mathrm{i}\varepsilon_p(t-t')\right]\Big\}\\ &= \delta(t-t')\,.\end{aligned} \tag{104}$$

The operator gives zero when acting on the function $G_0^{-+}(G_0^<)$ in (37), i.e.,

$$G_{0p}^<(t,t') = \mathrm{i}n_p\exp\left[-\mathrm{i}\varepsilon_p(t-t')\right], \tag{105}$$

$$(G_0^{\mathrm{R}})^{-1} G_{0p}^< = \left(\mathrm{i}\,\frac{\partial}{\partial t} - \varepsilon_p\right)\mathrm{i}n_p\exp\left[-\mathrm{i}\varepsilon_p(t-t')\right] = 0\,. \tag{106}$$

Therefore, in the original matrix representation [cf. (67)], we find that

$$\hat{G}_0^{-1}\hat{G}_0 = \hat{1}\,. \tag{107}$$

In passing to the triangular representation, the inverse operator matrix is also transformed. For transformation (65), it is given by

$$\hat{\hat{G}}_0^{-1} = L\hat{G}_0^{-1}L^{-1} = (G_0^{\mathrm{R}})^{-1}\sigma_x\,. \tag{108}$$

For transformation (91), it is given by

$$\hat{\hat{G}}_0^{-1} = V^{-1}\hat{G}_0^{-1}U^{-1} = (G_0^{\mathrm{R}})^{-1}\hat{1}\,. \tag{109}$$

In what follows, we mainly use the triangular matrix form with $G^<$ in (88). As already mentioned, by construction, this formulation is completely equivalent to the 'unitary' triangular form (65) and gives equivalent Dyson equations. The diagram rules for calculating irreducible parts in this representation are also derived automatically using the original matrix form symmetric in the Keldysh indices. All formulas below are almost 'literally' transferred to the canonical triangular form (65) with $G^<$ replaced by G^{K}. In triangular representation (88), (109), the (1,2) component of (107) is simply the action of the operator $(G_0^{\mathrm{R}})^{-1}$ on the left-hand and right-hand sides of Eqn (93):

$$G_0^{-1}G^< = \Sigma^< G^{\mathrm{A}} + \Sigma^{\mathrm{R}} G^<\,. \tag{110}$$

This equation explicitly contains the exact functions $G^<$ at current times and no function $G_0^<$. However, the information on the initial distribution function is contained in the initial conditions of the integro-differential equation.

Integral equation (93) for steady nonequilibrium states can be transformed such that the dependence on $G_0^<$ disappears completely. Rewriting Eqn (93) in the form

$$[1 - \hat{G}_0^{\mathrm{R}}\Sigma^{\mathrm{R}}]\hat{G}^< = \hat{G}_0^<[1 + \Sigma^{\mathrm{A}}\hat{G}^{\mathrm{A}}] + \hat{G}_0^{\mathrm{R}}\Sigma^<\hat{G}^{\mathrm{A}}\,, \tag{111}$$

using Eqn (75) for the retarded and advanced Green's functions,

$$[1 - \hat{G}_0^{\mathrm{R}}\Sigma^{\mathrm{R}}]\hat{G}^{\mathrm{R}} = \hat{G}_0^{\mathrm{R}}\,, \tag{112}$$

$$\hat{G}_0^{\mathrm{A}}[1 + \Sigma^{\mathrm{A}}\hat{G}^{\mathrm{A}}] = \hat{G}^{\mathrm{A}}\,, \tag{113}$$

and introducing the operators inverse to $G^{\rm R}$ and $G^{\rm A}$, we obtain

$$G^< = G^{\rm R}\big[(G_0^{\rm R})^{-1}G_0^<(G_0^{\rm A})^{-1}\big]G^{\rm A} + G^{\rm R}\Sigma^<G^{\rm A}\,. \qquad (114)$$

Because $(G_0^{\rm R})^{-1}G_0^< = 0$, the first term in the right-hand side of (114) must vanish, and hence the explicit dependence on the initial function $G_0^<$ disappears. In fact, there is a subtlety, to which we also return in what follows, discussing it from different perspectives. Indeed, if all transient processes from the initial state of any 'nonpathological' system are guaranteed to have completely terminated, then the function $G^<$ at the current time is defined only by the last term in (114). However, in passing from the original Dyson equation (93) to (114), we actually applied nonequivalent transformations related to the inverse operators $(G^{\rm R})^{-1}$ in (103). Roughly speaking, such transformations require solving some differential equations in time, and the last term in (114) describes only the inhomogeneous solutions. But homogeneous solutions, which were discarded in the transformation, are important for describing all transient processes at finite times. Thus, the original equation (93) does describe these transient processes, and it therefore naturally contains the initial function $G_0^<$, but transformed equation (114), strictly speaking, is suitable for large times only when it becomes independent of the initial state. (A system influenced by external perturbations can be in both nonequilibrium and unsteady states, however.) In Section 6, we illustrate this with a simple example.

It follows that if all transient processes from the initial state have terminated, we must solve the system of two equations

$$\hat G^{\rm K} = \hat G^{\rm R}\Sigma^{\rm K}\hat G^{\rm A} \quad \text{or} \quad \hat G^< = \hat G^{\rm R}\Sigma^<\hat G^{\rm A}\,, \qquad (115)$$

$$\hat G^{\rm R} = \hat G_0^{\rm R} + \hat G_0^{\rm R}\Sigma^{\rm R}\hat G^{\rm R}\,. \qquad (116)$$

In fact, there are two, not three, equations because the function $G^{\rm A}$ is always uniquely determined by $G^{\rm R}$ ($G^{\rm A}(r,t;r',t') = [G^{\rm R}(r',t';r,t)]^*$ or $G^{\rm A}(p,\omega) = [G^{\rm R}(p,\omega)]^*$).

It is important that the foregoing referred to the most general case, where some perturbation in the system is turned on at the initial time t_0, and we describe all time variations, including transient processes. In other words, the most general formulation of the NDT in the time representation allows describing not just nonequilibrium but also any nonstationary processes. The Green's function then depends on two times, which considerably complicates calculations compared to the stationary case, where all functions depend only on the time difference. We show in Section 5 how to pass from the Dyson equation to various types of differential equations similar to quantum kinetic equations, which are sometimes easier to use in the nonstationary case.

In many cases, we deal with a nonequilibrium but stationary state. For example, we have solid state problems with continuous radiation and the electron tunneling effect for a constant contact-potential difference. Then the initial time t_0 is to be pushed far into the past, i.e., $t_0 = -\infty$. In this case, the calculation is much simpler because we can use the Fourier transformation in time for stationary states.

The Green's functions of noninteracting particles (37) in the Fourier representation have the form

$$G_p^{\rm R}(\omega) = \frac{1}{\omega - \varepsilon(p) + {\rm i}\delta}\,, \qquad (117)$$

$$G_p^{-+}(\omega) \equiv G_p^{0<}(\omega) = 2\pi{\rm i}n_p\delta\big(\omega - \varepsilon(p)\big)\,. \qquad (118)$$

If particles are in thermodynamic equilibrium at the initial time, then, using the δ-function, we can represent $G^<$ as

$$G_p^{0<}(\omega) = 2\pi{\rm i}n_0(\omega)\delta\big(\omega - \varepsilon(p)\big) = n_0(\omega)[G_p^{0\rm A} - G_p^{0\rm R}] = 2{\rm i}n_0(\omega)\,{\rm Im}\,G_p^{0\rm A}(\omega)\,. \qquad (119)$$

The Green's function $G_p^{0<}$ is the product of the spectral function ${\rm Im}\,G_p^{0\rm A}(\omega)$ and the particle distribution function $n_0(\omega)$. We note that, generally speaking, replacing n_p with $n(\omega)$ is not quite an equivalence transformation, as was well illustrated in [30]. This subtlety is discussed using the example in Section 6.

In many cases, comparing formulas (115) and (119) allows introducing a nonequilibrium distribution function of particles in given states. If the irreducible part in a state $|\lambda\rangle$ is diagonal in some approximation, Eqn (115) can be transformed into a form analogous to (119).

Using the relation

$$\Sigma_{\lambda\lambda}^{\rm A} - \Sigma_{\lambda\lambda}^{\rm R} = (\hat G_{\lambda\lambda}^{\rm R})^{-1} - (\hat G_{\lambda\lambda}^{\rm A})^{-1} = \frac{\hat G_{\lambda\lambda}^{\rm A} - \hat G_{\lambda\lambda}^{\rm R}}{\hat G_{\lambda\lambda}^{\rm R}\hat G_{\lambda\lambda}^{\rm A}}\,, \qquad (120)$$

we can represent $G^<(\omega)$ in the form

$$\hat G_{\lambda\lambda}^<(\omega) = \frac{\Sigma_{\lambda\lambda}^<(\omega)}{\Sigma_{\lambda\lambda}^{\rm A}(\omega) - \Sigma_{\lambda\lambda}^{\rm R}(\omega)}\big[\hat G_{\lambda\lambda}^{\rm A}(\omega) - \hat G_{\lambda\lambda}^{\rm R}(\omega)\big] = 2{\rm i}N_\lambda(\omega)\,{\rm Im}\,\hat G_{\lambda\lambda}^{\rm A}(\omega)\,. \qquad (121)$$

The quantity appearing here can be called a nonequilibrium distribution function,

$$N_\lambda(\omega) = \frac{\Sigma_{\lambda\lambda}^<(\omega)}{\Sigma_{\lambda\lambda}^{\rm A}(\omega) - \Sigma_{\lambda\lambda}^{\rm R}(\omega)}\,. \qquad (122)$$

It follows that we do not need to solve kinetic equations in order to find the nonequilibrium distribution functions and nonequilibrium occupation numbers. It suffices to calculate the irreducible parts $\Sigma^<$ and $\Sigma^{\rm R,A}$ using the NDT rules.

Such formulas can describe nonequilibrium occupation of discrete electron states in tunneling problems, nonequilibrium excitation of optical modes and molecular vibrations, and occupation of optical modes in a resonator.

We note that the information contained in the nonequilibrium distribution functions is richer than the information about occupation numbers in a given state contained in the semiclassical balance equations, because the occupation numbers expressed in terms of nonequilibrium Green's functions are a more coarse integral characteristic:

$$N_\lambda = -{\rm i}G_{\lambda\lambda}^<(t,t) = \int {\rm d}\omega\, N_\lambda(\omega)\,\frac{1}{\pi}\,{\rm Im}\,\hat G_\lambda^{\rm A}(\omega)\,. \qquad (123)$$

Passing to the Fourier transform allows keeping track of what happens when the temperature tends to zero. In this case, the averaging is done with respect to the ground state of a many-body system, and the conventional diagram technique based only on the T-ordered functions G^{--} should be valid. It turns out that all diagrams for the function G^{--} having vertices with the '+' sign vanish. For example, the contribution of the diagram shown in Fig. 9a for fermions is given by

$$G^{-+}(r - r_1, \omega)G^{+-}(r_1 - r', \omega) \propto n(\omega)\big[n(\omega) - 1\big] \to 0 \qquad (124)$$

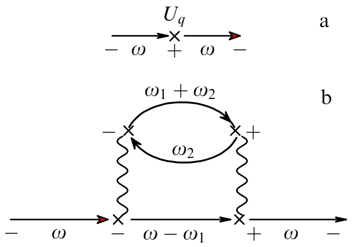

Figure 9. Diagrams vanishing at $T = 0$.

(for bosons, $G^{-+} \to 0$). In more complex cases, as in the diagram in Fig. 9b, occupation numbers appear in combinations that vanish anyway as $T \to 0$:

$$n(\omega-\omega_1)n(\omega_2+\omega_1)\big[n(\omega)-1\big]\big[n(\omega_2)-1\big]$$
$$\to \big[1-\theta(\omega+\omega_2)\big]\theta(\omega+\omega_2) = 0\,. \tag{125}$$

Therefore, in the case $T = 0$, there are only diagrams with the '$-$' signs in all vertices.

We note that the sum of all disconnected loops containing only G^{--} is not zero. Therefore, at zero temperature, we must either use standard arguments to cancel the overall factor in all disconnected diagrams and prove that there are only connected diagrams built of the usual GFs, or use the NDT, where the sum of all disconnected loops is equal to zero, and prove that the usual GFs remain in connected diagrams for the usual function G^{--}.

5. Quantum kinetic equations

Usually, classical kinetic equations describe the time evolution of the particle number in a given state (concentration at a given spatial point),

$$\frac{\partial}{\partial t}\, n_p(t) = \ldots\,. \tag{126}$$

In terms of the NDT, this implies that the left-hand side of these equations must be

$$-\mathrm{i}\,\frac{\partial}{\partial t}\,\hat{G}_p^{<}(t,t) = \ldots\,. \tag{127}$$

Observables are expressed in terms of the Green's functions at equal times. But the quantum kinetic equations can also describe the rate of change of a GF with respect to one of the arguments if the other plays the role of a parameter. These equations are sometimes easier to solve, and the observables then follow by setting $t' = t$ in the solution. The equations can be easily obtained from Dyson equation (93) by acting on each term in this equation with the operator $(G_0^{\mathrm{R}})^{-1}$ in (103). Since the action of this operator on the function $G_0^<$ gives zero, just two terms in the right-hand side of the Dyson equation remain [see (110)]. Hence, for the GF in the momentum representation, we obtain

$$\left[\mathrm{i}\,\frac{\partial}{\partial t}-\varepsilon_p\right]\hat{G}^<_{p,p'}(t,t') = \int \Sigma^<_{p,p_1}(t,t_1)\hat{G}^{\mathrm{A}}_{p_1,p'}(t_1,t')\,\mathrm{d}t_1$$
$$+\int \Sigma^{\mathrm{R}}_{p,p_1}(t,t_1)\hat{G}^<_{p_1,p'}(t_1,t')\,\mathrm{d}t_1\,. \tag{128}$$

There is no $G_0^<$ in this equation, nor is there any explicit information about the initial particle distribution function. The information about the initial state is contained in the solution of the integro-differential equations in the form of boundary conditions.

To derive a quantum-statistical analogue of the Boltzmann equation, we supplement the above equation with the adjoint equation obtained from the same Dyson equation written in a different form:

$$\hat{G}^<(t,t') = \hat{G}_0^<(t,t') + \hat{G}^<\Sigma^{\mathrm{A}}\hat{G}_0^{\mathrm{A}} + \hat{G}^{\mathrm{R}}\Sigma^<\hat{G}_0^{\mathrm{A}} + \hat{G}^{\mathrm{R}}\Sigma^{\mathrm{R}}\hat{G}_0^<\,. \tag{129}$$

To eliminate the function $G_0^<$, we now have to act on this equation with the operator G_0^{-1} 'from the right', or, equivalently, act on the second argument of the Green's function with the operator adjoint to $(G_0^{\mathrm{R}})^{-1}$:

$$(\hat{G}_0^{\mathrm{R}})^{*-1}(t') = -\mathrm{i}\,\frac{\partial}{\partial t'}-\varepsilon_{p'}\,. \tag{130}$$

Subtracting the resulting adjoint equation from Eqn (128), we arrive at the generalized kinetic equation

$$\left[\mathrm{i}\,\frac{\partial}{\partial t}-\varepsilon_p+\varepsilon_{p'}\right]\hat{G}^<_{pp'}(t,t) = \int \Sigma^<_{pp_1}(t,t_1)\hat{G}^{\mathrm{A}}_{p_1p'}(t_1,t)\,\mathrm{d}t_1$$
$$+\int \Sigma^{\mathrm{R}}_{pp_1}(t,t_1)\hat{G}^<_{p_1p'}(t_1,t)\,\mathrm{d}t_1 - \int \hat{G}^<_{pp_1}(t,t_1)\Sigma^{\mathrm{A}}_{p_1p'}(t_1,t)\,\mathrm{d}t_1$$
$$-\int \hat{G}^{\mathrm{R}}_{pp_1}(t,t_1)\Sigma^<_{p_1p'}(t_1,t)\,\mathrm{d}t_1\,, \tag{131}$$

where we set $t = t'$, and therefore

$$\mathrm{i}\left[\frac{\partial}{\partial t}+\frac{\partial}{\partial t'}\right]\bigg|_{t=t'}\hat{G}^<(t,t') = \mathrm{i}\,\frac{\partial}{\partial t}\,\hat{G}^<(t,t)\,. \tag{132}$$

We note that although the left-hand side of (131) is the Green's function at equal times corresponding to a certain physical quantity (or the distribution function), the Green's functions in the right-hand side of the equation, as well as the irreducible parts, depend on essentially different variables due to the quantum nature of this equation. Also, the 'collisional part' contains the Green's functions G^{R} and G^{A}, which cannot be determined from this equation. This is in contrast to the classical Boltzmann equation, which is a closed equation for the distribution function. Thus, in the quantum case, it is impossible to write a closed equation containing only the Green's functions at equal times. Therefore, the general equation

$$(\hat{G}_0^{-1}-\hat{G}_0^{*\,-1})\hat{G}^< = (\hat{\Sigma}\hat{G})^< - (\hat{G}\hat{\Sigma})^< \tag{133}$$

may be called the quantum kinetic equation (the generalized quantum Boltzmann equation), with the stipulation that retarded and advanced Green's functions have already been found from the Dyson equation (they may also depend on the function $G^<$!). The choice of variables in (133) and the exact meaning of the convolution operator product in the right-hand side depend on the particular representation. The right-hand side is a generalized collision integral, which can be written differently using relations between various components of nonequilibrium Green's functions (41) and irreducible part (64):

$$(\hat{\Sigma}\hat{G})^< - (\hat{G}\hat{\Sigma})^< = \hat{G}^<\hat{\Sigma}^> - \hat{G}^>\hat{\Sigma}^< + (\hat{\Sigma}^{\rm R}\hat{G}^< - \hat{G}^<\hat{\Sigma}^{\rm R}) + (\hat{\Sigma}^<\hat{G}^{\rm A} - \hat{G}^{\rm A}\hat{\Sigma}^<) = \hat{\Sigma}^{\rm R}\hat{G}^< + \hat{\Sigma}^<\hat{G}^{\rm A} - \hat{G}^{\rm R}\hat{\Sigma}^< - \hat{G}^<\hat{\Sigma}^{\rm A}\,. \qquad (134)$$

We can use a simpler semiclassical kinetic equation when the perturbation in the noninteracting system gives rise to slow variations in space and time. The phrase 'slow variations' means that if we consider all functions as depending on the central and relative variables,

$$G^<(r_1, t_1; r_2, t_2) = G^<\left(\frac{r_1 + r_2}{2}, \frac{t_1 + t_2}{2}; r_1 - r_2, t_1 - t_2\right), \qquad (135)$$

then the function must change much more slowly in the sum variable than in the difference variable. The GF oscillation rate in the time difference variable is determined by the particle energy scale.

If we write the Green's function in the coordinate representation

$$(\hat{G}_0^{\rm R})^{-1}\hat{G}^{0\rm R}(rt, r't') = \left[{\rm i}\,\frac{\partial}{\partial t} + \frac{1}{2m}\,\Delta\right]\hat{G}^{0\rm R}(rt, r't') = \delta(t - t')\delta(r - r') \qquad (136)$$

and then pass to the Wigner representation

$$G^<(R, t; p, \omega) = \int \exp\left[{\rm i}\omega(t_1 - t_2) - {\rm i}p(r_1 - r_2)\right] \times G^<\left(\frac{r_1 + r_2}{2} = R, \frac{t_1 + t_2}{2} = t; r_1 - r_2, t_1 - t_2\right) {\rm d}(r_1 - r_2)\,{\rm d}(t_1 - t_2)\,, \qquad (137)$$

then the right-hand side of Eqn (131) can be simplified. Because the mean variables vary sufficiently slowly, the integration of terms like ΣG in the relative variables can be approximately considered an independent operation. Therefore,

$$\int \Sigma^<_{pp_1}(t, t_1)\hat{G}^{\rm A}_{p_1p'}(t_1, t')\exp\left[{\rm i}\omega(t - t')\right]{\rm d}t_1\,{\rm d}(t - t') \simeq \Sigma^<_{pp_1}(t, \omega)\hat{G}^{\rm A}_{p_1p'}(t, \omega)\,. \qquad (138)$$

For the quadratic dispersion, we have

$$\varepsilon_{p+q} - \varepsilon_{p-q} = \frac{p}{m}\,2q \to \frac{p}{m}\frac{\partial}{\partial R}\,. \qquad (139)$$

Then the kinetic equation takes the familiar form of the classical Boltzmann equation

$$\left[{\rm i}\,\frac{\partial}{\partial t} + {\rm i}\,\frac{p}{m}\frac{\partial}{\partial R}\right]\hat{G}^<_{p,\omega}(R, t) = \Sigma^<_{p\omega}(R, t)\hat{G}^{\rm A}_{p\omega}(R, t) + \Sigma^{\rm R}_{p\omega}(R, t)\hat{G}^<_{p\omega}(R, t) - \hat{G}^<_{p\omega}(R, t)\Sigma^{\rm A}_{p\omega}(R, t) - \hat{G}^{\rm R}_{p\omega}(R, t)\Sigma^<_{p\omega}(R, t)\,. \qquad (140)$$

We note that by introducing a compact notation usually called the Moyal product [31], the convolution of functions in the right-hand side of (131) can be formally written in the Wigner representation in the local form as

$$\int {\rm d}r_1\,\Sigma(r, r_1)G(r_1, r') \Rightarrow \Sigma_p(R) \otimes G_p(R)\,, \qquad (141)$$

where

$$\Sigma_p(R) \otimes G_p(R) = \Sigma_p(R)\exp\left[{\rm i}\left(\overleftarrow{\partial_R}\,\overrightarrow{\partial_p} - \overleftarrow{\partial_p}\,\overrightarrow{\partial_R}\right)\right]G_p(R)\,. \qquad (142)$$

The same transformation can be done with respect to the time variables. In fact, this product is simply a compact notation for the Taylor series of functions in the right-hand side of the quantum kinetic equation. Because the Moyal product is highly nonlocal, it is applicable only when considering gradient expansions.

Quantum kinetic equations were already investigated in [32]. Equations of this type are also given in the book by Kadanoff and Baym [29]. However, these papers do not contain any general standard recipes for calculating irreducible parts. In [29], the equations are obtained directly from the Heisenberg equations for creation and annihilation operators, with the irreducible part being a functional derivative in the spirit of Schwinger. In the case of a system in thermodynamic equilibrium, the only (and cumbersome) method was to analytically continue finite-order perturbative expressions of the temperature diagram technique to real frequencies. In the NDT, kinetic equations arise as a consequence of the Dyson equations, as their differential form. Moreover, there is a standard machinery to calculate the irreducible parts, which is the same as in the conventional diagram technique.

6. Simple example as a testing ground for studying the properties of the nonequilibrium diagram technique

In this section, we use a simple example to discuss subtleties arising when applying the general theory. We consider a system consisting of an isolated, localized electronic state and free electrons in a metal or semiconductor,

$$\hat{H}_0 = \varepsilon_1 a_1^+ a_1 + \sum_k \varepsilon_k c_k^+ c_k\,. \qquad (143)$$

The state described by the operators a_1 can be a discrete state of atoms adsorbed on the surface of a metal, an impurity state in a semiconductor, etc. The operators c_k^+ and c_k correspond to band electrons. In all actual cases, there are overlap matrix elements between localized and free electron states. It follows that an electron can hop from the localized level into the free band and back. This interaction is considered a perturbation. Also, we consider the simplest external field, which is an additional potential U applied to the localized state. Then the total perturbation Hamiltonian has the form

$$\hat{V} = U a_1^+ a_1 + T\sum_k (c_k^+ a_1 + a_1^+ c_k)\,, \qquad (144)$$

where T is the transition matrix elements between localized and band states. As is often the case, we omit their dependence on k. The system is schematically shown in Fig. 10.

If the state ε_1 has any occupation at the initial instant, then, after turning on interaction (144), transition processes begin (we discuss them shortly). We first find a solution in the stationary case where all transient processes have terminated. The diagrams for the irreducible part of the localized state ε_1 are shown in Fig. 11.

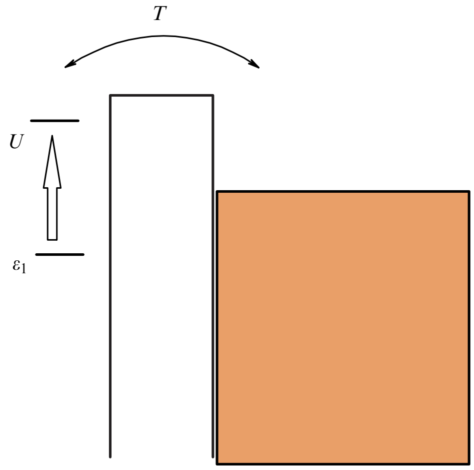

Figure 10. Simple model layout. The electron level ε_1 and bulk states are connected by transient processes.

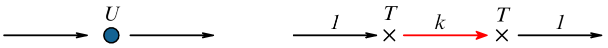

Figure 11. Two contributions to the irreducible part of the Green's function for a localized state.

The diagrams correspond to the following matrix of irreducible parts of the Green's function G_{aa} for the localized state in representation (88):

$$\hat{\Sigma}_{aa} = \begin{pmatrix} U + T^2 \sum_k G_k^{0\mathrm{R}}(\omega) & T^2 \sum_k G_k^{0<}(\omega) \\ 0 & U + T^2 \sum_k G_k^{0\mathrm{A}}(\omega) \end{pmatrix} . \tag{145}$$

The real part of the momentum integral appearing in (145) is frequently neglected in calculations, with only the pole contribution retained:

$$\sum_k G_k^{0\mathrm{R}}(\omega) = \sum_k \frac{1}{\omega - \varepsilon_k + \mathrm{i}\delta} \simeq -\mathrm{i}\pi \nu_k(\omega) , \tag{146}$$

where ν_k is the density of band electron states. This gives the simple expression

$$\Sigma_a^{\mathrm{R}}(\omega) = U + T^2 \sum_k G_k^{0\mathrm{R}}(\omega) = U - \mathrm{i}\gamma . \tag{147}$$

The characteristic quantity that appears here is the localized state decay rate (the rate of transitions from localized states to the continuous spectrum)

$$\gamma = \pi T^2 \nu_k . \tag{148}$$

The Dyson equation in the Fourier representation for G^{R},

$$\hat{G}^{\mathrm{R}} = \hat{G}_0^{\mathrm{R}} + \hat{G}_0^{\mathrm{R}} \Sigma_a^{\mathrm{R}}(\omega) \hat{G}^{\mathrm{R}} = \hat{G}_0^{\mathrm{R}} + \hat{G}_0^{\mathrm{R}} (U - \mathrm{i}\gamma) \hat{G}^{\mathrm{R}} , \tag{149}$$

can be solved easily, giving the trivial answer

$$\hat{G}^{\mathrm{R}} = \frac{1}{\omega - \varepsilon_1 - U + \mathrm{i}\gamma} . \tag{150}$$

The localized state energy level is shifted due to the applied potential and broadened due to transitions to the continuous spectrum.

We now use the formula $G^< = G^{\mathrm{R}} \Sigma^< G^{\mathrm{A}}$, Eqn (115), to determine the steady-state filling of the localized state. The irreducible part $\Sigma^<$ is given by

$$\Sigma^<(\omega) = -\Sigma^{-+}(\omega) = T^2 \sum_k G_k^{0<}(\omega) = 2\mathrm{i}\gamma n_0(\omega) \tag{151}$$

[we recall that $G_k^{0<}(\omega) = 2\pi\mathrm{i} n_0(\omega)\delta(\omega - \varepsilon(k))$, where n_0 is the equilibrium Fermi distribution of band electrons]. It follows that

$$\hat{G}^<(\omega) = \hat{G}^{\mathrm{R}} \Sigma^< \hat{G}^{\mathrm{A}} = \frac{2\mathrm{i}\gamma}{(\omega - \varepsilon_1 - U)^2 + \gamma^2} \, n_0(\omega) . \tag{152}$$

This relation has a clear meaning: the density of localized level states, broadened because of the coupling to the thermostat, is filled with band electrons that have the equilibrium Fermi distribution function n_0.

Letting $\gamma \to 0$ in the expressions (which means that the localized state becomes isolated), we calculate the occupation of the state as a function of the potential:

$$\begin{aligned} G^<(\omega) &= 2\pi\mathrm{i} n_0(\omega)\delta(\omega - \varepsilon_1 - U) \\ &= 2\pi\mathrm{i} n_0(\varepsilon_1 + U)\delta(\omega - \varepsilon_1 - U) . \end{aligned} \tag{153}$$

We have found that the energy level is changed, while the filling of this state is determined by the thermodynamic Fermi function with a shifted energy variable.

However, setting $T = 0$ ($\gamma = 0$) from the very beginning, we find that the nondiagonal (1,2) component is absent in the matrix of irreducible parts (145):

$$\hat{\Sigma} = \begin{pmatrix} U & 0 \\ 0 & U \end{pmatrix} , \qquad \Sigma^{\mathrm{R}} = \Sigma^{\mathrm{A}} = U . \tag{154}$$

Therefore, Eqn (115) cannot be used in this case. The functions G^{R} and G^{A} are still given by (150) with $\gamma = 0$. We return to Eqn (114) and consider the first term in the right-hand side,

$$\hat{G}^< = \hat{G}^{\mathrm{R}} \big[(\hat{G}_0^{\mathrm{R}})^{-1} \hat{G}_0^< (\hat{G}_0^{\mathrm{A}})^{-1} \big] \hat{G}^{\mathrm{A}} , \tag{155}$$

which we omit in what follows. Here, infinitesimal imaginary variations $\mathrm{i}\delta$ are treated as small but finite quantities. We then obtain

$$\hat{G}^<(\omega) = \hat{G}_0^<(\omega) \, \frac{(\omega - \varepsilon_1)^2 + \delta^2}{(\omega - \varepsilon_1 - U)^2 + \delta^2} . \tag{156}$$

The function $G_0^<(\omega)$ in (119) can be represented as

$$G_0^<(\omega) = 2\pi\mathrm{i} n_0(\varepsilon_1)\delta(\omega - \varepsilon_1) = 2\mathrm{i} n_0(\varepsilon_1) \frac{\delta}{(\omega - \varepsilon_1)^2 + \delta^2} . \tag{157}$$

Then $G^<(\omega)$ can be routinely found as

$$\begin{aligned} G_a^<(\omega) &= 2\mathrm{i} n_0(\varepsilon_1) \, \frac{\delta}{(\omega - \varepsilon_1 - U)^2 + \delta^2} \\ &= 2\pi\mathrm{i} n_0(\varepsilon_1)\delta(\omega - \varepsilon_1 - U) . \end{aligned} \tag{158}$$

We note that using (119), we can represent Eqns (114) and (155) in the form

$$\begin{aligned} G_a^<(\omega) &= G^{\mathrm{R}} \big[(\hat{G}_0^{\mathrm{R}})^{-1} \big(n_0(\varepsilon_1)(G_0^{\mathrm{A}} - G_0^{\mathrm{R}}) \big) (\hat{G}_0^{\mathrm{A}})^{-1} \big] G^{\mathrm{A}} \\ &= G^{\mathrm{R}} n_0(\varepsilon_1) \big[(\hat{G}_0^{\mathrm{R}})^{-1} - (\hat{G}_0^{\mathrm{A}})^{-1} \big] G^{\mathrm{A}} . \end{aligned} \tag{159}$$

Here, $2n_0 \operatorname{Im} \Sigma_0^{\mathrm{R}}(\varepsilon_1)$ plays the role of $\Sigma^<$ in general formula (115). This $\Sigma_0^{\mathrm{R}}(\varepsilon_1)$ is equal to $2\mathrm{i}\delta$ rather than zero, which again gives the above result. The result shows that the energy level changes due to the applied field, but the occupation is the same. However, the level occupation ε_1 does not change if we use (118) for the initial Green's function $G_0^<(\omega)$. But if we start with (119), where $n_0(\varepsilon_1)$ is replaced by $n_0(\omega)$ due to the δ-function, then the level occupation changes:

$$\begin{aligned} G_a^<(\omega) &= 2\mathrm{i}n_0(\omega)\delta(\omega - \varepsilon_1 - U) \\ &= 2\pi\mathrm{i}n_0(\varepsilon_1 + U)\delta(\omega - \varepsilon_1 - U)\,. \end{aligned} \tag{160}$$

In this case, the level occupation is determined by the thermodynamic distribution function at the energy shifted by the amount of the applied field. The question of why apparently equivalent representations for $G_0^<$ in some cases yield different results has been discussed in the literature. But the answer is quite simple: it depends on the 'degree of isolation' of the system (of any state or mode in the system).

Turning to Eqn (122), which determines steady-state occupation numbers, we find that by setting $\gamma = 0$ from the very beginning, we obtain the indeterminate expression 0/0:

$$N_a(\omega) = \frac{\Sigma_a^<(\omega)}{\Sigma_a^{\mathrm{A}}(\omega) - \Sigma_a^{\mathrm{R}}(\omega)} = \frac{2\mathrm{i}\gamma n_0(\omega)}{2\mathrm{i}\gamma}\,. \tag{161}$$

The resulting indeterminacy and possible dual answers are not a drawback of the technique. This is because there are actually two different physical situations. Let the discrete level under consideration be that of an atom located away from any solid (i.e., it is truly isolated). If we bring the capacitor plate toward the atom, thereby increasing the potential of all atomic states, then the electron occupation number of the level does not change. This is the answer in (157). We next consider the impurity level in a solid. Because of multiple interactions not included directly in Hamiltonian (160), changing the energy level of such a state inevitably leads to changing its occupation according to the thermodynamic distribution. Treating the imaginary variations in the GF denominators as very small but finite quantities means exactly that we implicitly turn on the coupling of the state to a large thermostat. Hence, the indeterminacy is, in fact, a well-posed and very old physical problem. The order in which the system is prepared is as follows: we first completely turn off the coupling to the thermostat and then send time to infinity; alternatively, we first wait while even a weak coupling to the thermostat yields thermalization, and then turn the coupling off to zero.

Therefore, the rule that is sometimes seen as a shaman spell, that n_p should be replaced by $n(\omega)$ in the Green's functions $G^<$ of a noninteracting system, simply means that the coupling of our system to the outside world (the thermostat) always exists, even if it is very small. Evaluating the indeterminate form using (161) yields Eqn (153). This phenomenon was already explained well in [30].

We now consider nonstationary transient processes. For this, we solve kinetic equation (131) for the function $G_{aa}^<$:

$$\begin{aligned} \mathrm{i}\,\frac{\partial}{\partial t}\,\hat{G}_{aa}^<(t,t) &= \int_0^\infty \Sigma^<(t,t_1)\hat{G}^{\mathrm{A}}(t_1,t)\,\mathrm{d}t_1 \\ &+ \int_0^\infty \Sigma^{\mathrm{R}}(t,t_1)\hat{G}^<(t_1,t)\,\mathrm{d}t_1 - \int_0^\infty \hat{G}^<(t,t_1)\Sigma^{\mathrm{A}}(t_1,t)\,\mathrm{d}t_1 \\ &- \int_0^\infty \hat{G}^{\mathrm{R}}(t,t_1)\Sigma^<(t_1,t)\,\mathrm{d}t_1\,. \end{aligned} \tag{162}$$

It is assumed here that the potential U and the interaction with band electrons are turned on at the initial instant $t_0 = 0$, while the localized state occupation number is $n_0(\varepsilon_1)$. Because the potential affects only variations of G^{R} and G^{A}, it can be taken into account simply by changing the energy value of the localized state by U.

The irreducible parts Σ^{R} and Σ^{A} in (146) and (147) in the wide-band approximation, where $v(\omega) \simeq \mathrm{const}$, are local in time:

$$\Sigma^{\mathrm{R}}(t_1,t_2) = -\mathrm{i}\gamma\delta(t_1 - t_2)\,. \tag{163}$$

The irreducible part $\Sigma^<$ in the time representation is obtained as the Fourier transformation of (151):

$$\Sigma^<(t_1,t_2) = \int \frac{\mathrm{d}\omega}{\pi}\,\mathrm{i}\gamma n_0(\omega)\exp\left[-\mathrm{i}\omega(t_1 - t_2)\right]. \tag{164}$$

The kinetic equation has the form

$$\begin{aligned} \mathrm{i}\,\frac{\partial}{\partial t}\,G^<(t,t) &= -2\mathrm{i}\gamma G^<(t,t) - \int \frac{\mathrm{d}\omega}{\pi}\,\frac{1}{(\omega - \varepsilon_1 - U)^2 + \gamma^2} \\ &\times \Big\{\gamma + \Big((\omega - \varepsilon_1 - U)\sin\left[(\omega - \varepsilon_1 - U)t\right] \\ &- \gamma\cos\left[(\omega - \varepsilon_1 - U)t\right]\Big)\exp(-\gamma t)\Big\}\,2\mathrm{i}\gamma n_0(\omega)\,. \end{aligned} \tag{165}$$

Under the condition $-\mathrm{i}G^<(0,0) = n_a(0) = n_0(\varepsilon_1)$ $(n_1(t) = -\mathrm{i}G^<(t,t))$, its solution is given by

$$\begin{aligned} n_1(t) &= n_0(\varepsilon_1)\exp(-2\gamma t) + \int \frac{\mathrm{d}\omega}{\pi}\,n_0(\omega)\,\frac{\gamma}{(\omega - \varepsilon_1 - U)^2 + \gamma^2} \\ &\times \Big[1 + \exp(-2\gamma t) - 2\cos\left[(\omega - \varepsilon_1 - U)t\right]\exp(-\gamma t)\Big]\,. \end{aligned} \tag{166}$$

The solution describes relaxation processes in our system. For large times $t \gg 1/\gamma$, the occupation tends to a steady-state value determined by the equilibrium broadened level occupation shifted by U:

$$n_1 = \int \frac{\mathrm{d}\omega}{\pi}\,n_0(\omega)\,\frac{\gamma}{(\omega - \varepsilon_1 - U)^2 + \gamma^2}\,. \tag{167}$$

Of course, this is the same steady-state value (152) found before.

The exact solution shows that the relaxation of the localized state occupation is not exponential. At the initial stage, the relaxation can even be nonmonotonic. An example of this behavior is shown in Fig. 12.

If we switch to a more coarse-grained picture by assuming that the oscillating terms in the right-hand side of (165) at times $> 1/\varepsilon_1$ make a small contribution, then we arrive at the same result that would follow from simple balance equations based on transition probabilities from the localized state to the continuous spectrum. Then Eqn (165) can be represented as a simple equation for $n_1(t) = -\mathrm{i}G^<(t,t)$:

$$\left[\frac{\partial}{\partial t} + 2\gamma\right]n_1(t) = 2\gamma n_0(\varepsilon_1 + U)\,. \tag{168}$$

Its solution is given by

$$n_1(t) = n_0(\varepsilon_1 + U)\big[1 - \exp(-2\gamma t)\big] + n_0(\varepsilon_1)\exp(-2\gamma t)\,. \tag{169}$$

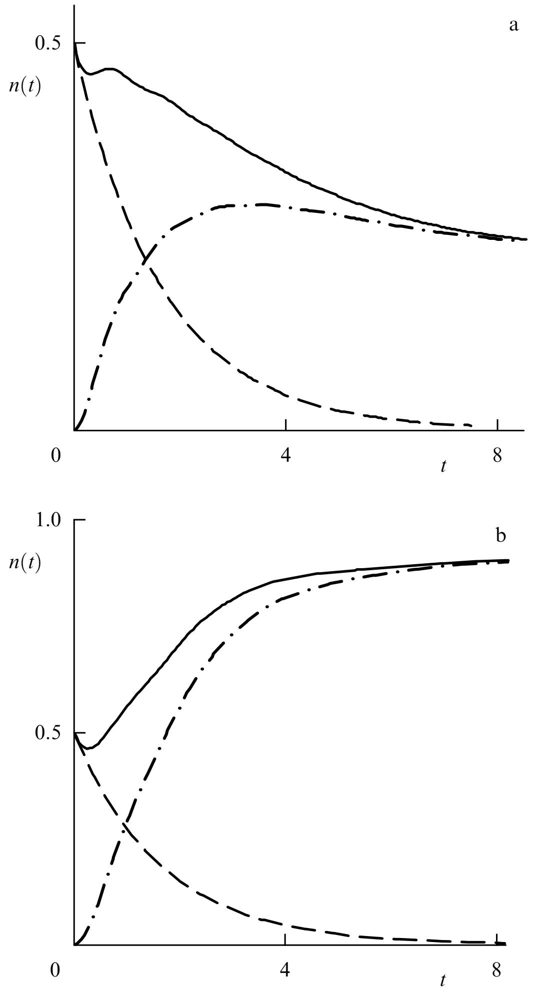

Figure 12. Density relaxation on the localized state for different model parameters. The initial occupation is $n = 1/2$. Dashed lines correspond to the contribution of the first term in (166), dashed-dotted lines correspond to the second term, and solid lines correspond to the general time dependence of the charge density (time is measured in $1/\gamma$ units). The initial interval of solid lines shows nonexponential behavior. (a) Energy of the localized state above the Fermi level; (b) energy of the localized state below the Fermi level.

This simplified formula shows that during the time period $t \simeq 1/\gamma$, the occupation numbers corresponding to the equilibrium distribution function for a thermostat are 'imposed' on the localized state.

Equation (169) clearly shows what happens if we start calculating the Green's function $G^{<}_{aa}$ step by step in the perturbation theory, treating transitions between localized and band states as perturbations (these are transitions that give rise to variations of the state occupation). This is the perturbation theory in the parameter $\gamma \propto T^2$ (see the second illustration in Fig. 11). But the first terms of solution (169) expanded in γ,

$$-\mathrm{i}G^{<}(t,t) = n_0(\varepsilon_1) + \big[n_0(\varepsilon_1 + U) - n_0(\varepsilon_1)\big]2\gamma t - \big[n_0(\varepsilon_1 + U) - n_0(\varepsilon_1)\big]2\gamma^2 t^2 + \ldots, \qquad (170)$$

have secular divergences in time, indicating that the perturbation theory should be applied with care. The same is obtained by a straightforward calculation of the first-order correction to $G^{(1)<}_{aa}(t,t)$:

$$G^{(1)<}_{aa}(t,t) = \int_0^{\infty}\int_0^{\infty}\Big[G^{<}_0(t,t_1)\Sigma^{\mathrm{A}}(t_1,t_2)G^{\mathrm{A}}_0(t_2,t)\,\mathrm{d}t_1\,\mathrm{d}t_2 \qquad (171)$$

$$+ G^{\mathrm{R}}_0(t,t_1)\Sigma^{<}(t_1,t_2)G^{\mathrm{A}}_0(t_2,t)\,\mathrm{d}t_1\,\mathrm{d}t_2$$

$$+ G^{\mathrm{R}}_0(t,t_1)\Sigma^{\mathrm{R}}(t_1,t_2)G^{<}_0(t_2,t)\,\mathrm{d}t_1\,\mathrm{d}t_2\Big]. \qquad (172)$$

Substituting irreducible parts (163) and (164), it is easy to see that the first correction diverges linearly in time.

A characteristic feature of the NDT is the occurrence of power-law time divergences in finite-order terms of the perturbation series for $G^{<}$ whenever there are nonstationary processes in the system. In fact, such a behavior of the perturbation series explicitly shows that the solution of the Dyson equation for $G^{<}$ is independent of $G^{<}_0$, although the integral equation still contains $G^{<}_0$. In some cases, the secular divergences make the calculation of $G^{<}$ useless and noninformative in the first orders. They indicate that the system flows from the original state into a completely different one. However, the NDT is, in this sense, a renormalizable theory giving rise to finite physically correct results. A proper method for describing the transition is to solve the kinetic equations derived from the Dyson equation.

7. Do we need the three-component technique as a generalization of the nonequilibrium diagram technique?

A simple example discussed in the preceding section demonstrated some of the technical features of the NDT. It also shows whether we need the so-called three-component technique. This technique is motivated by the following reasons. The study of kinetics of many-body systems is traditionally based on a response theory for a system in thermodynamic equilibrium. The response theory requires that time correlation functions of certain operators be calculated at a finite temperature. At the end of this section, we discuss the diagram technique for retarded correlators developed by Konstantinov and Perel' in 1960 [18]. Now, we consider the real-time Green's function at a finite temperature. It is defined as

$$\big\langle \hat{A}(t)\hat{B}(t')\big\rangle = \frac{1}{\mathrm{Sp}\big[\exp\left(-H/T\right)\big]} \times \mathrm{Sp}\left[\exp\left(-\frac{H}{T}\right)\exp\left(\mathrm{i}Ht\right)\hat{A}\exp\left(-\mathrm{i}Ht\right)\exp\left(\mathrm{i}Ht'\right)\hat{B}\exp\left(-\mathrm{i}Ht'\right)\right]. \qquad (173)$$

Expectation values of this type appeared in the famous work by Kubo [33] devoted to calculating the response of a system in equilibrium. Contrary to the original NDT equation (24), the density matrix here is always assumed to be Gibbsian,

$$\rho = \frac{\exp\left(-H/T\right)}{\mathrm{Sp}\big[\exp\left(-H/T\right)\big]}\,.$$

Then, extracting the perturbation $\hat{V}$ from the Hamiltonian, both the real-time evolution operators and the Boltzmann factor $\exp\left(-H/T\right)$ can be represented as T-ordered exponentials, exactly as in the temperature Matsubara technique.

Because there are now three T-ordered exponentials averaged in a certain order, the entire expression can be represented as a single T_{C_3}-ordering along the contour C_3

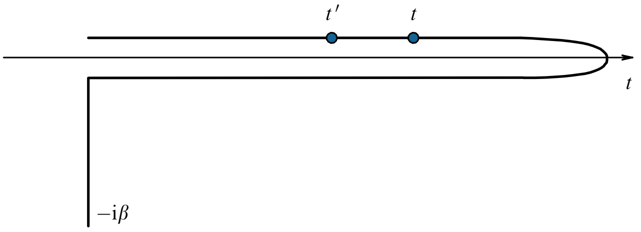

Figure 13. Contour with three branches.

shown in Fig. 13,

$$\langle \hat{A}(t)\hat{B}(t')\rangle = \frac{1}{Z}\,\mathrm{Sp}\left[T_{C_3}\left\{\exp\left[-\mathrm{i}\int_{C_3}\hat{V}(t_c)\,\mathrm{d}t_c\right]\hat{A}(t_c)\hat{B}(t'_c)\right\}\right]. \qquad (174)$$

If the originally averaged operators are placed in a certain order as in (173), then time arguments of the operators $\hat{A}$ and $\hat{B}$ must be assigned to different contour branches along the real axis, $t'_c = t'^-$ and $t_c = t^+$. In averaging the ordinary T-ordering, we set $t'_c = t'^-$, $t_c = t^-$, etc. Any correlation function of two (or more) operators can always be represented in form (174) using the T_{C_3}-ordering along the contour composed of three parts.

The contour has a part 'along the imaginary time axis'. Such a graphical interpretation emerges because within the Matsubara technique, operators in the interaction picture can be formally represented as

$$\begin{aligned}\hat{c}_p(\tau) &= \exp(H\tau)c_p\exp(-H\tau)\\ &= \exp\left[\mathrm{i}H(-\mathrm{i}\tau)\right]c_p\exp\left[-\mathrm{i}H(-\mathrm{i}\tau)\right]. \end{aligned}\qquad (175)$$

In the Matsubara technique, the parameter τ ranges from 0 to $\beta = 1/T$, and hence there is an 'imaginary time' segment from 0 to $-\mathrm{i}\beta$. In principle, such a figure should not be literally understood as a contour in the 'complex time plane'. It is just a visualization of the fact that there are three groups of operators arranged in a certain order in any term of the perturbation series, while each group of operators is ordered in accordance with its own rule.

If we consider only time correlators in thermodynamic equilibrium in a system with a time-independent Hamiltonian, the term 'contour in the complex time plane' can have a literal meaning. In this case, we introduce the evolution operator in complex time

$$U(z,z') = T_{Cz}\exp\left[-\mathrm{i}\int_z^{z'}\hat{V}(z_1)\,\mathrm{d}z_1\right], \qquad (176)$$

where z and z' represent a 'complex' time of the form $t + \mathrm{i}\tau$. The complex time parameters are also used to build the perturbation operator in the interaction picture [16, 34, 35]. However, there are a number of physical limitations. The convergence conditions for all expressions require that the imaginary part of the 'complex time' lie in the strip $[0, -\mathrm{i}\beta]$. On the other hand, the analyticity condition for the Green's functions requires that 'the imaginary part of time' on the contour decrease monotonically from 0 to $-\mathrm{i}\beta$ [36]. A possible diagram technique corresponding to the contour shown in Fig. 14 was developed by Umezawa, Matsumoto, and Tachiki [37] and called the Thermo Field Dynamics. Within this approach, the contour passes 'above' the real axis, then goes along a segment along the imaginary axis from zero to $-\mathrm{i}\beta/2$, then goes back parallel to the real axis until the initial instant, and finally passes along the imaginary axis from $-\mathrm{i}\beta/2$ to $-\mathrm{i}\beta$. In this theory, the averaging of operators belonging to vertical segments is factored. Hence, only the nontrivial averaging of operators on lines parallel to the real axis remains. It follows that the Thermal Field Dynamics is also a two-component technique, but for calculating time correlation functions in an equilibrium system.

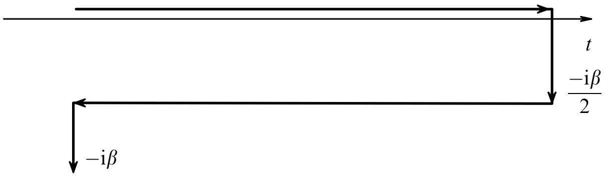

Figure 14. Thermo Field Dynamics contour.

We stress once again that all operations that look like an analytic continuation to the time plane are possible only for time correlators calculated by the thermodynamic equilibrium equations. If the Hamiltonian (or the perturbation to which the diagram technique is associated) is time-dependent, then discussing the 'analytic continuation' in time is not possible. We also note that the widely used Kubo–Martin–Schwinger-type relations [16, 29]

$$G^>(t - \mathrm{i}\beta) = -G^<(t)\,, \quad G^<(t + \mathrm{i}\beta) = -G^>(t) \qquad (177)$$

for the Green's functions of complex time are valid only in the case of thermodynamic equilibrium when the perturbation operator is time-independent. We recall that in the general case, the extension to the complex time plane is meaningless.

Moreover, a significant difference from the NDT is that in theories with time correlation functions, we always use the Gibbs density matrix $\rho = \exp(-H/T)/\mathrm{Sp}\,[\exp(-H/T)]$ in a state of thermodynamic equilibrium. In general, the NDT initial density matrix can be arbitrary, and the theory describes all transitions and relaxation processes occurring in the system after the perturbation is turned on. For large times, any nonpathological system eventually thermalizes and forgets its initial state. Therefore, it seems that it should make no difference whether we use the initial density matrix $\rho_0 = \exp(-H_0/T)/\mathrm{Sp}\,[\exp(-H_0/T)]$ for noninteracting particles, as is generally done in the NDT, or the total density matrix $\rho = \exp(-H/T)/\mathrm{Sp}\,[\exp(-H/T)]$, as in the three-component technique. Arguments that have led some authors to think that the three-component technique is necessary are that the spectrum obtained within the NDT is correct, while the occupation does not correspond to thermodynamic equilibrium.

We try to clarify the matter with simple examples.

The T_{C_3}-ordering allows generalizing Wick's theorem to this case as well. The Green's functions arise in which each of two operators can belong to one of three branches of the contour, i.e., the GFs become 3×3 matrices. In this case, it is better to use indices '1, 2' instead of '−, +', and the index '3' to denote operators on the 'imaginary' part of the contour.

We apply this technique to the simple example already thoroughly discussed in Section 6. We have seen that if the coupling of discrete states to the thermostat — band electrons — vanishes, then the result depends on how the limit transition is done. We examine the three-component technique in the case where there is a discrete state. Also, for a particle in this state, an additional potential U is turned on at a time t_0,

$$H_0 = \varepsilon_1 a_1^+ a_1\,, \qquad \hat{V} = U a_1^+ a_1\,. \tag{178}$$

In addition to the four NDT Green's functions, functions G_{13}, G_{23}, G_{31}, and G_{32} arise. Letting τ denote the variable along the vertical segment from 0 to $-\mathrm{i}\beta$, we find

$$\begin{aligned} G_{13}^0(t,\tau) &= -\mathrm{i}\big\langle T_{C_3} a_1(t) a_1^+(\tau)\big\rangle = \mathrm{i}\big\langle a_1^+(\tau) a_1(t)\big\rangle \\ &= \frac{\mathrm{Sp}\,\big[\exp\left(-H_0/T\right) a_1^+(\tau) a_1(t)\big]}{\mathrm{Sp}\,\big[\exp\left(-H_0/T\right)\big]}\,. \end{aligned} \tag{179}$$

Operators in the interaction picture for the 'imaginary' and real parts of the contour have different forms:

$$\begin{aligned} a(\tau) &= \exp\left(H_0\tau\right) a_1 \exp\left(-H_0\tau\right), \\ a(t) &= \exp\big[\mathrm{i}H_0(t-t_0)\big] a_1 \exp\big[-\mathrm{i}H_0(t-t_0)\big]\,. \end{aligned} \tag{180}$$

Therefore, even for a noninteracting system, the Green's functions G_{13} and G_{31} depend on two different variables:

$$\begin{aligned} G_{13}^0(t,\tau) &= \mathrm{i}n(\varepsilon_1) \exp\left(\tau\varepsilon_1\right) \exp\big[-\mathrm{i}\varepsilon_1(t-t_0)\big]\,, \\ G_{31}^0(\tau,t) &= \mathrm{i}\big(n(\varepsilon_1)-1\big) \exp\left(-\tau\varepsilon_1\right) \exp\big[\mathrm{i}\varepsilon_1(t-t_0)\big]\,. \end{aligned} \tag{181}$$

It follows that the Fourier-transformed GFs are to be considered as matrices $G(\omega,\omega')$. Then both the time and temperature parts of the matrix are diagonal, $G(\omega)\delta(\omega-\omega')$, $G_{33}(\omega_n)\delta_{\omega_n,\omega'_n}$, and G_{13} has the form

$$G_{13}^0(\omega,\omega_n) = \mathrm{i}\,\frac{1}{\mathrm{i}\omega_n-\varepsilon_1}\,2\pi\mathrm{i}\delta(\omega-\varepsilon_1)\exp\left(\mathrm{i}\omega t_0\right). \tag{182}$$

The interaction picture was chosen such that all operators at the initial instant coincide with those in the Schrödinger picture. We see that the functions G_{13}^0 essentially depend on the initial time due to their matrix nature. Therefore, the integrals in the Dyson equation must be bounded from below by the initial time t_0 first, and only then can we set $t_0 \to -\infty$ in the resulting expressions in the steady-state case.

This behavior of the off-diagonal components that relate the time and temperature sectors allows suggesting that the nondiagonal contribution is equal to zero due to fast oscillations at large times induced by the factor $\exp\left(\mathrm{i}\omega t_0\right)$ [34, 35]. It follows that the conventional NDT (or the conventional temperature technique, in the case of stationary properties) is sufficient to describe the system.

However, there have been counterexamples claiming that this is not necessarily so. The examples pertained to isolated states or isolated modes, and hence our example is relevant here.

Because the third, 'temperature', segment goes along the real axis following the two branches of the contour, the order of operators in the functions G_{23} and G_{13} is the same, and therefore $G_{23} = G_{13}$ and $G_{32} = G_{31}$.

The matrix structure of the Dyson equation remains the same. It is now just a 3 × 3 matrix equation, because there are vertices arising when expanding the Boltzmann factor $\exp\left(-H/T\right)$, which contain operators with the index '3' and relate the Green's functions $G^{\alpha 3} G^{3\beta}$.

Within the original formulation of the three-component technique, the GF matrix in the old NDT notation is given by

$$\hat{G} = \begin{pmatrix} G^{--} & G^{-+} & G_{13} \\ G^{+-} & G^{++} & G_{13} \\ G_{31} & G_{31} & G_{33} \end{pmatrix}. \tag{183}$$

It is convenient to perform the same transformations (65) that lead to the triangular representation in the NDT,

$$\hat{G} \Rightarrow \begin{pmatrix} 0 & 1 & 0 \\ 1 & 0 & 0 \\ 0 & 0 & 1 \end{pmatrix} \hat{L}\hat{G}\hat{L}^{-1}\,, \tag{184}$$

where

$$\hat{L} = \frac{1}{\sqrt{2}} \begin{pmatrix} 1 & -1 & 0 \\ 1 & 1 & 0 \\ 0 & 0 & \sqrt{2} \end{pmatrix}. \tag{185}$$

We then arrive at the triangular representation

$$\hat{G} = \begin{pmatrix} G^{\mathrm{R}} & G^{\mathrm{K}} & \sqrt{2}G_{13} \\ 0 & G^{\mathrm{A}} & 0 \\ 0 & \sqrt{2}G_{31} & G_{33} \end{pmatrix} \tag{186}$$

or, using transformations (88)–(91), at

$$\hat{G} = \begin{pmatrix} G^{\mathrm{R}} & G^{<} & G_{13} \\ 0 & G^{\mathrm{A}} & 0 \\ 0 & G_{31} & G_{33} \end{pmatrix}. \tag{187}$$

In this representation, the external potential corresponds to the irreducible part represented by the diagonal matrix

$$\hat{\Sigma} = U \begin{pmatrix} 1 & 0 & 0 \\ 0 & 1 & 0 \\ 0 & 0 & 1 \end{pmatrix}. \tag{188}$$

The equation for $G^<$ is the (1,2) component of the Dyson equation:

$$\begin{aligned} G^<(t,t') &= G_0^<(t,t') + \int_{t_0}^{\infty} G_0^<(t,t_1) U G^{\mathrm{A}}(t_1,t')\,\mathrm{d}t_1 \\ &+ \int_{t_0}^{\infty} G_0^{\mathrm{R}}(t,t_1) U G^<(t_1,t')\,\mathrm{d}t_1 + \int_0^{\beta} G_{13}^0(t,\tau) U G_{31}(\tau,t')\,\mathrm{d}\tau\,, \end{aligned} \tag{189}$$

while the (3,1) component of the Dyson equation allows representing the equation for G_{31} as

$$\begin{aligned} G_{31}(\tau,t') &= G_{31}^0(\tau,t') + \int_{t_0}^{\infty} G_{31}^0(\tau,t_1) U G^{\mathrm{A}}(t_1,t')\,\mathrm{d}t_1 \\ &+ \int_0^{\beta} G_{33}^0(\tau-\tau_1) U G_{31}(\tau_1,t')\,\mathrm{d}\tau_1\,. \end{aligned} \tag{190}$$

As in the conventional temperature technique, Eqn (190) can be solved using the Fourier transformation with respect to τ. In the fermionic case, we expand in the odd Matsubara frequencies $\omega_n = (2n+1)\pi T$. However, it is not so convenient to use the Fourier transformation with respect to time in Eqn (189). The variables of the functions G_{31} and G_{13} are mixed, and hence the limit $t_0 \to -\infty$ is to be taken carefully. Indeed, before the limit is taken, the Green's functions $G^<$ depend on two variables, and not only on their difference. Therefore, it is easier to use the mixed representation

$G_{13}(t, \omega_n)$, where the solution of (190) is given by

$$G_{31}(\omega_n, t') = \frac{\mathrm{i}}{\mathrm{i}\omega_n - \varepsilon_1} \, \frac{1}{1 - G^0_{33}(\omega_n)} \exp\left[\mathrm{i}(\varepsilon_1 + U)(t' - t_0)\right]. \qquad (191)$$

Without solving the equation for G^{A} (because the answer is obvious), we use the explicit form

$$G^{\mathrm{A}}(t, t') = \mathrm{i}\theta(t' - t) \exp\left[-\mathrm{i}(\varepsilon_1 + U)(t - t')\right]. \qquad (192)$$

In this formalism, the function G_{33} is the usual Matsubara function

$$G^0_{33}(\omega_n) = \frac{1}{\mathrm{i}\omega_n - \varepsilon_1}. \qquad (193)$$

After substituting the solution G_{31} in (189) and replacing

$$\int_0^{\beta} G^0_{13}(t, \tau) U G_{31}(\tau, t') \, \mathrm{d}\tau = T \sum_{\omega_n} G^0_{13}(t, \omega_n) U G_{31}(\omega_n, t'), \qquad (194)$$

we find that the last term $G^0_{13} U G_{31}$ takes the form

$$\begin{aligned} &T \sum_{\omega_n} G^0_{13}(t, \omega_n) U G_{31}(\omega_n, t') \\ &= T \sum_{\omega_n} \left[\frac{1}{\mathrm{i}\omega_n - \varepsilon_1 - U} - \frac{1}{\mathrm{i}\omega_n - \varepsilon_1} \right] \\ &\times \exp\left[-\mathrm{i}\varepsilon_1 (t - t')\right] \exp\left[\mathrm{i}U(t' - t_0)\right] \qquad (195) \\ &= \mathrm{i}\left[n(\varepsilon_1 + U) - n(\varepsilon_1)\right] \exp\left[-\mathrm{i}\varepsilon_1(t - t')\right] \exp\left[\mathrm{i}U(t' - t_0)\right]. \qquad (196) \end{aligned}$$

We see that the term $G_{13} G_{31}$ is a source in the equations for $G^<$, thereby providing a transition from the original occupation numbers $n(\varepsilon_1)$ to new equilibrium numbers $n(\varepsilon_1 + U)$. It is easily seen that the solution of Eqn (189) in the time representation with this additional term is given by

$$G^<(t, t') = \mathrm{i}n(\varepsilon_1 + U) \exp\left[-\mathrm{i}(\varepsilon_1 + U)(t - t')\right]. \qquad (197)$$

In this case, the functions $G^<_0(t, t') = \mathrm{i}n(\varepsilon_1) \exp\left[-\mathrm{i}\varepsilon_1(t - t')\right]$ completely disappear from the equation, and the memory of the initial occupation $n(\varepsilon_1)$ is lost.

The argument justifying the use of the three-component technique is that when applying the potential, the occupation changes consistently. On the other hand, a straightforward (and thoughtless) use of the NDT should give Eqn (158), containing the original occupation $n(\varepsilon_1)$. However, the same correct result with the new occupation number $n(\varepsilon_1 + U)$ in (158) is obtained within the NDT if we assume that our system is still coupled to the external thermostat very weakly. It turns out that the three-component technique is relevant only if we consider a completely isolated system (state), but at the same time wish the occupation to be described by the thermodynamic equilibrium Gibbs distribution! It is clear that this is an extremely illogical standpoint: the Gibbs distribution always implies a coupling to the thermostat. Moreover, if we explicitly or implicitly consider a weak coupling with the thermostat as above, then the occupation numbers are the same as in the three-component technique, and hence no further complication of the theory is required.

In the example with one isolated state, the rapidly oscillating factors in the off-diagonal Green's functions cancel. This is because we are dealing with a singular density of states described by a delta-function.

In more complex cases, the problem can be implicit. Because there are doubts as to whether the Keldysh technique works properly in all cases, we here briefly describe the correct way to solve a more complicated problem considered in [38]. That paper claims that the three-component technique is necessary for calculating the spin susceptibility in the Heisenberg model with the Hamiltonian

$$H = \sum_{i,j} J_{ij} \hat{S}_i \hat{S}_j - \sum_i h \hat{S}_i, \qquad (198)$$

where h is an external magnetic field. For our purposes, it is more convenient to rewrite the Hamiltonian in terms of the electron creation and annihilation operators. Then the original Hamiltonian is

$$H_0 = -h(c^+_{i\uparrow} c_{i\uparrow} - c^+_{i\downarrow} c_{i\downarrow}), \qquad (199)$$

and the perturbation is given by the exchange interaction:

$$V = J(S^+ S^- + \ldots) = J(c^+_{i\uparrow} c_{i\downarrow} c^+_{i+1\downarrow} c_{i+1\uparrow} + \ldots). \qquad (200)$$

The contradiction allegedly discovered in [38] is as follows. In the framework of the RPA approach, we can find the magnon spectrum determined by the poles of the correlator (susceptibility) $\chi_R(\Omega, q)$. The spectrum is given by the same expression in both the NDT and the three-component techniques. However, when calculating occupation numbers of the collective modes, i.e., calculating the functions $\chi^<$, the author concludes that the correct thermodynamic equilibrium occupation of the magnon modes can be obtained only within the three-component technique. We show that this is not true and outline the calculation of the transverse response correlator $\langle S^+ S^- \rangle$ allowing us, in particular, to obtain the correct occupation of the collective modes. The correlator in terms of the electron operators is given by

$$\begin{aligned} \chi(q, \omega) &= \int \mathrm{d}t \sum_{R_{i0}} \left\langle S^+_i(t) S^-_0(0) \right\rangle \exp\left(\mathrm{i}\Omega t - \mathrm{i}qR_{i0}\right) \\ &= \int \mathrm{d}t \sum_{R_{i0}} \exp\left(\mathrm{i}\Omega t - \mathrm{i}qR_{i0}\right) \left\langle c^+_{i\uparrow}(t) c_{i\downarrow}(t) c^+_{0\downarrow}(0) c_{0\uparrow}(0) \right\rangle. \qquad (201) \end{aligned}$$

The right-hand side of (201) shows that the correlator corresponds to the simple two-particle correlation Green's function G^{-+}_2; we therefore let it be denoted by $\chi^<$. The calculation of the two-particle function can be done within the RPA, which corresponds to the simple Bethe–Salpeter equation shown in Fig. 15.

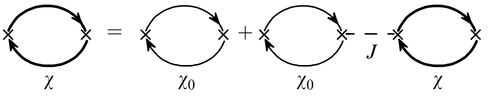

Figure 15. Spin susceptibility equation within the RPA approach.

Equations for the two-particle function in the RPA approximation are fully consistent with single-particle Dyson equations (75) and (93). To find the function $\chi^< = G^{-+}_2$, we first need to determine the corresponding retarded and advanced two-particle functions $\chi^{\mathrm{R}} = G^{\mathrm{R}}_2$ and $\chi^{\mathrm{A}} = G^{\mathrm{A}}_2$. Their equations are of the same graphical form (see

Fig. 15). As a result, $\chi^<$ has a form similar to (115):

$$\chi^<(q,\Omega) = \left[1 + J(q)\chi^{\mathrm{R}}(q,\Omega)\right]\chi_0^<(\Omega)\left[1 + J(q)\chi^{\mathrm{A}}(q,\Omega)\right], \tag{202}$$

where $\chi^{\mathrm{R,A}}(q,\Omega)$ is a solution of equations that are completely analogous to (75) and have a simple irreducible part $\Sigma^{\mathrm{R}} = J(q)$,

$$\chi^{\mathrm{R}}(q,\Omega) = \frac{\chi_0^{\mathrm{R}}(\Omega)}{1 - J(q)\chi_0^{\mathrm{R}}(\Omega)}, \tag{203}$$

while $\chi_0^<(\Omega)$ and $\chi_0^{\mathrm{R}}(\Omega)$ are the two-particle Green's functions (loops) of the zeroth order. Thus,

$$\chi_0^<(\Omega) = \int \frac{\mathrm{d}\omega}{2\pi}\, G_\downarrow^>(\omega - \Omega) G_\uparrow^<(\omega). \tag{204}$$

(A similar expression for $\chi_0^{\mathrm{R}}(\Omega)$ can also be easily obtained using the general NDT rules.) The one-electron Green's functions corresponding to Hamiltonian (199) are quite simple. Moreover, we take the weak coupling of electrons to the external thermostat into account to obtain

$$G^{\mathrm{R}}_{\uparrow,\downarrow}(\omega) = \frac{1}{\omega \pm h + \mathrm{i}\gamma}, \quad G^<_{\uparrow,\downarrow}(\omega) = n_{\mathrm{F}}(\omega)\big(G^{\mathrm{A}}(\omega) - G^{\mathrm{R}}(\omega)\big). \tag{205}$$

Equation (203) has a pole corresponding to collective modes, magnons with the dispersion $\Omega_q = 2h + J(q)\tanh(h/2T)$. The function $\chi^<(q,\Omega)$ must determine their occupation numbers. From (202), it follows that

$$\chi^<(q,\Omega) = \frac{\Omega - 2h + \mathrm{i}\gamma}{\Omega - \omega_q + \mathrm{i}\gamma}\,\frac{2\gamma n_{\mathrm{F}}^2(\Omega/2)}{(\Omega - 2h)^2 + \gamma^2}\,\frac{\Omega - 2h - \mathrm{i}\gamma}{\Omega - \omega_q - \mathrm{i}\gamma}. \tag{206}$$

Using the ratio $n_{\mathrm{F}}^2(\Omega/2) = n_{\mathrm{B}}(\Omega)\tanh(\Omega/4T)$, we obtain

$$\begin{aligned}\chi^<(q,\Omega) &= \tanh\left(\frac{\Omega}{4T}\right)\frac{2\gamma}{(\Omega - \omega_q)^2 + \gamma^2}\, n_{\mathrm{B}}(\Omega) \\ &\underset{\gamma\to 0}{\to} \tanh\left(\frac{\omega_q}{4T}\right) 2\pi n_{\mathrm{B}}(\omega_q)\delta(\Omega - \omega_q).\end{aligned} \tag{207}$$

The resulting expression is fully consistent with the (1,2) spin susceptibility component given by Eqn (3.33) in [38] and contains the correct thermodynamic equilibrium magnon occupation numbers given by the Bose distribution $n_{\mathrm{B}}(\omega_q)$.

The formal difficulties encountered in [38] are, again, that within the RPA approach, magnons are isolated excitations not interacting either with each other or with other excitations, just like the electron level in the simple example in Section 6. We have to repeat that requiring the Gibbs distribution for an isolated branch of excitations not coupled to anything at all is simply wrong. We merely introduce a small coupling to the thermostat — in our analysis, the constant γ, which provides thermodynamic equilibrium — and in the end set it equal to zero, and hence there are no miracles and no need to modify the NDT.

Thus, it turns out that correct application of both the three-component technique and the NDT always yields the same result, despite the difference in the initial density matrices. As already noted by Keldysh [1], in any physically relevant system without external perturbations, the NDT initial density matrix evolves such that the correct thermodynamic equilibrium is finally restored. Therefore, there is no specific need in the three-component technique.

In this section, we considered various techniques in which time and temperature are mixed variables. We also mention the important work by Konstantinov and Perel' [18], which preceded Keldysh's work. They formulated a diagram technique for calculating the linear response of a system with interparticle interaction, taking the calculation of conduction as an example. In the linear response theory, the relevant quantities (in the spirit of the Kubo formula [33]) contain an integral like

$$\begin{aligned}&\int_0^\beta \mathrm{d}\lambda\, \frac{1}{\mathrm{Sp}\left[\exp(-H/T)\right]} \\ &\times \mathrm{Sp}\left\{\exp(-H/T)\exp\left[-\mathrm{i}H(t + \mathrm{i}\lambda)\right] a_p^+ a_{p'} \exp\left[\mathrm{i}H(t + \mathrm{i}\lambda)\right] a_{p_1}^+ a_{p_2}\right\},\end{aligned} \tag{208}$$

where t is the response time, a_p are the electron operators, and the Hamiltonian H describes all interactions in the system. Considering both the time evolution and the Boltzmann factor $\exp(-H/T)$ in the interaction picture, Konstantinov and Perel' put forward the idea of Green's functions defined as the operator ordering along the particular contour C_{KP} shown in Fig. 16.

Because the contour has four different segments, multicomponent Green's functions emerge, but we can already see in Fig. 16 that a quite tricky technique arises with much more complicated rules than those of the Keldysh NDT. Using these rules for summing any series, writing the Dyson equation, etc, is not so simple as in the conventional technique. Unfortunately, starting from retarded correlators, it is not easy to develop a simple technique for calculating them. Indeed, a closed technique operating only with retarded correlators does not exist, but following this route to construct the NDT, which also allows calculating the retarded correlators, is not easy.

Historically, nonstationary and nonequilibrium problems in many-body quantum theory were considered primarily in terms of the response theory. Constructing the theory was divided into two phases. The first was to derive Kubo-type formulas that give response functions via retarded correlators. The second was to develop methods to calculate retarded correlators. Great progress in this direction was achieved in [2, 15], where analytic continuation methods were developed, which made it possible to calculate retarded correlation functions in the temperature (Matsubara) technique.

This standpoint was supported by tradition and habit. However, it turned out that corrections to a current or density

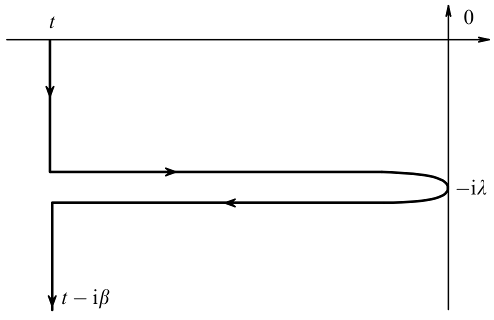

Figure 16. Konstantinov and Perel' contour [18].

are much easier to compute directly (in the case of conduction or susceptibility) because they are expressed in terms of the Green's function $G^<$, for which there is a regular and simple diagram technique. It turns out that the desire to follow the traditional route starting from retarded correlators and using the Gibbs distribution made the authors of [18] do a more difficult job than was necessary.

In the next section, we show that any response theory can be easily formulated within the NDT.

8. Response theory within the nonequilibrium diagram technique

Many papers are devoted to applying the NDT to the response theory (see review [39]). We therefore give only a brief summary, along with an example that has not been discussed in other papers. For definiteness, we consider the response of a system of electrons to an electric field determined by a scalar potential $\phi(r,t)$. In the linear response theory, a (charge) density is determined by the response function χ:

$$\delta n(r,t) = \int \mathrm{d}t_1\,\mathrm{d}r_1\,\chi(r-r_1,t-t_1)\phi(r_1,t_1)\,. \tag{209}$$

The usual response theory deals with finding the response function χ. Alternatively, the variation $\delta n(r,t)$ can be calculated directly, because it is simply a variation of the Green's function $G^<(rt,rt)$ caused by the perturbation

$$H_{\text{int}} = \int \mathrm{d}r\,\hat{n}(r,t)\phi(r,t)\,. \tag{210}$$

A variation of the function $G^<$ is defined in the first order by the diagrams shown in Fig. 17:

$$G^{(1)<}(rt,rt) = \int \mathrm{d}t_1\,\mathrm{d}r_1\,\big[G^{\mathrm{R}}(rt,r_1t_1)G^<(r_1t_1,rt) + G^<(rt,r_1t_1)G^{\mathrm{A}}(r_1t_1,rt)\big]\phi(r_1,t_1)\,. \tag{211}$$

Because

$$\delta n(r,t) = -\mathrm{i}G^{(1)<}(rt,rt)\,, \tag{212}$$

it immediately follows that in terms of the NDT Green's functions, the response function is given by

$$\chi(r-r_1,t-t_1) = -\mathrm{i}\int \mathrm{d}t_1\,\mathrm{d}r_1\,\big[G^{\mathrm{R}}(rt,r_1t_1)G^<(r_1t_1,rt) + G^<(rt,r_1t_1)G^{\mathrm{A}}(r_1t_1,rt)\big]\,. \tag{213}$$

Using this equation and Fig. 18, we can easily establish a correspondence between the expression obtained and the conventional formulation of the linear response theory based on calculating the correlator

$$\chi(r-r_1,t-t_1) \propto \big\langle\big[n(rt),n(r_1t_1)\big]\big\rangle\theta(t-t_1)\,. \tag{214}$$

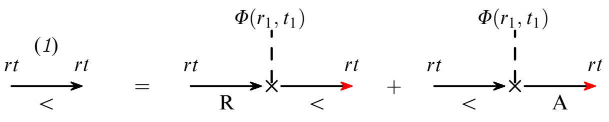

Figure 17. Diagram equation for a linear correction to the normal Green's function G_1^{-+}.

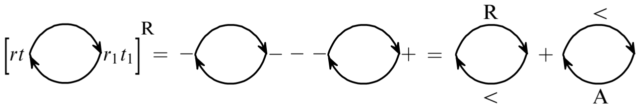

Figure 18. Diagrams for the retarded polarization operator.

In the NDT terms, the retarded density–density correlation function is the two-particle Green's function (the polarization operator) defined by the same formulas (67) as the one-particle Green's function,

$$\Pi^{\mathrm{R}} = \Pi^{--} - \Pi^{-+}\,. \tag{215}$$

The diagrams for the retarded polarization operator are shown in Fig. 18.

The readers who are familiar with the Matsubara diagram technique can see that two terms in (213) are exactly the two terms in the Eliashberg analytic continuation of the polarization operator (see Fig. 18) from discrete imaginary frequencies to the real axis.

8.1 Gauge-invariant response function of a superconductor

If a system describes interactions between particles, finding the linear response is a more complicated problem because an external field then acts on each particle both explicitly and implicitly. For example, a change in the density of particles in the external field in a region of space in the presence of a Coulomb interaction produces an additional potential acting on particles in another region. In what follows, we illustrate some advantages of the NDT when calculating the response function in the case of the electromagnetic response of superconductors. Soon after the BCS theory was proposed, the transverse field response was calculated (in fact, the problem of a constant magnetic field and radiation absorption by quasiparticle excitations in a superconductor was given a proper solution). However, the longstanding problem was to properly describe the response to a longitudinal electric field, because gauge invariance is realized in superconductors in a nontrivial way. Thanks to the work of many authors [40–42], the physical mechanism for the gauge invariance restoration is now clear. Also, it was realized that imposing the continuity equation allows finding correct equations for the response of a superconductor to a longitudinal field.

However, it is not widely recognized that within the NDT, we *automatically* obtain completely gauge-invariant equations that describe the response of a superconductor to the electromagnetic field. This is explicitly considered in [43]. Here, we describe only the basic idea of the calculation within the general linear response theory in the NDT.

To describe the response of a superconductor, we use the BCS Hamiltonian

$$\widehat{H} = \int \widehat{\Psi}_\alpha^+(x)\left(\frac{\hat{\mathbf{p}}^2}{2m}-\mu\right)\widehat{\Psi}_\alpha(x)\,\mathrm{d}^3\mathbf{r} - \int\big[\Delta(x)\widehat{\Psi}_\downarrow^+(x)\widehat{\Psi}_\uparrow^+(x) + \text{h.c.}\big]\,\mathrm{d}^3\mathbf{r}\,. \tag{216}$$

Then, in an external field defined by potentials $\mathbf{A}(x)$ and $\varphi(x)$, the total Hamiltonian is

$$\widehat{H} = \int \widehat{\Psi}^{+}_{\alpha}(x)\left(\frac{\left(\widehat{\mathbf{p}} - (e/c)\mathbf{A}(x)\right)^2}{2m} - \mu\right)\widehat{\Psi}_{\alpha}(x)\,\mathrm{d}^3\mathbf{r}$$
$$+ \int e\varphi(x)\delta\hat{n}(x)\,\mathrm{d}^3\mathbf{r} - \int\left[\Delta(x)\widehat{\Psi}^{+}_{\downarrow}(x)\widehat{\Psi}^{+}_{\uparrow}(x) + \text{h.c.}\right]\mathrm{d}^3\mathbf{r}$$
$$+ \frac{1}{2}\int \delta\hat{n}(x)V(\mathbf{r} - \mathbf{r}')\delta\hat{n}(x')\,\mathrm{d}^3\mathbf{r}\,\mathrm{d}^3\mathbf{r}'\,. \tag{217}$$

In this section, indices α and β refer to the spin of the electron, and $x = (\mathbf{r}, t)$. For generality, we added the Coulomb interaction between electrons, which is required to obtain the actual spectrum of collective modes in superconductors. Hamiltonian (217) also describes the positive homogeneous charged background that provides the electrical neutrality of the system, thereby leading to the operator of density fluctuations

$$\delta\hat{n}(x) \equiv \widehat{\Psi}^{+}_{\alpha}(x)\widehat{\Psi}_{\alpha}(x) - n \tag{218}$$

(where n is the electron density in the absence of the field), which arise in the terms containing the scalar potential and the Coulomb interaction between electrons $V(\mathbf{r} - \mathbf{r}') = e^2/|\mathbf{r} - \mathbf{r}'|$.

We note that Hamiltonian (217) is not invariant under the gauge transformations

$$\mathbf{A}(x) \to \mathbf{A}'(x) = \mathbf{A}(x) + \nabla\chi(x)\,,$$
$$\varphi(x) \to \varphi'(x) = \varphi(x) - \frac{1}{c}\frac{\partial\chi(x)}{\partial t}\,, \tag{219}$$
$$\widehat{\Psi}_{\alpha}(x) \to \widehat{\Psi}'_{\alpha}(x) = \widehat{\Psi}_{\alpha}(x)\exp\left[\mathrm{i}\,\frac{e}{c}\,\chi(x)\right],$$

if the order parameter Δ is considered as a fixed external parameter. In fact, we must remember that Δ is self-consistently defined by

$$\Delta(x) = g\left\langle\widehat{\Psi}_{\uparrow}(x)\widehat{\Psi}_{\downarrow}(x)\right\rangle, \tag{220}$$

where g is the superconducting coupling constant. It is then possible to build a fully gauge-invariant linear response theory of superconductors such that the final equations for the current and electron density contain only gauge-invariant combinations of the electromagnetic four-potentials.

The external field changes the electron states in a superconductor. Hence, order parameter (220) is obviously a function of the external field. External fields in the linear response theory are supposed to be weak and therefore the resulting variations of the order parameter are also small:

$$\Delta = \Delta^{(0)} + \Delta^{(1)}\,, \tag{221}$$

where $\Delta^{(1)}$ is the order parameter correction due to the field. Thus, the correct perturbation Hamiltonian for a superconductor in an external field described by BCS Hamiltonian (216) is given by

$$\widehat{H}_{\text{int}} = -\frac{1}{c}\int \hat{\mathbf{j}}^{0}(x)\mathbf{A}(x)\,\mathrm{d}^3\mathbf{r}$$
$$+ e\int \delta\hat{n}(x)\left[\varphi(x) + \frac{1}{e}\int V(\mathbf{r} - \mathbf{r}')\left\langle\delta\hat{n}(x')\right\rangle^{(1)}\mathrm{d}^3\mathbf{r}'\right]\mathrm{d}^3\mathbf{r}$$
$$- \int \Delta^{(1)}(x)\widehat{\Psi}^{+}_{\downarrow}(x)\widehat{\Psi}^{+}_{\uparrow}(x)\,\mathrm{d}^3\mathbf{r} - \int \Delta^{+(1)}(x)\widehat{\Psi}_{\uparrow}(x)\widehat{\Psi}_{\downarrow}(x)\,\mathrm{d}^3\mathbf{r}\,, \tag{222}$$

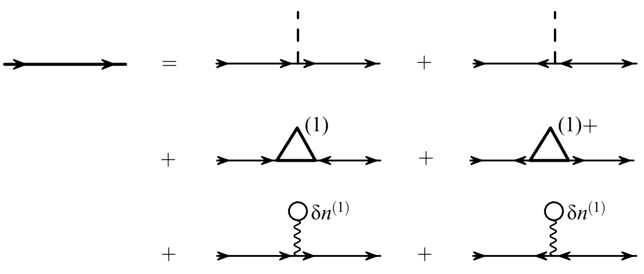

Figure 19. Complete diagram equation for a linear correction to the normal Green's function G_1^{-+} of a superconductor in the presence of an external electromagnetic field. Dashed lines correspond to the 'bare' interaction between electrons and the potentials $\mathbf{A}$ and φ. The triangle denotes the order parameter correction $\Delta^{(1)}$. Wavy lines denote the Coulomb interaction between electrons V. Open circles in the third row correspond to the electron density δn changed by the field.

where

$$\hat{\mathbf{j}}^{0}(x) = \frac{\mathrm{i}e}{2m}\left[\left(\nabla\widehat{\Psi}^{+}_{\alpha}(x)\right)\widehat{\Psi}_{\alpha}(x) - \widehat{\Psi}^{+}_{\alpha}(x)\nabla\widehat{\Psi}_{\alpha}(x)\right] \tag{223}$$

is the 'paramagnetic' part of the current density operator, and the Coulomb interaction is taken into account in the RPA.

If the density and order parameter corrections are considered in Hamiltonian (222) as given but yet unknown quantities linear in the external field, it is easy to calculate the correction linear in perturbation (222) to the Green's function $G^{<}$. This correction consists of three pairs of terms shown in Fig. 19.

The diagram technique for a superconductor uses both the normal Green's functions G and the anomalous functions F, including the function $F^{-+}_{\alpha\beta}$ defined without the T-ordering symbol:

$$G^{-+}_{\alpha\beta}(x, x') = \mathrm{i}\left\langle\widehat{\Psi}^{+}_{\beta}(x')\widehat{\Psi}_{\alpha}(x)\right\rangle,$$
$$F^{-+}_{\alpha\beta}(x, x') = \mathrm{i}\left\langle\widehat{\Psi}_{\beta}(x')\widehat{\Psi}_{\alpha}(x)\right\rangle. \tag{224}$$

Taking these functions into account, density fluctuations (218), the current, and order parameter (220) can be represented as

$$\delta n(x) = -2\mathrm{i}G_1^{-+}(x, x)\,, \tag{225}$$

$$\mathbf{j}(x) = -2\,\frac{\mathrm{i}e}{2m}(\nabla' - \nabla)G_1^{-+}(x, x')\Big|_{x'=x} - \frac{e^2 n}{mc}\,\mathbf{A}(x)\,, \tag{226}$$

$$\Delta^{(1)}(x) = \mathrm{i}gF_1^{-+}(x, x)\,. \tag{227}$$

Because we consider the linear response theory, the subscript 1 denotes the correction to the corresponding Green's function of the first order in perturbation operator (222). The prefactor 2 in (225) and (226) is due to the summation over spin (here, $G_{\alpha\beta} = \delta_{\alpha\beta}G$ and $F_{\alpha\beta} = \mathrm{i}\sigma^{y}_{\alpha\beta}F$, because the interaction of the electron spin with the magnetic field is neglected).

Figure 19 clearly shows that compared to the case of noninteracting particles, the diagrams for the linear response of a superconductor, in addition to the external field itself, involve corrections to the order parameter and electron density, which play the role of 'additional external fields' (for the Coulomb interaction in the mean-field approximation).

To find the variation of the function G^{-+} determining the total linear response, we need equations for $\Delta^{(1)}$ and $\delta n(x)$ as

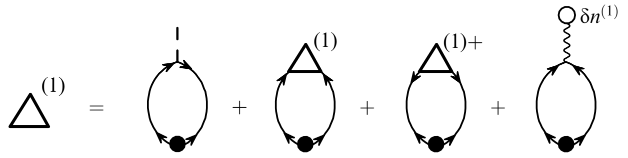

Figure 20. Graphic representation of the self-consistency equation for the order parameter correction $\Delta^{(1)}$ linear in the external field. Filled circles denote the BCS coupling constant g.

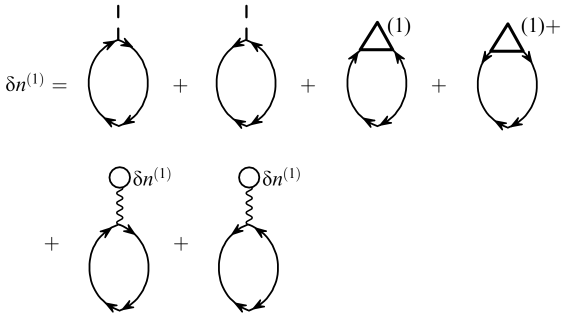

Figure 21. Graphic representation of the self-consistency equation for the electron density variation δn in the linear approximation in the external field.

functions of the external field. The usual procedure originally proposed within the temperature technique in [44] is that, having calculated the Green's functions for the current and density variation (225) and (226) using the diagrams shown in Fig. 19, we have to impose the continuity equation $e\,\partial\delta n/\partial t + \operatorname{div}\mathbf{j} = 0$. This equation gives $\Delta^{(1)}$ as a function of the external fields $\mathbf{A}$ and φ (without the Coulomb interaction). This restores the gauge invariance of the response function.

However, there is a method that 'respects' gauge invariance at each step of the calculation. The method employs the self-consistency equation for the order parameter and electron density fluctuations. The quantity $\Delta^{(1)}$ in the right-hand side of the diagram equation in Fig. 19 is determined by the anomalous Green's function F^{-+} at equal times (227). We also have an equation for F^{-+}, quite similar to the equation for G^{-+}, describing a variation of the anomalous function in the first order in H_{int} (see Fig. 19). Therefore, there is an equation for $\Delta^{(1)}$ shown in Fig. 20, where joining the ends of the anomalous Green's function reminds us of the coincident arguments x and x'.

Similarly, we arrive at the equation for the electron density variation $\delta n(x) = -2\mathrm{i}G_1^{-+}(x,x)$ shown in Fig. 21. In the case of a normal metal, this equation accounts for the usual screening within the RPA.

To properly take the gauge invariance into account, we should accurately extract the effects associated with the order parameter phase; corrections to the *phase gradient* and the *modulus* of the order parameter are small, while the phase variations (hence, variations of the order parameter) can be of the order of unity.

We explicitly split the order parameter variation into the modulus and phase variations in the external field:

$$\Delta(x) = (\Delta_0 + \Delta_1)\exp\left[\mathrm{i}\theta(\mathbf{A},\varphi)\right].$$

By a gauge transformation, the order parameter can be made real. (We note that the phase θ is still an unknown function of $\mathbf{A}$ of φ.) Then, in accordance with (219), the potentials are modified as

$$\begin{aligned}\mathbf{A}'(x) &= \mathbf{A}(x) - \frac{c}{2e}\left(\nabla\theta(x)\right)^{(1)},\\ \varphi'(x) &= \varphi(x) + \frac{1}{2e}\left(\frac{\partial\theta(x)}{\partial t}\right)^{(1)}.\end{aligned} \tag{228}$$

Substituting $\mathbf{A}'$ and φ' as the external fields in the diagrams in Fig. 19, we obtain the following equation for the current and charge density combined into a four-vector current $j = (\delta n, \mathbf{j})$:

$$j_\mu(q) = -\frac{e}{c}\left(Q^{\mathrm{A}}_{\mu\nu}(q) + \frac{n}{m}\,\delta_{\mu\nu}(1-\delta_{\mu 0})\right)A'_\nu(q)\,. \tag{229}$$

Here, we introduced the four-vector notation for potentials (228), $A'(q) = (c\varphi'(q), \mathbf{A}'(q))$, and performed the Fourier transformation in space and time variables $q = (\omega, \mathbf{q})$. The polarization operator Q^{A} is a loop of two Green's functions, and its explicit form is given below. For simplicity, the expression is given in the case of a superconductor without Coulomb interaction and neglecting variations of the order parameter modulus. The equation does not yet describe the response of the current to an external electromagnetic field, because the transformed potential A' contains not only the external field but also a still unknown function — the order parameter phase gradient $\nabla\theta(x)$. This unknown function can be determined from the self-consistency equation (see Fig. 20), which, after a gauge transformation, is given by

$$\Delta^{(1)}(q) = -\frac{e}{c}\,\Pi^{\mathrm{A}}_\nu(q)A'_\nu(q) - \left(\Pi^{\Delta}(q) + \Pi^{\Delta^+}(q)\right)\Delta^{(1)}(q)\,. \tag{230}$$

At the moment, we are not interested in the particular form of the different polarization operators Π (loops of two Green's functions), which can be easily found from the diagram in Fig. 17.

The phase θ is identified such that the order parameter $\Delta^{(1)}$ is real. However, Eqn (230) is complex, and it therefore allows finding both the real correction Δ_1, which is the real part of Eqn (230), and the relation of θ to the external field, which is the imaginary part of Eqn (230). Using the imaginary part of the self-consistency equation, the phase θ can be expressed in terms of the external potentials φ and $\mathbf{A}$. Then the right-hand side of (229) contains the given external potentials. In this way, we obtain the linear response equations relating the external field to the current in a superconductor.

Details of the calculations can be found in [43]. Here, we just emphasize that within the NDT, it is only required to calculate several polarization operators (two-particle functions) quite similar to the simplest polarization operator (213) (see Fig. 18). The difference is that these polarization operators consist of both normal and anomalous Green's functions, as follows from Figs 20 and 21. The summation over Keldysh indices is the same as in the simple polarization operator (213), and hence all the polarization loops used are also retarded.

We describe polarization loops that enter the resulting response functions (they can be obtained using the diagrams shown in the first row of Fig. 21):

$$\begin{aligned} Q^{\mathrm{A}}_{kl}(q) &= -2\mathrm{i}\,\frac{1}{m^2}\int\left(p_k+\frac{q_k}{2}\right)\left(p_l+\frac{q_l}{2}\right) \\ &\times\Big[G_0^{\mathrm{R}}(p+q)G_0^{-+}(p)+G_0^{-+}(p+q)G_0^{\mathrm{A}}(p) \\ &- F_0^{\mathrm{R}}(p+q)(F^+)_0^{-+}(p)-F_0^{-+}(p+q)(F^+)_0^{\mathrm{A}}(p)\Big]\,\frac{\mathrm{d}^4p}{(2\pi)^4}\,, \end{aligned} \tag{231}$$

$$\begin{aligned} Q^{\mathrm{A}}_{k0}(q) = Q^{\mathrm{A}}_{0k}(q) &= -2\mathrm{i}\,\frac{1}{m}\int\left(p_k+\frac{q_k}{2}\right) \\ &\times\Big[G_0^{\mathrm{R}}(p+q)G_0^{-+}(p)+G_0^{-+}(p+q)G_0^{\mathrm{A}}(p) \\ &+ F_0^{\mathrm{R}}(p+q)(F^+)_0^{-+}(p)+F_0^{-+}(p+q)(F^+)_0^{\mathrm{A}}(p)\Big]\,\frac{\mathrm{d}^4p}{(2\pi)^4}\,, \end{aligned} \tag{232}$$

$$\begin{aligned} Q^{\mathrm{A}}_{00}(q) &= -2\mathrm{i}\int\Big[G_0^{\mathrm{R}}(p+q)G_0^{-+}(p)+G_0^{-+}(p+q)G_0^{\mathrm{A}}(p) \\ &- F_0^{\mathrm{R}}(p+q)(F^+)_0^{-+}(p)-F_0^{-+}(p+q)(F^+)_0^{\mathrm{A}}(p)\Big]\,\frac{\mathrm{d}^4p}{(2\pi)^4}\,. \end{aligned} \tag{233}$$

The resulting equations for the response of a superconductor in terms of the polarization operators in the Fourier representation are given by

$$\begin{aligned} \delta n &= \mathrm{i}eq_k\left(\left(Q^{\mathrm{A}}_{kl}+\frac{n}{m}\,\delta_{kl}\right)Q^{\mathrm{A}}_{00}-Q^{\mathrm{A}}_{k0}Q^{\mathrm{A}}_{0l}\right)E_l \\ &\times\Bigg[q_{k'}\left(Q^{\mathrm{A}}_{k'l'}+\frac{n}{m}\,\delta_{k'l'}\right)q_{l'}-2\omega Q^{\mathrm{A}}_{0l'}q_{l'}+\omega^2Q^{\mathrm{A}}_{00} \\ &- Vq_{k'}q_{l'}\left(\left(Q^{\mathrm{A}}_{k'l'}+\frac{n}{m}\,\delta_{k'l'}\right)Q^{\mathrm{A}}_{00}-Q^{\mathrm{A}}_{k'0}Q^{\mathrm{A}}_{0l'}\right)\Bigg]^{-1}, \end{aligned} \tag{234}$$

$$\begin{aligned} j_k &= -\frac{e^2}{c}\left(Q^{\mathrm{A}}_{kl}+\frac{n}{m}\,\delta_{kl}\right)\left(A_l-\frac{q_lq_{l'}}{q^2}\,A_{l'}\right) \\ &+ \mathrm{i}e^2\left(\left(Q^{\mathrm{A}}_{kl}+\frac{n}{m}\,\delta_{kl}\right)Q^{\mathrm{A}}_{00}-Q^{\mathrm{A}}_{k0}Q^{\mathrm{A}}_{0l}\right)\omega \\ &\times\Bigg[q_{k'}\left(Q^{\mathrm{A}}_{k'l'}+\frac{n}{m}\,\delta_{k'l'}\right)q_{l'}-2\omega Q^{\mathrm{A}}_{0l'}q_{l'}+\omega^2Q^{\mathrm{A}}_{00} \\ &- Vq_{k'}q_{l'}\left(\left(Q^{\mathrm{A}}_{k'l'}+\frac{n}{m}\,\delta_{k'l'}\right)Q^{\mathrm{A}}_{00}-Q^{\mathrm{A}}_{k'0}Q^{\mathrm{A}}_{0l'}\right)\Bigg]^{-1}\frac{q_lq_{l''}}{q^2}\,E_{l''}\,. \end{aligned} \tag{235}$$

Here, $V = 4\pi e^2/q^2$ is the Fourier transform of the Coulomb potential. Most importantly, the potentials $\mathbf{A}$ and φ appear in a manifestly gauge-invariant manner, entering the electric field $\mathbf{E} = -(1/c)\,(\partial\mathbf{A}/\partial t) - \nabla\varphi$ and the transverse part of the vector potential $(A_l - (q_lq_{l'}/q^2)A_{l'})$.

Ensuring that transformation (228) actually compensates the order parameter phase at all steps of the calculation, we arrive at a well-defined relation between the phase and the external field, resulting from the gauge invariance of the system in arbitrary fields. Therefore, the approach based on self-consistency equation (230) is equivalent to imposing the continuity equation for the current used by Ambegaokar and Kadanoff [44]. We note that although the correct results within the temperature technique have been finally obtained, a consistent derivation of the linear response of a superconductor in the presence of an essentially time-dependent quantity — the order parameter phase — is much simpler and more logical within the NDT framework.

9. Tunneling systems

Tunneling systems are a problem of a different kind than finding the density matrix variations of systems (often homogeneous) in external fields within the response theory. In such systems, we deal with at least three subsystems: two junction banks and the area between them (Fig. 22). The junction banks are two different thermal reservoirs with different chemical potentials and possibly different temperatures.

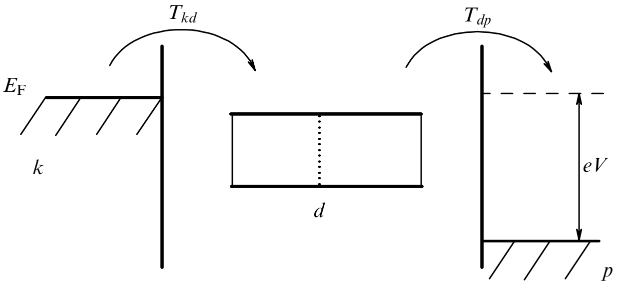

Figure 22. Overall schematic of the tunneling system.

The perturbation here is not the applied potential but transitions between the subsystems due to the tunneling matrix elements. It follows that the initial density matrix of the entire system is the product of the initial (equilibrium) density matrices for the left and right banks and the intermediate subsystem

$$\rho_0 = \rho^0_{\mathrm{L}} \times \rho^0_d \times \rho^0_{\mathrm{R}}\,. \tag{236}$$

Once transitions between the subsystems start to occur, the total density matrix changes such that it cannot be factored into a product of three independent density matrices. The problem of the density matrix variations in a complex system can be consistently considered only within the NDT framework. One of the first consistent descriptions of tunneling problems in the NDT was given in [3–5].

9.1 General equations for the tunneling current

Some general equations for the tunneling current can be obtained even without specifying the properties of the intermediate system. The junction banks are assumed to be described by the Hamiltonian for free particles with the chemical potentials shifted by eV:

$$\hat{H}_0 = \sum_k(\varepsilon_k-\mu)c_k^+c_k+\sum_p(\varepsilon_p-\mu-eV)c_p^+c_p+\hat{H}_d\,, \tag{237}$$

where c_k is the left-bank electron operator, c_p is the right-bank operator, and the term $\hat{H}_d$ describes an isolated intermediate system (with all possible interactions). The perturbation here is given by the tunneling Hamiltonian describing transitions between the left and right banks and the intermediate system,

$$H_{\mathrm{tun}} = T_{\mathrm{L}}\sum_{k,i}(c_k^+d_i+d_i^+c_k)+T_{\mathrm{R}}\sum_{p,i}(c_p^+d_i+d_i^+c_p)\,, \tag{238}$$

where d_i is the annihilation operator of a particle in the ith state of the intermediate system, and T_{L} and T_{R} are tunneling

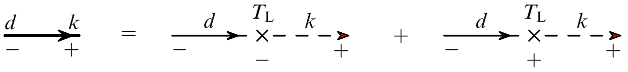

Figure 23. Diagrams that determine the function G_{dk} in tunneling problems. Here, T_L is the tunneling matrix element between a junction bank and the intermediate system.

matrix elements connecting the intermediate system to the left and right banks.

First and foremost, we are interested in calculating the current at a given voltage across the junction. The current operator from the left bank to the intermediate system can be found in a standard way from the continuity equation, which determines variations of the left-bank particle number,

$$\frac{\partial}{\partial t} n_L = -i[n_L, H_T] = \hat{I}_L \, . \qquad (239)$$

Explicitly,

$$\hat{I}_L = iT_L \sum_k (c_k^+ d - d^+ c_k) \, . \qquad (240)$$

The same equation can be written for the current from the intermediate system into the right bank, but these currents are equal in the steady-state case (this can be shown by straightforward calculation in each particular case). Therefore, we consider a current only on one side. The current operator expectation value can be expressed in terms of the NDT Green's functions:

$$I_L = iT_L \sum_k \big(\langle c_k^+ d \rangle - \langle d^+ c_k \rangle \big) \, , \qquad (241)$$

$$\langle c_k^+ d \rangle = \big\langle c_k^+(t^-) d(t^+) \big\rangle = G^<_{dk}(t,t) = \int \frac{d\omega}{2\pi} \, G^<_{dk}(\omega) \, . \qquad (242)$$

In the steady-state case,

$$I = \sum_k T_{kd} \int \frac{d\omega}{2\pi} \, \big(G^<_{kd}(\omega) - G^<_{dk}(\omega) \big) \, . \qquad (243)$$

The Green's functions $G^<_{dk}$ are given by the diagrams in Fig. 23. When there is no other interaction between the left bank and the intermediate system except the one-particle transitions, the expression shown in Fig. 23 is not a first-order correction to the tunneling matrix element but the exact Dyson equation.

The functions G_k correspond to the original left-bank Green's functions, while the functions G_d are exact and take all junction transitions and all interactions within the intermediate system into account:

$$G^<_{dk}(t,t) = T_L \int dt_1 \, \big[G^R_d(t,t_1) G^{0<}_k(t_1,t) + G^<_d(t,t_1) G^{0A}_k(t_1,t) \big] \, . \qquad (244)$$

Using the explicit form of the left-bank Green's function, we find

$$I(V) = 2T_L T_L^* \sum_k \int \operatorname{Im} G_k^{R0}(\omega) \times \big[2 \operatorname{Im} G_d^A(\omega) n_k^0(\omega) - i G_d^<(\omega) \big] \frac{d\omega}{2\pi} \, . \qquad (245)$$

This equation is also valid for the intermediate system with electron–electron or electron–phonon interactions. In terms of the NDT, it seems to have been first obtained in [6]. The left–right junction symmetry is hard to see in the above equation. The symmetry is explicitly restored once the exact Green's functions G_d^R and $G_d^<$ are found. (We note that in the interacting case, the approximations used to obtain the exact Green's function G_d must satisfy the relevant Ward identities. In other words, they must be consistent; otherwise, equations for the right and left currents would give different results!)

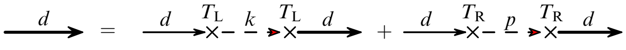

Figure 24. Graphic representation of the Dyson equation for the function G_d of the intermediate system without interaction.

If there are no interactions among particles in the intermediate system, then the exact Green's function G_d satisfies the simple Dyson equation graphically shown in Fig. 24.

After solving the NDT matrix equation and substituting the exact functions G_d^R and $G_d^<$ in (245), the equation for the current is simplified to the standard Landauer equation, which is manifestly symmetric with respect to the left and right junction banks,

$$I(V) = \int 4\gamma_L \gamma_R G_d^A(\omega) G_d^R(\omega) \big[n_L^0(\omega) - n_R^0(\omega) \big] \frac{d\omega}{2\pi} \, , \qquad (246)$$

where the standard tunneling rates are introduced:

$$\gamma_{L,R} = \pi |T_{L,R}|^2 \nu_{L,R} \, . \qquad (247)$$

Here, $\nu_{L,R}$ is the density of states on the left (right) bank, and $n^0_{L,R}(\omega)$ is the Fermi distribution function in the left (right) bank.

We note that if the tunneling occurs through a single isolated electron level (as in Fig. 25), i.e., the intermediate system Hamiltonian in (237) is equal to

$$\hat{H}_d = \varepsilon_1 d^+ d \, , \qquad (248)$$

then $G_d^R(\omega) = 1/(\omega - \varepsilon_1 + i(\gamma_L + \gamma_R))$, and Eqn (246) takes the characteristic resonant-tunneling form

$$I(V) = \int \frac{4\gamma_L \gamma_R}{(\omega - \varepsilon_1)^2 + (\gamma_L + \gamma_R)^2} \big[n_L^0(\omega) - n_R^0(\omega) \big] \frac{d\omega}{2\pi} \, . \qquad (249)$$

This formula can be obtained by calculating the transmission coefficient and using the temperature diagram technique. But

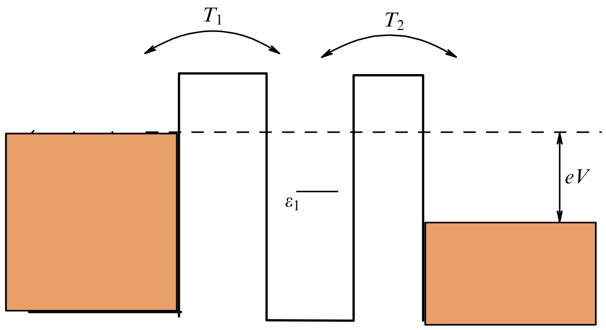

Figure 25. Tunneling system with an electron resonance level.

even in this case, calculating $G_d^<$ in the Dyson equation (see Fig. 24) gives a nonequilibrium electron distribution function in the intermediate system, which cannot be obtained via the temperature technique:

$$n_d(\omega) = \frac{\gamma_L n_L^0(\omega) + \gamma_R n_R^0(\omega)}{\gamma_L + \gamma_R}\,. \tag{250}$$

The same two-step nonequilibrium distribution function appears in ballistic junctions with lengths less than the characteristic scattering length. These essentially nonequilibrium distributions are important when considering the electron–phonon and electron–electron interaction in the junction area.

In the nonstationary case, when the voltage applied across the junction or any other parameters of the system are time-dependent, the NDT is the only method that allows consistently deriving the current equation. The calculations are more complicated, but the computational strategy remains the same [45].

9.2 Tunneling current fluctuations (noise)

Calculating the noise spectrum or the current fluctuations in tunnel junctions is an example where the NDT gives the most general equations describing both the shot and thermal Nyquist noise in a unified and simple manner. In what follows, we describe this phenomenon using the tunnel junction in which the tunneling occurs through discrete electronic levels of the intermediate system. This can be a quantum dot, a molecule in the STM, etc.

The junction is shown in Fig. 25, where only one discrete electron level is shown for simplicity. The corresponding Hamiltonian is given by

$$\hat{H} = \varepsilon_1 a_1^+ a_1 + \sum_k \varepsilon_k c_k^+ c_k + T_L \sum_k (c_k^+ a_1 + a_1^+ c_k) + \sum_p \varepsilon_p c_p^+ c_p + T_R \sum_p (c_p^+ a_1 + a_1^+ c_p)\,. \tag{251}$$

The current through the left and right barriers is defined by (240) and (241) (the electron charge e is shown here explicitly):

$$\hat{I}_L = \mathrm{i}eT_L(a_1^+ c_k - c_k^+ a_1)\,, \quad \hat{I}_R = \mathrm{i}eT_R(a_1^+ c_p - c_p^+ a_1)\,. \tag{252}$$

In the steady-state regime, the currents from the left bank to the intermediate system and from the intermediate system to the right bank are the same: $I_L = \langle \hat{I}_L \rangle = -\langle \hat{I}_R \rangle = -I_R$. However, even for a constant mean current, its fluctuations are different in different parts of the system, $S_{LL}(\omega) \equiv \langle I_L^2 \rangle_\omega \neq \langle I_R^2 \rangle_\omega \equiv S_{RR}(\omega)$. It can be shown that the charge conservation equation implies that the zero-frequency current fluctuations in the steady-state regime is the same throughout the system, $S_{LL}(0) = -S_{RL} = -S_{LR} = S_{RR}$. If we are interested only in the noise power at zero frequency, it is sufficient to calculate one of the current–current correlators, for example,

$$S_{LL}(t) = \langle \hat{I}_L(t) \hat{I}_L(0) \rangle = -e^2 T_L^2 \big\langle \big(a_1^+ c_k(t) - c_k^+ a_1(t)\big)\big(a_1^+ c_k(0) - c_k^+ a_1(0)\big)\big\rangle\,. \tag{253}$$

From the NDT perspective, the correlator corresponds to the diagrams shown in Fig. 26.

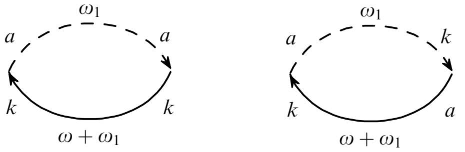

Figure 26. Diagrams that define the correlator $S_{LL}(\omega)$.

The Fourier-transformed correlator is given by

$$S_{LL}(\omega) = e^2 T_L^2 \sum_k \int \frac{\mathrm{d}\omega_1}{2\pi} \big[G_{aa}^<(\omega_1) G_{kk}^>(\omega + \omega_1) + G_{kk}^<(\omega_1) G_{aa}^>(\omega + \omega_1) - G_{ak}^<(\omega_1) G_{ak}^>(\omega + \omega_1) - G_{ka}^<(\omega_1) G_{ka}^>(\omega + \omega_1)\big]\,.$$

Calculating this, we find the final result for the current fluctuations:

$$S_{LL}(0) = e^2 \frac{4\gamma_L \gamma_R}{\gamma_L + \gamma_R} \int \frac{\mathrm{d}\omega}{2\pi} \operatorname{Im} G_1^A(\omega) \bigg\{ \big[n_L(1 - n_R) + n_R(1 - n_L)\big] - \frac{4\gamma_L \gamma_R}{\gamma_L + \gamma_R} \operatorname{Im} G_1^A(\omega)(n_L - n_R)^2 \bigg\}\,. \tag{254}$$

(We recall that $\gamma_L = T_L^2 \nu_k$ and $\gamma_R = T_R^2 \nu_p$ are the tunneling transition rates, and $n_L = n(\omega)$ and $n_R = n(\omega - eV)$.) This simple equation is interesting because it contains both the shot and thermal Nyquist noise. ‘Classic’ Nyquist noise can be obtained from (254) in the equilibrium case with a zero voltage $V = 0$ across the junction as follows. At $V = 0$, $T \neq 0$ $(n_L - n_R) = 0$, formula (254) becomes

$$S_{11}(0) = 4\,\frac{\gamma_L \gamma_R}{\gamma_L + \gamma_R} \int \frac{\mathrm{d}\omega}{2\pi} \operatorname{Im} G_1^A(\omega) \big[n_L(1 - n_R) + n_R(1 - n_L)\big]\,. \tag{255}$$

If the temperature is less than the characteristic electron energy, say, the level width $\gamma = \gamma_L + \gamma_R$, then

$$n(\omega)\big(1 - n(\omega)\big) = \frac{1}{4} \cosh^{-2}\left(\frac{\omega}{2T}\right) \simeq T\delta(\omega)\,. \tag{256}$$

Equation (254) reduces to the Nyquist equation

$$S_{11}(0) = 2Tg(0) = \frac{2T}{R_{\text{tun}}}\,, \tag{257}$$

where the junction conduction (the inverse tunneling resistance) is given by

$$g(0) = \frac{\gamma_L \gamma_R}{\gamma_L + \gamma_R} \frac{2}{\pi} \operatorname{Im} G_1^A(0)\,. \tag{258}$$

On the other hand, to find the standard form of the shot noise, we consider $T \to 0$. We also have $n_L(1 - n_R) + n_R(1 - n_L) \simeq n_L - n_R$ and $(n_L - n_R)^2 \simeq n_L - n_R$. Therefore, the noise is proportional to the tunneling current, as it should be for shot noise. This can be easily seen by comparing formulas (254) and (249) for the noise and the current. However, the coefficient between the noise power and the current depends on the particular junction regime. At low voltages $V \ll \gamma$, we find the well-known equation whereby the transmission coefficient determines the noise power [46, 47]:

$$S_{11} = eI(V)\left[1 - \frac{4\gamma_{\mathrm{L}}\gamma_{\mathrm{R}}}{\varepsilon_1^2 + (\gamma_{\mathrm{L}} + \gamma_{\mathrm{R}})^2}\right] = eI(1 - \mathcal{T})\,, \tag{259}$$

where

$$\mathcal{T} = \frac{4\gamma_{\mathrm{L}}\gamma_{\mathrm{R}}}{\varepsilon_1^2 + (\gamma_{\mathrm{L}} + \gamma_{\mathrm{R}})^2}$$

is the transmission coefficient of the resonant tunneling structure.

We see that the current fluctuations are smaller than the usual Poisson shot noise, for which $S(\omega \to 0) = eI$. Moreover, in the full resonance case, when $\gamma_{\mathrm{L}} = \gamma_{\mathrm{R}}$ and $\varepsilon_1 = 0$, we find that $\mathcal{T} = 1$ and the current fluctuations are completely suppressed. It is interesting that at high voltages $V \gg \varepsilon_1, \gamma$, the noise power is also proportional to the current, but the coefficient is different:

$$S_{11} = eI\left[1 - \frac{2\gamma_{\mathrm{L}}\gamma_{\mathrm{R}}}{(\gamma_{\mathrm{L}} + \gamma_{\mathrm{R}})^2}\right] \geqslant \frac{1}{2}\,eI\,. \tag{260}$$

The study of noise in quantum systems, in atomic and molecular junctions, using the NDT can be found in numerous papers (for a more extended discussion, see [48]). Of particular interest is the case of inelastic tunneling with vibrational interaction [49–52].

9.3 Vibrations excited by the tunneling current

In any system, electrons interact with vibrational modes. Therefore, the tunneling current flow can be accompanied by excitation of vibrations. The excitation can occur in the junction banks and be determined by the electron–phonon interaction in the bulk of a material. The effect gives rise to features on the current–voltage characteristic, whose positions are related to the phonon frequencies (one of the first papers here is [53]).

The electron–vibrational interaction and vibrations of such small objects as quantum dots, or even individual molecules located near the tunnel junction, are different from the case of massive junctions. The NDT is the most appropriate language to formulate the theory of such systems. Here, we mention Ref. [5] as one of the first papers where the electron–phonon interaction was considered by means of the NDT. To date, a huge number of papers apply the NDT to study vibrations excited by the tunneling current in molecules, atomic chains, etc. [54–60]. Some aspects of tunneling and vibrations are reviewed in [61]. Thanks to the progress in experimental techniques, these theoretical results can be compared with experiment, for example, with the results on individual molecules on a substrate, obtained by a scanning tunneling microscope (STM).

Much research work is devoted to the classification of features in the tunneling characteristics in the presence of electron–vibrational interaction.

In this review, we focus on another aspect of this interaction. We discuss the calculation of the intensity of vibrations excited by the tunneling current. Such a theory is needed, for example, to estimate the heating of small tunnel junctions. Moreover, there is a very interesting area in the STM experiments on controlling dissociation, desorption, and molecular and atomic motion over the surface by means of the tunneling current (see, e.g., [62]).

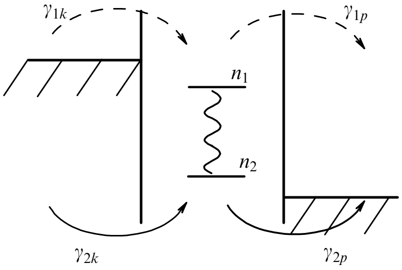

Figure 27. Two-level tunneling system with electron–vibrational interaction.

The idea behind these NDT calculations is very simple. Because the oscillation modes (or heating) are determined in secondary quantization by the occupation number, we have to find the corresponding Green's functions $D^{<}(t, t') = -\mathrm{i}\langle b^{+}(t) b(t')\rangle$ (where b^{+} is the creation operator of a vibration quantum), which immediately define the nonequilibrium occupation numbers $N(t) = \mathrm{i}D^{<}(t, t)$.

As discussed in Section 5, from the Dyson equation for the phonon Green's function, we can find the kinetic equations and use them to consider transient effects associated with the vibrations.

To see how this strategy works, we consider the simple example of two discrete electron levels in the intermediate system shown in Fig. 27 [63].

The Hamiltonian consists of three parts:

$$\hat{H} = \hat{H}_{\mathrm{dot}} + \hat{H}_0 + \hat{H}_{\mathrm{tun}}\,. \tag{261}$$

The term $\hat{H}_{\mathrm{dot}}$ describes a quantum dot or molecule that is the intermediate system with only two electron states (levels); the electron–vibrational interaction with a single vibrational mode makes transitions between the levels possible:

$$\hat{H}_{\mathrm{dot}} = \sum_{i=1,2} \varepsilon_i a_i^{+} a_i + g(a_1^{+} a_2 + a_2^{+} a_1)(b + b^{+}) + \omega_0 b^{+} b\,, \tag{262}$$

where a_i are the first and second state electron operators, b is the operator of the vibrational mode with a frequency ω_0, and g is the electron–phonon coupling constant. Here, ε_i are two discrete energy levels in the quantum dot; in what follows, we assume that level '1' is above level '2': $\varepsilon_1 > \varepsilon_2$.

The second term in (261) represents the right and left junction banks described as a system of noninteracting particles, with the chemical potential of one of the banks shifted by the applied voltage eV:

$$\hat{H}_0 = \sum_{\mathbf{k}} (\varepsilon_k - \mu) c_{\mathbf{k}}^{+} c_{\mathbf{k}} + \sum_{\mathbf{p}} (\varepsilon_p - \mu - eV) c_{\mathbf{p}}^{+} c_{\mathbf{p}}\,. \tag{263}$$

As usual, the tunneling Hamiltonian describes transitions between the junction banks and the intermediate system:

$$\hat{H}_{\mathrm{tun}} = \sum_{\mathbf{p},\, i=1,2} T_{\mathbf{p},i}(c_{\mathbf{p}}^{+} a_i + \text{h.c.}) + \sum_{\mathbf{k},\, i=1,2} T_{\mathbf{k},i}(c_{\mathbf{k}}^{+} a_i + \text{h.c.})\,. \tag{264}$$

The diagram technique for nonequilibrium processes gives the Dyson equation with a first-order irreducible part (Fig. 28), which determines all the phonon Green–Keldysh functions.

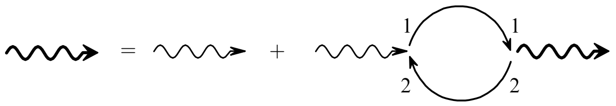

Figure 28. Dyson equation for the vibrational Green's function.

The matrix Dyson equation in triangular NDT representation (75) and (93) gives rise to the system of equations

$$\hat{D}^{<} = \hat{D}_0^{<} + \hat{D}_0^{<} \Pi^{\mathrm{A}} \hat{D}^{\mathrm{A}} + \hat{D}_0^{\mathrm{R}} \Pi^{<} \hat{D}^{\mathrm{A}} + \hat{D}_0^{\mathrm{R}} \Pi^{\mathrm{R}} \hat{D}^{<} , \tag{265}$$

$$\hat{D}^{\mathrm{R}} = \hat{D}_0^{\mathrm{R}} + \hat{D}_0^{\mathrm{R}} \Pi^{\mathrm{R}} \hat{D}^{\mathrm{R}} , \tag{266}$$

where D_0 is the equilibrium Green's function,

$$\begin{aligned} D_0^{\mathrm{R}}(\Omega) &= \frac{2\omega_0}{(\Omega + \mathrm{i}\delta)^2 - \omega_0^2} , \\ D_0^{<}(\Omega) &= N_0(\Omega)\big(D_0^{\mathrm{R}}(\Omega) - D_0^{\mathrm{A}}(\Omega)\big) , \end{aligned} \tag{267}$$

and N_0 is the Bose distribution.

We can easily write the irreducible components (polarization operators) in the lowest order in electron–phonon interaction (the first order in g^2), depicted in Fig. 28 as loops of the two-electron Green's functions:

$$\begin{aligned} &\Pi^{\mathrm{A}}(\Omega) - \Pi^{\mathrm{R}}(\Omega) \\ &\quad = -4\mathrm{i}g^2 \int \frac{\mathrm{d}\omega}{2\pi} \Big[\mathrm{Im}\, G_2^{\mathrm{A}}(\omega) \mathrm{Im}\, G_1^{\mathrm{A}}(\omega - \Omega) \big(n_2(\omega) - n_1(\omega - \Omega)\big) \\ &\quad + \mathrm{Im}\, G_1^{\mathrm{A}}(\omega)\, \mathrm{Im}\, G_2^{\mathrm{A}}(\omega - \Omega) \big(n_1(\omega) - n_2(\omega - \Omega)\big)\Big] , \\ &\Pi^{<}(\Omega) \\ &\quad = -4\mathrm{i}g^2 \int \frac{\mathrm{d}\omega}{2\pi} \Big[n_1(\omega)\big(n_2(\omega - \Omega) - 1\big)\, \mathrm{Im}\, G_1^{\mathrm{A}}(\omega)\, \mathrm{Im}\, G_2^{\mathrm{A}}(\omega - \Omega) \\ &\quad + n_2(\omega)\big(n_1(\omega - \Omega) - 1\big)\, \mathrm{Im}\, G_2^{\mathrm{A}}(\omega)\, \mathrm{Im}\, G_1^{\mathrm{A}}(\omega - \Omega)\Big] . \end{aligned} \tag{268}$$

In this case, the perturbation theory is based on the electron–phonon interaction under the assumption that the tunneling problem without this interaction is already exactly solved. Therefore, all the electron Green's function in (268) are defined exactly within the tunneling problem. We recall that the nonequilibrium electron occupation numbers n_1 and n_2 contained in these functions are defined by tunneling processes (250): $n_i(\omega) = (\gamma_i^p n_p^0(\omega) + \gamma_i^k n_k^0(\omega))/\gamma_i$. As usual, the tunneling rates are defined by the tunneling matrix elements $T_{k,(p),i}$ and the state density $\nu_{k,p}$ on the junction banks: $\gamma_i^k = \pi T_{k,i}^2 \nu_k$, $\gamma_i^p = \pi T_{p,i}^2 \nu_p$. Here and hereafter, the total discrete level broadening caused by hybridization with the banks is denoted by $\gamma_i = \gamma_i^p + \gamma_i^k$.

The solution of the Dyson equation in the form with nonequilibrium distribution functions was found in (121) and (122) in Section 4:

$$D^{<} = -2\, \frac{\Pi^{<}}{2\, \mathrm{Im}\, \Pi^{\mathrm{R}}}\, \mathrm{Im}\, D^{\mathrm{R}} . \tag{269}$$

Therefore, the nonequilibrium vibrational occupation number is given by the simple formula

$$N(\Omega) = \frac{\mathrm{i}\Pi^{<}(\Omega)}{2\, \mathrm{Im}\, \Pi^{\mathrm{R}}(\Omega)} . \tag{270}$$

(Here, we discuss the steady-state case, when the voltage across the junction is independent of time, and hence the occupation of vibrational modes is nonequilibrium but stationary.)

It follows from the form of the irreducible part $\Pi^{<}$ that it can be explicitly divided into two terms:

$$\mathrm{i}\Pi^{<}(\Omega) = 2\, \mathrm{Im}\, \Pi^{\mathrm{R}}(\Omega) N_0(\Omega) + P^{<}(\Omega) , \tag{271}$$

where the function $P^{<}$ is given below. Then

$$N(\Omega) = N_0(\Omega) + \Delta N(\Omega) , \qquad \Delta N(\Omega) = \frac{P^{<}(\Omega)}{2\, \mathrm{Im}\, \Pi^{\mathrm{R}}(\Omega)} , \tag{272}$$

where the first term is simply the equilibrium Bose distribution function for the phonon mode in equilibrium with an electron thermostat (junction banks), and the second term describes nonequilibrium effects associated with the tunneling current flow and vanishes in the absence of voltage across the junction.

We note that the resulting nonequilibrium distribution has an important symmetry property, which is easily verified by Eqns (268) for the polarization operators: $N(\Omega) = -N(-\Omega) - 1$, with the nonequilibrium correction $\Delta N(\Omega) = -\Delta N(-\Omega)$. In other words, the nonequilibrium distribution function has the same properties as the Bose equilibrium function. This is closely related to the fact that the nonequilibrium distribution is also a solution of the kinetic equation, and therefore the collision integral resulting from integral Dyson equation (265) vanishes. However, using the kinetic equation, we can only say that the distribution does have the above property, but finding the specific form of the stationary distribution is impossible.

Substituting the occupation numbers n_1 and n_2 expressed in terms of the equilibrium Fermi distributions n_p and n_k on the banks in (268), we find

$$\begin{aligned} P^{<}(\Omega) = \frac{-4g^2}{\gamma_1 \gamma_2} &\int \frac{\mathrm{d}\omega}{2\pi} \big(n_p^0(\omega - \Omega) - n_k^0(\omega - \Omega)\big) \\ &\times \Big[\mathrm{Im}\, G_1^{\mathrm{R}}(\omega)\, \mathrm{Im}\, G_2^{\mathrm{R}}(\omega - \Omega) \\ &\times \big(\gamma_1^k \gamma_2^p n_k^0(\omega) - \gamma_2^k \gamma_1^p n_p^0(\omega) + (\gamma_1^k \gamma_2^p - \gamma_2^k \gamma_1^p) N_0(\Omega)\big) \\ &+ \mathrm{Im}\, G_1^{\mathrm{R}}(\omega - \Omega)\, \mathrm{Im}\, G_2^{\mathrm{R}}(\omega) \\ &\times \big(\gamma_2^k \gamma_1^p n_k^0(\omega) - \gamma_1^k \gamma_2^p n_p^0(\omega) - (\gamma_1^k \gamma_2^p - \gamma_2^k \gamma_1^p) N_0(\Omega)\big)\Big] , \end{aligned} \tag{273}$$

$$\begin{aligned} \mathrm{Im}\, \Pi^{\mathrm{A}} = \frac{-2g^2}{\gamma_1 \gamma_2} &\int \frac{\mathrm{d}\omega}{2\pi} \Big[\mathrm{Im}\, G_1^{\mathrm{A}}(\omega)\, \mathrm{Im}\, G_2^{\mathrm{A}}(\omega - \Omega) \\ &\times \Big(\gamma_1^k \gamma_2 \big(n_k^0(\omega) - n_k^0(\omega - \Omega)\big) + \gamma_2 \gamma_1^p \big(n_p^0(\omega) - n_p^0(\omega - \Omega)\big) \\ &+ (\gamma_1^k \gamma_2^p - \gamma_2^k \gamma_1^p)\big(n_k^0(\omega - \Omega) - n_p^0(\omega - \Omega)\big)\Big) \\ &+ \mathrm{Im}\, G_1^{\mathrm{A}}(\omega - \Omega)\, \mathrm{Im}\, G_2^{\mathrm{A}}(\omega) \Big(\gamma_2^k \gamma_1 \big(n_k^0(\omega) - n_k^0(\omega - \Omega)\big) \\ &+ \gamma_1 \gamma_2^p \big(n_p^0(\omega) - n_p^0(\omega - \Omega)\big) \\ &- (\gamma_1^k \gamma_2^p - \gamma_2^k \gamma_1^p)\big(n_k^0(\omega - \Omega) - n_p^0(\omega - \Omega)\big)\Big)\Big] . \end{aligned} \tag{274}$$

The sign of the tunneling rate combination $(\gamma_1^k \gamma_2^p - \gamma_2^k \gamma_1^p)$ in (274) determines the relative occupation of two-electron states in the presence of the tunneling current,

$$\frac{\gamma_1^k \gamma_2^p - \gamma_2^k \gamma_1^p}{\gamma_1 \gamma_2} \big(n_k^0(\omega) - n_p^0(\omega)\big) = n_1(\omega) - n_2(\omega) . \tag{275}$$

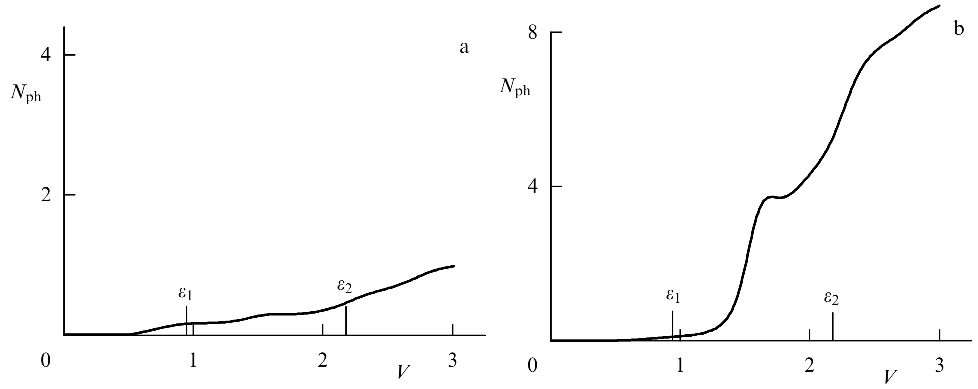

Figure 29. (a) Weak and (b) strong vibrational modes. Electron levels are labeled by vertical tags, the frequency is $\omega_0 = 0.5$. (a) $\gamma_1^k\gamma_2^p < \gamma_2^k\gamma_1^p$, (b) $\gamma_1^k\gamma_2^p > \gamma_2^k\gamma_1^p$.

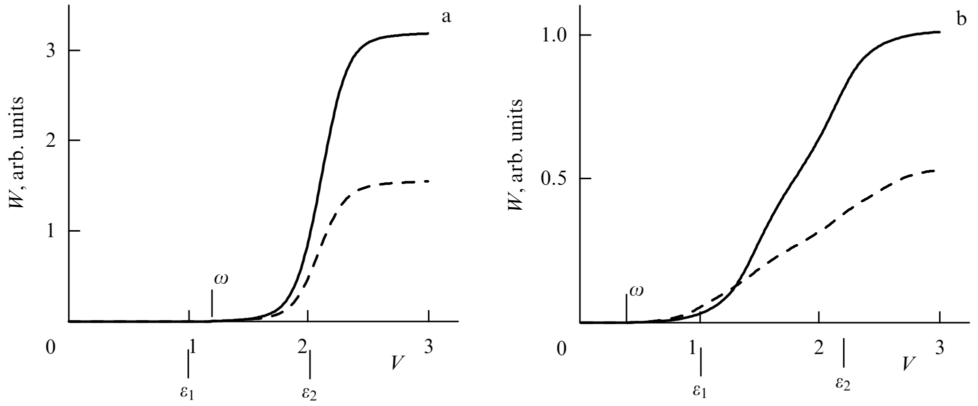

Figure 30. Voltage dependence of the power of vibration generation induced by the tunneling current. Solid lines refer to the zero temperature and dashed lines to $T = 0.2\omega_0$. Electron levels are labeled by vertical tags.

Phonon generation processes occur in different ways depending on the particular case realized in the system: the 'normal' occupation $(n_1(\omega) - n_2(\omega) < 0)$ or the 'inverted' occupation $(n_1(\omega) - n_2(\omega) > 0)$ (we recall that $\varepsilon_1 > \varepsilon_2$). Figures 29 and 30 show the dependence of the nonequilibrium vibrational occupation and phonon power generation on voltage for the particular configuration of discrete electron levels shown in Fig. 27. The positive potential applied to the right bank decreases the Fermi level of electrons such that it first crosses the level ε_1, and then ε_2.

In the case of normal occupation, the phonon emission rate is small. In this regime, the maximum values of the nonequilibrium occupation numbers are not higher than a few units (Fig. 29a).

In the case of the inverted occupation of two levels in the presence of a current, the phonon generation is quite different. Here, the vibrations are much stronger; see Fig. 29b (the vertical scales of the left and right figures differ twofold). Moreover, the generation increases sharply for a certain value of the applied voltage, such that the phonon occupation numbers defined by (272) blow up to infinity. Figure 29 shows only the initial segment of the plot extending from the origin to the threshold. The nonequilibrium phonon occupation numbers diverge because the function $\mathrm{Im}\,\Pi^{\mathrm{A}}$ defined by (274) passes through zero, changing from positive to negative at some finite voltage across the junction. The effect is very similar to how lasing develops in the case of inverted occupation. To correctly describe the vibrational subsystem in this case, it is necessary to either build a theory of a higher order in the electron–phonon interaction [63] or consider other relaxation channels.

The NDT methods clarify the conditions that give rise to strong or weak vibrations. This information makes it possible to adjust the phonon emission rate in those systems where we can vary the tunnel junction parameters. For quantum wells, this can be achieved by both preparing wells of a special shape and controlling the shape by an external electric field. For molecules, we focus the tunneling microscope by increasing or decreasing the tunneling coupling between the STM tip and the molecule.

The theory shows that the generation of phonons (vibrations) is greatly increased if the tunneling current in the system with discrete levels creates inverted occupation. The suppression of generation is essential for the creation of semiconductor cascade lasers based on a system of tunnel junctions. Optical generation requires the creation of inverted occupation. However, as shown in this section, phonon generation inevitably develops at the same time, thereby preventing light emission. An NDT analysis similar to that in this section allows estimating whether the light emission can be achieved and how we can vary the tunnel junction parameters to achieve the required properties of the system.

Furthermore, using the NDT, it is very easy to study temperature effects, because the general equations are valid at any temperature. In our case, the temperature enters the distribution function of electrons on the junction banks.

If nonequilibrium phonons are rapidly emitted from the junction area such that there is no actual increase in the phonon (vibrational) occupation numbers, then Eqns (272) and (265) can be used to determine the phonon intensity (power) on the junction.

In many cases, the situation where nonequilibrium phonons rapidly leave the junction area or there are fast vibrational relaxation channels that are difficult to estimate accurately is more physically relevant. Leaving aside all other mechanisms of such fast relaxation (the simplest one is the ballistic escape in systems with good heat conduction), we see that using the NDT, the relaxation can be taken into account by adding a relaxation term to the right-hand side of the kinetic equation obtained from Dyson equation (265) [see (133)]:

$$\mathrm{i}\,\frac{\Omega}{\omega_0}\,\frac{\partial}{\partial t}\,D^<(\Omega,t) = (\Pi D)^< - (D\Pi)^< - \Gamma\left(D^< - D_0^<\right). \quad (276)$$

The appearance of the relaxation term $\mathcal{R} = -\Gamma(D^< - D_0^<)$ with a large constant Γ implies that the nonequilibrium phonon Green's functions are little different from the original equilibrium functions in the case of the balance between pumping and relaxation. Then, calculating the right-hand side of (276) using the original 'zeroth' Green's functions without knowledge of the details about the relaxation, we can find the phonon (vibration) power generation in the presence of the tunneling current.

Because $\mathrm{Im}\,D^{\mathrm{R}}$ almost always has a sharp peak at the phonon frequency ω_0,

$$\mathrm{i}\int\frac{\mathrm{d}\Omega}{2\pi}\,\frac{\Omega}{\omega_0}\,\mathcal{D}^<(\Omega,t) \approx -\int\frac{\mathrm{d}\Omega}{2\pi}\,\mathrm{Im}\,D^{\mathrm{R}}(\Omega)N_{\omega_0}(t,\Omega) = N_{\omega_0}(t)\,, \quad (277)$$

integrating the left- and right-hand sides of (276), we obtain the balance equation for the number of vibrational quanta:

$$\frac{\partial}{\partial t}\,N_{\omega_0}(t) = \int\frac{\mathrm{d}\Omega}{2\pi}\left[(\Pi D)^< - (D\Pi)^<\right] = W - \Gamma\left(N_{\omega_0}(t) - N_0\right). \quad (278)$$

It follows from (278) that the phonon generation rate is given by

$$\begin{aligned} W &= \int\frac{\mathrm{d}\Omega}{2\pi}\left[(\Pi D)^< - (D\Pi)^<\right] \\ &= \int\frac{\mathrm{d}\Omega}{2\pi}\left[D^<(\Pi^{\mathrm{R}} - \Pi^{\mathrm{A}}) - \Pi^<(D^{\mathrm{R}} - D^{\mathrm{A}})\right]. \end{aligned} \quad (279)$$

Using the splitting in (271) for the generation power, we obtain a very simple result,

$$W = P^<(\omega_0)\,. \quad (280)$$

This expression can also be represented in another form:

$$W = \int\frac{\mathrm{d}\Omega}{\pi}\,\mathrm{Im}D^{\mathrm{R}}(\Omega)\mathcal{G}(\Omega)\Delta N(\Omega) \approx -\mathcal{G}(\omega_0)\Delta N(\omega_0)\,, \quad (281)$$

where $\mathcal{G} = 2\,\mathrm{Im}\,\Pi^{\mathrm{R}}$ is the effective generation rate and $\Delta N(\omega_0) = \mathrm{i}\Pi^</2\,\mathrm{Im}\,\Pi^{\mathrm{R}}$ is the 'nonequilibrium correction' to the equilibrium occupation number. This is the nonequilibrium excitation level that was calculated above, i.e., the occupation numbers that the vibrational excitation would reach due to the tunneling current in the absence of fast relaxation due to other mechanisms. The generation rate is determined by values of these functions at the frequency equal to the phonon frequency ω_0.

Using (273) for the two-level model, we can find how the vibration intensity depends on the applied voltage for different relations between the position of electron levels and the frequency. Examples are shown in Fig. 30. We note that real transitions in an isolated system are possible only with $\omega_0 = \varepsilon_1 - \varepsilon_2$, while the vibration frequency in an open tunneling system can be arbitrary compared to the difference of electron energies $\varepsilon_1 - \varepsilon_2$. However, both the voltage at which a noticeable generation begins and the nature of the growth rate with a voltage depend on the relation between ω_0 and ε_1, ε_2. We also see that increasing the temperature significantly reduces the generation rate.

Recently, there has been much interest in vibrations and tunneling current for molecules adsorbed on a surface. Indeed, vibrations allow explaining the mechanisms and characteristics of experimentally observed phenomena: current stimulated desorption, dissociation, and controlled molecular motions on the surface (see, e.g., [62]). Junctions of thin wires and even of monoatomic chains are actively being investigated. Also, the NDT, along with numerical density functional methods, is now applied to the study of tunneling current and vibrations [64–66].

9.4 Tunneling problems within the effective mass approach

Usually, tunneling problems arise in quantum mechanics in the context of one-dimensional wave-tunneling phenomena. For some systems, such as planar semiconductor heterostructures and superlattices, it is convenient to use the general NDT formalism in a 'continuum' representation based on the effective mass approximation. Moreover, this representation clarifies the relation to the transmission and reflection coefficients of (free) electrons on a barrier.

We examine the NDT Green's functions in the 'continuum' representation. For a homogeneous semiconductor or metal, the Green's functions in the momentum representation have the simple form

$$G^{\mathrm{R}}(k,\omega) = \frac{1}{\omega - \varepsilon(k) + \mathrm{i}\gamma}\,, \quad (282)$$

$$G^<(k,\omega) = 2\mathrm{i}n(\omega)\delta\left(\omega - \varepsilon(k)\right) \quad (283)$$

(here γ is an infinitesimal quantity). Planar wave-tunneling problems are conveniently considered using the Green's functions in the mixed representation, where the plane parallel to the interface is transformed into the momentum representation, but the dependence of the coordinate along the axis perpendicular to the boundaries is preserved. Let this axis be z. In the case of a quadratic spectrum $\varepsilon(k) = k^2/2m$, the symbolic equation

$$G_{\mathrm{R}}^{-1}G^{\mathrm{R}} = 1$$

in various representations takes the form (with $\hbar = 1$ here and hereafter)

$$\left(\omega - \varepsilon(k)\right)G^{\mathrm{R}}(k,\omega) = 1\,, \quad (284)$$

$$\left(\frac{1}{2m}\,\Delta + \omega\right)G^{\mathrm{R}}(r,r',\omega) = \delta(r - r')\,, \quad (285)$$

$$\left[\frac{1}{2m}\,\frac{\partial^2}{\partial z^2} + \omega - \frac{p^2}{2m} + \mathrm{i}\gamma\right]G^{\mathrm{R}}(z,z',p,\omega) = \delta(z - z')\,. \quad (286)$$

In the last equation, an infinitesimal imaginary part is indicated explicitly because it fixes the solution uniquely. We introduce the notation

$$\kappa = \sqrt{2m(\omega + \mathrm{i}\gamma) - p^2} \tag{287}$$

and choose the branch $\operatorname{Im}\kappa > 0$. (The convention applies to any root of this type.) Then there is a unique solution of Eqn (286) that is finite at $|z - z'| \to \infty$:

$$G^{\mathrm{R}}(z, z', p, \omega) = \frac{\exp\left(\mathrm{i}\kappa|z - z'|\right)}{\mathrm{i}\kappa}\, m\,. \tag{288}$$

The advanced function is always related to the retarded one as $G^{\mathrm{A}}(z, z', p, \omega) = [G^{\mathrm{R}}(z', z, p, \omega)]^*$. Therefore,

$$G^{\mathrm{A}}(z, z', p, \omega) = \frac{\exp\left(-\mathrm{i}\kappa^*|z - z'|\right)}{-\mathrm{i}\kappa^*}\, m\,. \tag{289}$$

The function $G^<$ satisfies the relation

$$\begin{aligned} G^<(z, z', p, \omega) &= n(\omega)\left[G^{\mathrm{A}}(z, z', p, \omega) - G^{\mathrm{R}}(z, z', p, \omega)\right] \\ &= \mathrm{i}n(\omega)\left[\frac{\exp\left(\mathrm{i}\kappa|z - z'|\right)}{\kappa} + \frac{\exp\left(-\mathrm{i}\kappa^*|z - z'|\right)}{\kappa^*}\right] m\,, \end{aligned} \tag{290}$$

while the function $G^<$ at equal arguments, defining the electron density, is given by [see (287)]

$$\begin{aligned} G^<(0, 0, p, \omega) &= \mathrm{i}n(\omega)\,\frac{\kappa^* + \kappa}{|\kappa|^2}\, m \\ &= \begin{cases} \dfrac{\mathrm{i}n(\omega)}{\kappa}\, m\,, & \dfrac{p^2}{2m} < \omega\,, \\ 0\,, & \dfrac{p^2}{2m} > \omega\,. \end{cases} \end{aligned} \tag{291}$$

This form of $G^<$ for a free-electron gas immediately follows from $G^<(k, \omega) = n(\omega)(G^{\mathrm{A}}(k, \omega) - G^{\mathrm{R}}(k, \omega))$. However, the same equation can be obtained from more general equations of the Keldysh technique. We introduce a small scattering of electrons by random impurities. An irreducible part corresponding to such interaction can be calculated in the standard manner as

$$\Sigma^{\mathrm{R}}(\omega) = \sum_k V^2 G^{\mathrm{R}}(k, \omega) = -\mathrm{i}\gamma\,, \tag{292}$$

$$\Sigma^{\mathrm{R}}(z, z', \omega) = -\mathrm{i}\gamma\delta(z - z')\,, \tag{293}$$

$$\Sigma^<(\omega) = \sum_k V^2 G^<(k, \omega) = 2\mathrm{i}\gamma n(\omega)\,, \tag{294}$$

$$\Sigma^<(z, z', \omega) = 2\mathrm{i}\gamma n(\omega)\delta(z - z')\,, \tag{295}$$

where V is the impurity scattering matrix element and $\gamma = \pi V^2 \nu_{\mathrm{F}}$.

The above equations can be viewed in two ways: the appearance of Σ can be considered a consequence of scattering by impurities, and then $n(\omega)$ are the occupation numbers in our electron system, which are postulated by the equilibrium Fermi function for a given potential. But exactly the same irreducible parts arise in the case of a transition of electrons to the thermostat and back with random spatial transition amplitudes. Then $n(\omega)$ is the equilibrium electron distribution function of the thermal reservoir. Using this trick, it is possible to introduce a different potential and temperature for the left and right junction banks, 'incorporated' into the occupation numbers $n(\omega)$ corresponding to $\Sigma^<$. If we move the region of interaction with the thermostat [i.e., the region where irreducible parts (292)–(295) are defined] some distance from the tunneling structure (Fig. 31), then the method gives the nonequilibrium occupation numbers over the entire junction area. The diagram shown in Fig. 31 allows modeling many different junction types. The thermostat areas described by the Gibbs distribution are massive parts of the junction where the temperature and potential are considered fixed. Solving the NDT equations (sometimes, approximately) in the intermediate area allows finding all nonequilibrium characteristics in the transition region.

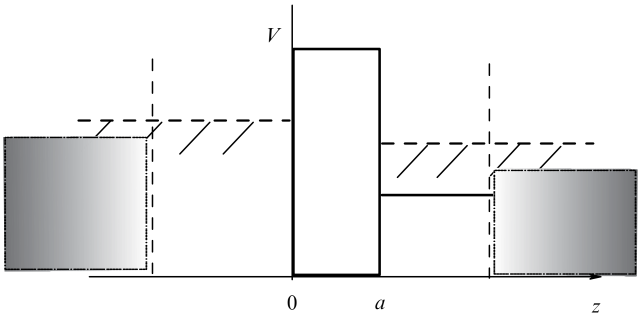

Figure 31. Tunneling system with regions outside the junction, which are considered to be thermostats.

The function $G^<$ can be found using the general formula of the nonequilibrium technique $G^< = G^{\mathrm{R}}\Sigma^< G^{\mathrm{A}}$,

$$\begin{aligned} &G^<(z, z', p, \omega) \\ &\quad = \int \mathrm{d}z_1\,\mathrm{d}z_2\, G^{\mathrm{R}}(z, z_1, p, \omega)\Sigma^<(z_1, z_2, p, \omega)G^{\mathrm{A}}(z_2, z', p, \omega) \\ &\quad = \int \mathrm{d}z_1 G^{\mathrm{R}}(z, z_1, p, \omega) 2\mathrm{i}\gamma n(\omega) G^{\mathrm{A}}(z_1, z', p, \omega) \end{aligned} \tag{296}$$

or, using the equivalent differential equation $(G_0^{-1} - \Sigma^{\mathrm{R}})G^< = \Sigma^< G^{\mathrm{A}}$,

$$\begin{aligned} &\left[\frac{1}{2m}\frac{\partial^2}{\partial z^2} + \omega - \frac{p^2}{2m} + \mathrm{i}\gamma\right] G^<(z, z', p, \omega) \\ &\qquad = 2\mathrm{i}\gamma n(\omega) G^{\mathrm{A}}(z, z', p, \omega)\,. \end{aligned} \tag{297}$$

Substituting (288) and (289) in these equations, we find that Eqn (290) for $G^<$ is reproduced, and γ can now take not only infinitesimal (for an ideal gas) but also finite values, appearing due to scattering on impurities or coupling to an external thermal reservoir.

We briefly discuss how the exact solution of the one-barrier tunneling problem found in terms of the Green's functions in Section 1 is related to the solution obtained via the tunneling Hamiltonian method. We assume that the tunneling structure is as shown in Fig. 32.

The energy is referenced to the bottom of the conduction band of the left junction bank. The applied voltage U enters the chemical potential shift in the electron occupation functions for regions on either side of the barrier. All quantities on the left of the barrier are assigned the index '0', and all quantities on the right are assigned the index '1'. The occupation numbers on the left and on the right are $n_0(\omega) = n_{\mathrm{F}}(\omega - \mu)$ and $n_1(\omega) = n_{\mathrm{F}}(\omega - \mu - eU)$. The z axis is perpendicular to the structure layers. The barrier is located at $0 < z < a$, where a is the thickness of the barrier.

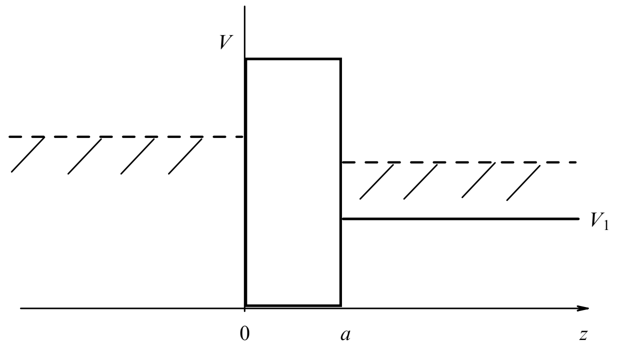

Figure 32. Potential shape defining a one-dimensional tunneling system.

Solving differential equations for $G^{\mathrm{R}}(z,z')$ of the type of Eqn (286) in each region and matching the corresponding solutions (the Green's function and its first derivative must be continuous in z and z') gives the following result for $z' > a$ and $z < 0$:

$$G^{\mathrm{R}}(z,z',p,\omega) = m\,\frac{-2q}{D}\exp\left[-\mathrm{i}\kappa_0 z + \mathrm{i}\kappa_1(z'-a)\right], \tag{298}$$

$$D = (q-\mathrm{i}\kappa_1)(q-\mathrm{i}\kappa_0)\exp(qa) - (q+\mathrm{i}\kappa_1)(q+\mathrm{i}\kappa_0)\exp(-qa), \tag{299}$$

where

$$\begin{aligned}\kappa_0 &= \sqrt{2m(\omega+\mathrm{i}\gamma)-p^2}\,,\\ \kappa_1 &= \sqrt{2m(\omega-V_1+\mathrm{i}\gamma)-p^2}\,,\\ q &= \sqrt{p^2+2m(V-\omega+\mathrm{i}\delta)}\end{aligned} \tag{300}$$

(δ is infinitely small). For simplicity, we assume that the coupling to the thermostat (the quantity γ) is the same on either side of the barrier. Because we are interested in the energy region where electrons tunnel through the barrier, $\omega < p^2/2m + V$, and therefore $q > 0$ is real in the sub-barrier region.

Full correspondence to the tunneling Hamiltonian method is achieved if we assume that $\exp(2qa) \gg 1$ (that is, 'double' (back and forth) tunneling processes have little effect on the states in each bank.) Then G^{R} in (298) takes the form

$$\begin{aligned}&G^{\mathrm{R}}(z,z',p,\omega)\\ &\quad= 2m\,\frac{-2q\exp(-qa)}{(q-\mathrm{i}\kappa_1)(q-\mathrm{i}\kappa_0)}\exp\left[-\mathrm{i}\kappa_0 z+\mathrm{i}\kappa_1(z'-a)\right]\\ &\quad= \frac{-(4q/m)\exp(-qa)\,\mathrm{i}\kappa_1\mathrm{i}\kappa_0}{(q-\mathrm{i}\kappa_1)(q-\mathrm{i}\kappa_0)}\\ &\quad\times m\,\frac{\exp\left[\mathrm{i}\kappa_1(z'-a)\right]}{\mathrm{i}\kappa_1}\,m\,\frac{\exp(-\mathrm{i}\kappa_0 z)}{2\mathrm{i}\kappa_0}\\ &\quad= T(p,\omega)G_0^{\mathrm{R}}(z,0,p,\omega)G_1^{\mathrm{R}}(a,z',p,\omega)\,,\end{aligned} \tag{301}$$

where G_1^{R} and G_0^{R} are the original Green's functions (288) for the regions on each side of the barrier, and the tunneling matrix element is

$$T(p,\omega) \equiv \frac{-(4q/m)\exp(-qa)\,\mathrm{i}\kappa_1\mathrm{i}\kappa_0}{(q-\mathrm{i}\kappa_1)(q-\mathrm{i}\kappa_0)}\,. \tag{302}$$

Here, the functions of an infinite system are used for the left and right bank Green's functions. However, it seems more reasonable to choose the nonperturbed Green's functions as solutions of the semi-infinite system bounded by a potential wall of the same height as the height of the barrier. In other words, the Green's functions are taken 'separately' for the left and right junction banks. They are given by

$$\begin{aligned}G_0^{\mathrm{R}}(z,0,p,\omega) &= \frac{\exp(-\mathrm{i}\kappa_0 z)}{\mathrm{i}\kappa_0-q}\,2m\,,\quad z<0\,,\\ G_1^{\mathrm{R}}(a,z',p,\omega) &= \frac{\exp\left[+\mathrm{i}\kappa_1(z'-a)\right]}{\mathrm{i}\kappa_1-q}\,2m\,,\quad z'>a\,.\end{aligned} \tag{303}$$

Then the function G^{R} of the entire system in Eqn (301) at $z' > a$ and $z < 0$ can also be represented as

$$\begin{aligned}&G^{\mathrm{R}}(z,z',p,\omega)\\ &\quad= \frac{\exp(-\mathrm{i}\kappa_0 z)}{\mathrm{i}\kappa_0-q}\,2m\,\frac{-2q\exp(-qa)}{2m}\,\frac{\exp\left[\mathrm{i}\kappa_1(z'-a)\right]}{\mathrm{i}\kappa_1-q}\,2m\\ &\quad= G_0^{\mathrm{R}}(z,0,p,\omega)T(p,\omega)G_1^{\mathrm{R}}(a,z',p,\omega)\,.\end{aligned} \tag{304}$$

This is identical to the equation $G_{12}^{\mathrm{R}} = G_1^{\mathrm{R}}T_{12}G_2^{\mathrm{R}}$ characteristic of the tunneling Hamiltonian method, and the tunneling matrix element takes the very simple form

$$T(p,\omega) \equiv \frac{-q\exp(-qa)}{m}\,. \tag{305}$$

The function $G^{<}(z,z')$, which is needed for calculating the current, is simpler to find using equations of type (296) if solutions for $G^{\mathrm{R(A)}}(z,z')$ are found in different regions in z. Because an equation similar to (296) now contains $\Sigma^{<}$ in regions on the left- and right-hand sides of the barrier, the function $G^{<}(z,z')$ contains both occupation numbers $n_0(\omega)$ and $n_1(\omega)$, i.e., it contains information on the potential difference applied.

The current through the barrier is given by the usual expression

$$j = -\frac{1}{2m}\left(\frac{\partial}{\partial z}-\frac{\partial}{\partial z'}\right)G^{<}(z,z')\bigg|_{z=z'}\,. \tag{306}$$

In the regions where the total current is conserved (i.e., there is no escape of electrons into an external thermostat), this equation can be used for any plane of z. It is convenient to take $z = 0$ or $z = a$. The exact calculation of $G^{<}(z,z')$ yields the following current [in the same approximation $\exp(2qa) \gg 1$]:

$$j(p,\omega) = \frac{-4q^2\exp(-2qa)(\kappa_1+\kappa_1^*)(\kappa_0+\kappa_0^*)}{|q-\mathrm{i}\kappa_1|^2|q-\mathrm{i}\kappa_0|^2}\big(n_0(\omega)-n_1(\omega)\big)\,. \tag{307}$$

This is the current density for particles with the energy ω and momentum p along the layers. The total current is $J = \int \mathrm{d}p\,\mathrm{d}\omega\, j(p,\omega)$. It turns out that using the same tunneling matrix element $T(p,\omega)$ introduced in (304) and (305), the above equation can be represented in the form completely equivalent to that of the tunneling Hamiltonian method:

$$\begin{aligned}j(p,\omega) = T(p,\omega)\big[&\operatorname{Im}G_1^{\mathrm{R}}(a,a,p,\omega)T^*(p,\omega)G_0^{<}(0,0,p,\omega)\\ &- G_1^{<}(a,a,p,\omega)T^*(p,\omega)\operatorname{Im}G_0^{\mathrm{R}}(0,0,p,\omega)\big]\,.\end{aligned} \tag{308}$$

For the left-bank Green's functions, we have [see (290)]

$$G_0^<(0,0,p,\omega) = \mathrm{i}n_0(\omega)\,\frac{\kappa_0+\kappa_0^*}{|q-\mathrm{i}\kappa_0|^2}\,,\qquad \operatorname{Im} G_0^{\mathrm{R}}(0,0,p,\omega) = \frac{\kappa_0+\kappa_0^*}{|q-\mathrm{i}\kappa_0|^2}\,, \tag{309}$$

and similarly for the right bank.

Thus, we find the following correspondence. Initially, in the tunneling Hamiltonian method, there are two Green's functions G_k and G_p describing electrons in the left and right junction banks (or quantum well) with the tunneling Hamiltonian of the form

$$H_{\mathrm{tun}} = \sum_{k,p} T_{k,p} c_k^+ c_p + \mathrm{h.c.}\,, \tag{310}$$

which describes transitions from states k on the left of the barrier to states p on the right of the barrier (or vice versa). The situation is as follows: the original 'zeroth' Green's functions are also Green's functions separately taken on the left and right sides of the barrier, while the tunneling matrix element depending on the frequency and longitudinal momentum can be symbolically written as $\delta(z_1)T(p,\omega)\delta(z_2-a)$. This means that the spatial variables of the Green's functions related by the tunneling matrix element must be taken at the edge of the barrier (each variable on its own edge). If the off-diagonal function G_{kp} in the case of the tunneling Hamiltonian has the form

$$G_{kp} = G_k T_{k,p} G_p\,, \tag{311}$$

then this nondiagonal Green's function now corresponds to the function $G(z,z')$ with the arguments z and z' taken on different sides of the barrier, for example, $z<0$ and $z'>a$. Then

$$G_{kp} \to G(z,z')\,,\quad z<0\,,\quad z'>a\,, \tag{312}$$

$$G_k T_{k,p} G_p \to G_0(z,0,p,\omega)T(p,\omega)G_1(a,z',p,\omega)\,. \tag{313}$$

The junction current in the tunnel Hamiltonian approach is given by

$$J = \sum_{k,p}(T_{kp}G_{kp}^< - T_{kp}^* G_{pk}^<) \to \big(T(p,\omega)G^<(0,a,p,\omega) - T^*(p,\omega)G^<(a,0,p,\omega)\big)\,. \tag{314}$$

It follows that in the case of weak tunneling, all observables are expressed in terms of the effective tunneling element $T(p,\omega)$ and the Green's functions of the right and left isolated banks are taken at arguments z on the edge of the barrier.

9.5 Thermal emission

As a practical example of using the continuum representation, we show how to find the thermal emission current from a metal surface by means of the NDT [67]. This is the problem of the flow of electrons through the structure shown in Fig. 33. We formalize the condition that all the electrons evaporating from the metal to the vacuum region (on the right) quickly escape to infinity, while the zero particle density is maintained on the left. For this, we can use the general approach in the preceding section, assuming that the chemical potential on the right has a large negative value.

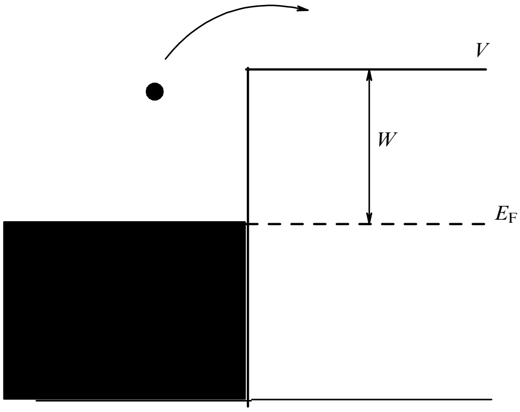

Figure 33. Thermal emission of metal with the work function W.

The exact function $G^{\mathrm{R}}(z,z',p,\omega)$ at $z>0$ and $z'<0$ necessary for calculating the current is given by

$$G^{\mathrm{R}}(z,z',p,\omega) = \frac{2m}{\mathrm{i}(\kappa_1+\kappa_0)}\exp(-\mathrm{i}\kappa_0 z' + \mathrm{i}\kappa_1 z)\,, \tag{315}$$

where

$$\kappa_0 = \sqrt{2m(\omega+\mathrm{i}\gamma)-p^2}\,,\quad \kappa_1 = \sqrt{2m(\omega-V+\mathrm{i}\delta)-p^2}\,. \tag{316}$$

Using the same equations (292) that ensure the equilibrium electron populations in the metal,

$$\Sigma^{\mathrm{R}}(z,z',\omega) = -\mathrm{i}\gamma\delta(z-z')\,, \tag{317}$$

$$\Sigma^<(z,z',\omega) = 2\mathrm{i}\gamma n(\omega)\delta(z-z')\,, \tag{318}$$

and using general equation (296), we obtain

$$G^<(z,z',p,\omega) = \int_{-\infty}^0 \mathrm{d}z_1\, G^{\mathrm{R}}(z,z_1,p,\omega)2\mathrm{i}\gamma n_0(\omega)G^{\mathrm{A}}(z_1,z',p,\omega)\,. \tag{319}$$

Because the right-hand vacuum maintains the zero concentration of electrons, the integral in (319) over the region $z>0$ where $n(\omega)=0$, in contrast to the tunneling problem, is absent. Using the function $G^<$ in (306), we find that the metal-to-vacuum flow of electrons is given by

$$J = \int\frac{\mathrm{d}\omega\,\mathrm{d}p}{(2\pi)^3}\,\frac{(\kappa_1+\kappa_1^*)(\kappa_0+\kappa_0^*)}{|\kappa_0+\kappa_1|^2}\,n_0(\omega)\,. \tag{320}$$

Here, only propagating states are taken into account due to the factors $(\kappa_1+\kappa_1^*)$, which are nonzero only when $\omega > V + p^2/2m$.

It follows that the characteristic dependence of the thermal emission current on the work function $W = V - E_{\mathrm{F}}$ and the temperature $T \ll W$ is given by

$$J \propto \exp\left(-\frac{W}{T}\right)T^2\sqrt{\frac{T}{W}}. \tag{321}$$

9.6 Thermal conduction and thermal effects

With the same methods that we used to calculate the current, i.e., the particle flow, we can find the energy flowing from one thermostat to another. In the cases where we can use the semiclassical kinetic equation, the NDT has no clear benefits. But the NDT is the most appropriate method to study the heat transfer in quantum junctions in essentially nonequilibrium distributions. In tunneling systems, the energy carried away by particles, say, from the left thermostat (junction bank) can be found from a relation similar to (239) for the particle flow:

$$Q = \frac{\partial}{\partial t}\langle H_{\mathrm{L}}\rangle = -\mathrm{i}\big\langle [H_{\mathrm{L}}, H_{\mathrm{T}}]\big\rangle = \mathrm{i}T_{\mathrm{L}}\sum_k \varepsilon_k\big\langle (c_k^+ d - d^+ c_k)\big\rangle \,. \tag{322}$$

Using the Green's functions, the energy flow in the steady-state case can be found similarly to (243):

$$I = \sum_k T_{kd}\varepsilon_k \int \frac{\mathrm{d}\omega}{2\pi}\,\big(G^<_{kd}(\omega) - G^<_{dk}(\omega)\big)\,. \tag{323}$$

In the simple case of a noninteracting intermediate system, the heat transfer between two reservoirs is given by

$$\begin{aligned} Q &= \int 4\gamma_{\mathrm{L}}\gamma_{\mathrm{R}}\,\omega G_d^{\mathrm{A}}(\omega) G_d^{\mathrm{R}}(\omega)\big[n^0_{\mathrm{L}}(\omega) - n^0_{\mathrm{R}}(\omega)\big]\,\frac{\mathrm{d}\omega}{2\pi} \\ &= \int \omega j(\omega)\,\frac{\mathrm{d}\omega}{2\pi}\,. \end{aligned} \tag{324}$$

Actually, the expression for the heat flux in the form $\int \omega j(\omega)\,\mathrm{d}\omega$ is fairly obvious: if a flow of particles $j(\omega)$ with energy ω escapes from the thermostat, the energy lost by the thermostat is $\omega j(\omega)$.

The NDT allows finding both the particle flow and heat flux in a system placed between thermostats with different chemical potentials and temperatures. Thus, it becomes possible to study a variety of thermoelectric effects in quite general terms [68–70]. In the case of inelastic effects like the already discussed vibration excitation in the presence of a current, calculating the heat flux can be difficult, but the NDT method can solve such problems [71]. The nonstationary thermal effects can also be described in this manner; in some cases, an increase in thermoeffects in a tunneling system is predicted [72].

We are not able to discuss all possible effects in junctions of various types here. For example, current fluctuations in junctions can produce electromagnetic radiation. In the case of an STM-to-metal junction, such radiation was considered within the NDT in [73].

There is the so-called Luttinger liquid appearing in one-dimensional structures due to electron interactions. In this state, the collective modes (such as plasmons) are well defined in equilibrium, but there are no well-defined single-particle excitations. If such a one-dimensional system is excited by an external field or included in a junction, it is a nontrivial problem to describe the nonequilibrium state. The nonequilibrium Luttinger liquid and the tunneling current flow through one-dimensional channels with such an electron state were described by means of NDT methods in [74–79].

10. Strong electromagnetic coupling to electrons in semiconductors

In the case of a weak incident electromagnetic perturbation, it is sufficient to apply the linear response theory. All usual equations for light absorption in semiconductors are obtained in this way. But in the case of strong coupling or lasing generation, the electron system is strongly excited, and hence the system nonequilibricity can no longer be ignored. The incident electromagnetic wave is absorbed, creating electron–hole pairs. At a high density of electrons and holes, the initial incident wave absorption conditions begin to change. Moreover, electrons and holes are scattered by impurities, interact with each other and with phonons, and recombine, with emission of light. As a result, quite a complex system is created whose behavior depends on the field strength, the relation between different relaxation rates in the electron–hole system, etc. The excitation spectrum in this system is determined by nonequilibrium distribution functions of electrons and holes, and therefore the use of the NDT in such cases is quite natural [80–82].

The starting-point Hamiltonian is simple:

$$\hat{H} = \sum_k \big[\varepsilon^{\mathrm{c}}_k a^+_k a_k + \varepsilon^{\mathrm{v}}_k b^+_k b_k\big] + \sum_{k,k'}\big[\lambda_{k,k'} a^+_k b_{k'} \exp(-\mathrm{i}\omega_0 t) + \mathrm{h.c.}\big]\,, \tag{325}$$

where a and b are electron annihilation operators in both the conduction and valence bands, $\varepsilon^{\mathrm{c}}_k$ and $\varepsilon^{\mathrm{v}}_k$ are the spectra of the conduction and valence bands, and the interaction with the electromagnetic wave of frequency ω_0 is described by the last term $\lambda_{k,k'} = E_{k-k'} d_{\mathrm{cv}}$, where E is the field amplitude and d_{cv} is the dipole matrix element of a transition from the valence to conduction band.

Because the interaction part is explicitly time-dependent, the Green's functions of conduction electrons $G_{\mathrm{cc}}(\omega)$ in the diagram series are related to the valence band Green's functions depending on a shifted frequency, $G_{\mathrm{vv}}(\omega - \omega_0)$. To remove the explicit time dependence of the Hamiltonian, we can pass to the 'rotating reference frame' using the operator $U = \exp\big[-\mathrm{i}\omega_0 t/2 \sum (a^+_k a_k + b^+_k b_k)\big]$. The interaction then gives rise to a system of equations for four Green's functions $G_{\mathrm{cc}}(\omega)$, $G_{\mathrm{cv}}(\omega)$, $G_{\mathrm{vc}}(\omega)$, $G_{\mathrm{vv}}(\omega)$. The spectrum can be determined by means of any pair of equations for $G^{\mathrm{R}}_{\mathrm{cc}}(\omega)$ and $G^{\mathrm{R}}_{\mathrm{vc}}(\omega)$ or for $G^{\mathrm{R}}_{\mathrm{cv}}(\omega)$ and $G^{\mathrm{R}}_{\mathrm{vv}}(\omega)$.

The quasiparticle spectrum of the transformed Hamiltonian has a gap if the light frequency is greater than the width of the forbidden band E_{g}:

$$\omega(k) = \frac{1}{2}\left[\varepsilon^{\mathrm{c}}_k + \varepsilon^{\mathrm{v}}_k \pm \sqrt{(E_{\mathrm{g}} - \omega_0 + \varepsilon^{\mathrm{c}}_k - \varepsilon^{\mathrm{v}}_k)^2 + 4\lambda^2}\,\right]. \tag{326}$$

Here, $\varepsilon^{\mathrm{c}}_k = k^2/2m_{\mathrm{e}}$, $\varepsilon^{\mathrm{v}}_k = -k^2/2m_{\mathrm{h}}$, and E_{g} is the width of the forbidden band. In the original formulation, this gives rise to the electron spectrum with a gap at the point where states in the conduction and valence bands are resonantly bound by an external field, $E_{\mathrm{g}} + \varepsilon^{\mathrm{c}}_k - \varepsilon^{\mathrm{v}}_k = \omega_0$,

$$E_{\mathrm{c}}(k) = \begin{cases} \dfrac{1}{2}\left[\varepsilon^{\mathrm{c}}_k + \varepsilon^{\mathrm{v}}_k + \omega_0 + \sqrt{(E_{\mathrm{g}} - \omega_0 + \varepsilon^{\mathrm{c}}_k - \varepsilon^{\mathrm{v}}_k)^2 + 4\lambda^2}\,\right], \\ \qquad\qquad \varepsilon^{\mathrm{c}}_k - \varepsilon^{\mathrm{v}}_k > \omega_0 - E_{\mathrm{g}}\,, \\ \dfrac{1}{2}\left[\varepsilon^{\mathrm{c}}_k + \varepsilon^{\mathrm{v}}_k + \omega_0 - \sqrt{(E_{\mathrm{g}} - \omega_0 + \varepsilon^{\mathrm{c}}_k - \varepsilon^{\mathrm{v}}_k)^2 + 4\lambda^2}\,\right], \\ \qquad\qquad \varepsilon^{\mathrm{c}}_k - \varepsilon^{\mathrm{v}}_k < \omega_0 - E_{\mathrm{g}}\,. \end{cases} \tag{327}$$

Using the functions G^{R} and G^{A} that determine the spectrum, it is easy to find the nonequilibrium distribution functions for electrons and holes. For this, we find the functions $G^<_{\mathrm{cc}} = \mathrm{i}\langle a^+ a\rangle$ and $G^<_{\mathrm{vv}} = \mathrm{i}\langle b^+ b\rangle$ from the conventional NDT equations as follows:

$$G^{<}_{\rm cc}(\omega) = G^{0<}_{\rm cc}(\omega) + G^{0<}_{\rm cc}(\omega)\lambda G^{\rm A}_{\rm vc}(\omega) + G^{0\rm R}_{\rm cc}(\omega)\lambda G^{<}_{\rm vc}(\omega)\,,$$
$$G^{<}_{\rm vc}(\omega) = G^{0<}_{\rm vv}(\omega)\lambda G^{\rm A}_{\rm cc}(\omega) + G^{0\rm R}_{\rm vv}(\omega)\lambda G^{<}_{\rm cc}(\omega)\,. \qquad (328)$$

There is a nonzero concentration of electrons in the conduction band and holes in the valence band due to the excitation by light, even at zero temperature. Moreover, the distribution function has the form

$$n_{\rm c}(k) = \frac{1}{2}\left[1 - \frac{|E_{\rm g} - \omega_0 + \varepsilon^{\rm c}_k - \varepsilon^{\rm v}_k|}{\sqrt{(E_{\rm g} - \omega_0 + \varepsilon^{\rm c}_k - \varepsilon^{\rm v}_k)^2 + 4\lambda^2}}\right], \qquad (329)$$

different from that of the temperature functions. This distribution function has a sharp peak at resonance values of the electron energy, where the frequency of light is equal to the energy transition from the valence to conduction band, $E_{\rm g} + \varepsilon^{\rm c}_k - \varepsilon^{\rm v}_k = \omega_0$. But the emergence of a highly nonequilibrium distribution of electrons and holes reduces wave absorption at the frequency ω_0. In the case of lasing with population inversion, the light emission 'burns a hole' in the electron distribution at the resonance frequency. In other words, electromagnetic waves and electrons form a rather complex coupled system, where the interaction gives rise to nonequilibrium distributions. In particular, the intensity of the interaction between waves and electrons also changes. An important role here is played by the off-diagonal Green's function $G^{<}_{\rm cv}(t,t) = {\rm i}\langle a^+(t)b(t)\rangle$, which determines the polarization magnitude. The full system of equations describing a strong pulse moving through a medium or the appearance of lasing must also include the electromagnetic field equation in which the source term is the polarization (current). A system of equations that takes the scattering of electrons on impurities, interaction with phonons, and the Coulomb interaction into account was derived in [83] but is very cumbersome. In many cases, particular calculations can be done only approximately (for a more detailed discussion, see books [7, 84]). The simplest example considered above deals with a nonequilibrium steady state. However, apart from stationary irradiation of a semiconductor by light, there is the very topical question of short and ultrashort pulses of intense light propagating through a substance. In this case, the Green's functions depend essentially on two times, and the problem becomes more complicated. The dynamics of electron–hole correlations, the dynamics of the screening, and plasma modes in the semiconductor after a short strong laser pulse were studied by means of the NDT in [85, 86].

The subject of nonequilibrium and unsteady states in systems such as a cascade laser (semiconducting superlattices) is particularly topical. Here, apart from the usual scattering by impurities and phonons, there is an additional dynamic effect — the tunneling of electrons from one quantum well to another. Using the NDT, we can show how different approximate approaches are related to each other and find the validity limits of simplified approaches [87]. The semiclassical solutions of the Boltzmann equation and more accurate NDT equations in the nonlinear transport regime in superlattices with inelastic scattering were compared in [88]. The study of the gain factor and emission linewidth in cascade lasers continued, for example, in [89, 90]. Moreover, it has been shown by means of the NDT that the cascade laser emission line broadening related to impurity scattering can be less than estimated by simple theories [90].

Finally, the NDT can be used in studying a nonequilibrium Bose condensate. Presently, such exciton and photon Bose condensates appearing in semiconductor structures and microcavities in a strong electromagnetic field are being widely studied (see, e.g., [91]).

11. Pseudoparticle method in the nonequilibrium diagram technique

It seems that the pseudoparticle (slave-particle) approach was originally formulated in the work by Abrikosov [92] to describe Kondo impurities. The basic idea of the method was formulated within the temperature diagram technique [92]. Later, there were attempts to establish general diagram rules within the pseudoparticle method [93–95], but the resulting technique was very different from the ordinary one. To overcome the difficulties, the mean-field approximation was used, which 'kills' the very essence of the approach. A generalization of the pseudoparticle method to the NDT was proposed in [96–98]. However, the authors considered diagrams in the lowest orders only, and therefore the general NDT diagram rules were not found.

In this section, we explain the method with the example of the Hubbard (Anderson) model, showing how to properly formulate the NDT [99].

Originally, the Hubbard Hamiltonian was formulated to describe the motion of band electrons in the tight-binding approximation taking the strong Coulomb interaction between two electrons at the same site (atom) into account,

$$\hat{H} = \sum_{ij\sigma} t_{ij} c^+_{i\sigma} c_{j\sigma} + \sum_{i\sigma} U n_{i\sigma} n_{i-\sigma} + \sum_{i\sigma} (\varepsilon_i - \mu) c^+_{i\sigma} c_{i\sigma}\,, \qquad (330)$$

where $c^+_{i\sigma}$ is the operator creating an electron with spin σ in the lattice site 'i', ε_i is the electron energy level, μ is the chemical potential, t_{ij} are the hopping matrix elements, and U is the on-site Coulomb repulsion of electrons.

The pseudoparticle method is that each of four possible states at a single site — no electrons, one electron with either spin, and two electrons with opposite spins — is described as an independent pseudoparticle. The pseudoparticle creation operators correspond to certain physical on-site states:

$$b^+ \Rightarrow |0\rangle\,, \qquad f^+_\sigma \Rightarrow c^+_\sigma|0\rangle\,, \qquad d^+ \Rightarrow c^+_\uparrow c^+_\downarrow|0\rangle\,. \qquad (331)$$

Physically, b and d are Bose operators, and f are Fermi operators. We note that the pseudoparticle vacuum state is completely unphysical. It should be absent in any equation, because the physical states are those pseudoparticle states with exactly one pseudoparticle b, f_σ, d on each site. Thus, in the pseudoparticle representation, we have to consider those physical states that satisfy the relation

$$\hat{N}_i = \sum_\sigma f^+_\sigma f_\sigma + b^+ b + d^+ d = 1\,. \qquad (332)$$

The original 'physical' electron creation operator is expressed in terms of pseudoparticles as

$$c^+_\sigma = f^+_\sigma b + d^+ f_{-\sigma}\,. \qquad (333)$$

In the pseudoparticle representation, the single-site part of the Hamiltonian with the Coulomb interaction between electrons is converted into the noninteracting Hamiltonian

$$\hat{H}^0 = \sum_i \left(\sum_\sigma \varepsilon f^+_{i\sigma} f_{i\sigma} + (2\varepsilon + U)\, d^+_i d_i + 0\, b^+_i b_i\right). \qquad (334)$$

But the hopping between sites now looks like interaction between pseudoparticles,

$$\hat{H}_{\rm int} = \sum_{ij\sigma} t_{ij}(f_{i\sigma}^+ b_i + d_i^+ f_{i-\sigma})(f_{j\sigma} b_j^+ + d_j f_{j-\sigma}^+)\,. \qquad (335)$$

It is therefore clear that the pseudoparticle method makes sense only in the case of strong Coulomb interaction, more precisely, for $t_{ij}/U \ll 1$. Otherwise, it is more natural to use the original formulation with conventional electron operators.

As already mentioned, any physical state should contain only one pseudoparticle at each site. The mapping between the original problem and the pseudoparticle method is exact only in this subspace defined by constraint (332). The projection onto the subspace can be done in different ways. Here, we follow the prescription proposed by Abrikosov [92]. For this, we add a large positive constant λ_i to the energy of every pseudoparticle state at site 'i',

$$\hat{H}_\lambda^0 = \sum_i \left[\sum_\sigma (\varepsilon + \lambda_i)\, f_{i\sigma}^+ f_{i\sigma} + \lambda_i b_i^+ b_i + (2\varepsilon + U + \lambda_i) d_i^+ d_i\right]. \qquad (336)$$

The thermodynamic average is treated as the initial conditions in the NDT. Then the average over states with n pseudoparticles on site 'i' has the Boltzmann weight $\langle n|\ldots|n\rangle \propto \exp(-n\lambda_i/T)$ for large λ (where T is the temperature). Therefore, we can retain the average with respect to only single pseudoparticle states on each site by means of the operation

$$\lim_{\lambda_i \to \infty} \left\{\exp\left(\frac{\lambda_i}{T}\right) \times \langle\ldots\rangle\right\}. \qquad (337)$$

States with two or more pseudoparticles have exponentially small weights and vanish in the limit $\lambda_i \to \infty$. The unphysical 'vacuum state' without pseudoparticles also has a vanishing contribution, because the Hamiltonian and any physical operator are normally ordered such that the pseudoparticle annihilation operator is on the far right.

Ensuring that $N_i = 1$ for the initial state, we consider only those states that obey this condition, because each term in the Hamiltonian preserves the number of pseudoparticles on each site. It follows that the evolution operator also preserves the constraint $N_i = 1$.

After taking the limit, the pseudoparticle occupation numbers are given by

$$\begin{aligned}
n_0 &= (Z_0)^{-1} \lim_{\lambda\to\infty} \left[\exp\left(\frac{\lambda}{T}\right) n_\lambda\right] \\
&= \frac{\exp(-\varepsilon/T)}{1 + 2\exp(-\varepsilon/T) + \exp\left[-(2\varepsilon+U)/T\right]}\,, \\
b_0 &= (Z_0)^{-1} \lim_{\lambda\to\infty} \left[\exp\left(\frac{\lambda}{T}\right) b_\lambda\right] \\
&= \frac{1}{1 + 2\exp(-\varepsilon/T) + \exp\left[-(2\varepsilon+U)/T\right]}\,, \qquad (338)\\
d_0 &= (Z_0)^{-1} \lim_{\lambda\to\infty} \left[\exp\left(\frac{\lambda}{T}\right) d_\lambda\right] \\
&= \frac{\exp\left[-(2\varepsilon+U)/T\right]}{1 + 2\exp(-\varepsilon/T) + \exp\left[-(2\varepsilon+U)/T\right]}\,,
\end{aligned}$$

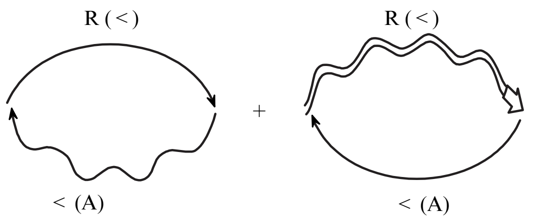

Figure 34. Retarded on-site electron Green's function. The solid line corresponds to a pseudofermion function, the wavy line to an 'empty-site' pseudoboson function, and the double wavy line to a pseudoboson double-occupied site function.

[where n_λ, b_λ, and d_λ are the equilibrium occupation numbers for Hamiltonian (336)] with

$$\begin{aligned}
Z_0 &= {\rm Sp}_{N=1}\left[\exp(-\beta\hat{H})\right] \\
&= \lim_{\lambda\to\infty}\left\{\exp(\beta\lambda)\,{\rm Sp}\left[\exp(-\beta\hat{H}_\lambda)\hat{N}\right]\right\}. \qquad (339)
\end{aligned}$$

These occupation numbers naturally satisfy the required constraint

$$b_0 + 2n_0 + d_0 = 1\,. \qquad (340)$$

The spectrum, state density, occupation numbers, and other characteristics we are interested in can be obtained from the ordinary NDT electron Green's functions

$$G_{\sigma ij}^{\alpha,\beta}(t,t') = -{\rm i}\left\langle T_C c_{i\sigma}(t), c_{j\sigma}^+(t')\right\rangle. \qquad (341)$$

In the pseudoparticle representation, the two-particle Green's functions have the form

$$\begin{aligned}
&G_{\sigma ij}^{--}(t,t') \\
&= -{\rm i}\left\langle T b_i^+ f_{i\sigma}(t), f_{j\sigma}^+ b_j(t')\right\rangle - {\rm i}\left\langle T f_{-\sigma i}^+ d_i(t), d_j^+ f_{-\sigma j}(t')\right\rangle \\
&- {\rm i}\left\langle T f_{-\sigma i}^+ d_i(t), f_{\sigma j}^+ b_j(t')\right\rangle - {\rm i}\left\langle T b_i^+ f_{\sigma i}(t), d_j^+ f_{-\sigma j}(t')\right\rangle. \qquad (342)
\end{aligned}$$

Hence, the retarded Green's function on an isolated Hubbard site is the sum of two simple loops in the pseudoparticle representation (Fig. 34).

After projection onto the physical subspace, the electron Green's function is given by

$$\begin{aligned}
&G_{ii\sigma 0}^{\rm R}(t-t') \\
&= {\rm i}\int \frac{{\rm d}\omega_1}{2\pi}\,\Big[B_0^<(t'-t)N_{\sigma 0}^{\rm R}(t-t') + B_0^{\rm A}(t'-t)N_{\sigma 0}^<(t-t') \\
&- N_{-\sigma 0}^<(t'-t)D_0^{\rm R}(t-t') - N_{-\sigma}^{\rm A}(t'-t)D^<(t-t')\Big], \qquad (343)
\end{aligned}$$

where the pseudoparticle Green's functions B, N, and D are

$$\begin{aligned}
&N_{0\sigma}^<(t-t') = {\rm i}n_0 \exp\left[-{\rm i}\varepsilon(t-t')\right], \\
&B_0^<(t-t') = -{\rm i}b_0\,, \qquad (344)\\
&D_0^<(t-t') = -{\rm i}d_0 \exp\left[-{\rm i}(2\varepsilon+U)(t-t')\right],
\end{aligned}$$

and n_0, b_0, and d_0 are given by (338). The retarded pseudoparticle functions have the form

$$\begin{aligned}
&N_{0\sigma}^{\rm R}(t-t') = -{\rm i}\theta(t-t')\exp\left[-{\rm i}\varepsilon(t-t')\right], \\
&B_0^{\rm R}(t-t') = -{\rm i}\theta(t-t')\,, \qquad (345)\\
&D_0^{\rm R}(t-t') = -{\rm i}\theta(t-t')\exp\left[-{\rm i}(2\varepsilon+U)(t-t')\right].
\end{aligned}$$

After the Fourier transformation in time, we obtain the usual electron Green's function for the one-site Hubbard model

$$G^{\mathrm{R}}_{0\sigma}(\omega) = \frac{n_0 + b_0}{\omega - \varepsilon + \mathrm{i}\delta} + \frac{n_0 + d_0}{\omega - \varepsilon - U + \mathrm{i}\delta} \,. \tag{346}$$

Pseudoparticle functions (344) and (345) are the basic elements of the NDT in the pseudoparticle representation. However, both the diagram rules and possible types of diagrams are different from the usual ones. To understand the implications of constraint (332) on the particle numbers, we must see what happens in the limit $\lambda \to \infty$, Eqn (337). For a finite parameter λ, all the ordinary NDT rules work as if the pseudoparticles were usual bosons and fermions. In this case, the diagrams contain various pseudoparticle functions $G^<$:

$$\begin{aligned}
&G^<_{f\sigma}(t - t') = \mathrm{i}n_\lambda \exp\left[-\mathrm{i}(\varepsilon + \lambda)(t - t')\right] \,, \\
&G^<_b(t - t') = -\mathrm{i}b_\lambda \exp\left[-\mathrm{i}\lambda(t - t')\right] \,, \\
&G^<_d(t - t') = -\mathrm{i}d_\lambda \exp\left[-\mathrm{i}(2\varepsilon + U + \lambda)(t - t')\right] \,.
\end{aligned} \tag{347}$$

It is important that any of the pseudoparticle occupation numbers n_λ, b_λ, and d_λ is proportional to $\exp(-\lambda/T)$ at large λ. Accordingly, any of the pseudoparticle Green's functions $G^<$ in (347) contains this exponentially small factor. Therefore, after taking limit (337), only diagrams with exactly one pseudoparticle function $G^<$ are retained, which are to be replaced by expressions (344). This requirement is very strong; for example, it forbids the existence of a Dyson equation.

Interactions in the pseudoparticle representation are always represented as annihilation of a particle of one type and creation of a particle of another type. For the Hubbard model, this is interaction (335). For the Anderson model with on-site Coulomb repulsion, the interaction is given by

$$\hat{H}_{\mathrm{int}} = \sum_{k\sigma} \left[t_k (f^+_\sigma b + d^+ f_{-\sigma}) c_{k\sigma} + \mathrm{h.c.} \right] \,, \tag{348}$$

where $c_{k\sigma}$ is the annihilation operator of a conduction band electron. This form of the interaction Hamiltonians implies that any diagram is represented as a number of closed loops of the pseudoparticle Green's functions related to the site and connected to each other either by intersite hopping t_{ij} in the Hubbard model or by the Green's functions of band electrons in the Anderson model. It is clear that at least one function $G^<$ must exist in any closed pseudoparticle loop. If signs of all vertices in a given loop are equal, i.e., pairs of $G^<$ and $G^>$ do not appear explicitly, then we can use the representation $G^{--} = G^{\mathrm{R}} + G^<$ or $G^{++} = G^< - G^{\mathrm{A}}$. Not all functions in a closed loop can be equal to G^{R} or G^{A}, because the expression $G^{\mathrm{R}}(t - t_1) G^{\mathrm{R}}(t_1 - t_2) \ldots G^{\mathrm{R}}(t_{n-1} - t_n) G^{\mathrm{R}}(t_n - t)$ (and similarly for G^{A}) vanishes. Hence, each loop involves either a manifest sign change from $-$ to $+$ or at least one $G^<$ function, as part of the functions G^{--} and G^{++}. Therefore, the requirement that any diagram contain just one function $G^<$ immediately implies that diagrams with exactly one on-site pseudoparticle loop are retained.

The structure of this pseudoparticle loop also turns out to be rigidly fixed. The function $G^<_{ii}$ can change its sign from '+' to '$-$' only in one vertex on each part of the loop; otherwise, there would be several functions $G^<$. Except for one function $G^<$ in the top loop and one function $G^>$ in the bottom loop, all other functions are G^{--} and G^{++}. Because $G^{--} = G^{\mathrm{R}} + G^<$ and $G^{++} = G^< - G^{\mathrm{A}}$, only G^{R} and G^{A} are left of the respective functions. Further simplifications are due to summing the diagrams with all possible positions of the propagator $G^>$ in the bottom loop. Because one of the pseudoparticle occupation numbers already appears in the upper part of the diagram, any propagator $G^>$ contributes only the constant $-2\mathrm{i}$, and we can write the propagator as $G^> = G^{\mathrm{R}} - G^{\mathrm{A}}$. Taking into account that the vertices in the loop are related either by the Green's functions of band electrons (in the Anderson model) or by electron lines leading to other lattice sites (in the Hubbard model), we can show that when consistently moving the propagator $G^> = G^{\mathrm{R}} - G^{\mathrm{A}}$ along the bottom loop, vanishing closed cycles of only retarded and advanced functions arise. The only possible remaining types of diagrams for $G^<_{ii}$ are shown in Fig. 35. In the upper part (starting with the pseudofermion line from time t), we have to successively replace each pseudoparticle line with the appropriate occupation number n_0, b_0, or d_0; the lines before this point are R lines, and after it, the A lines. For the bottom line, there are two possibilities: all lines are replaced with G^{R} if $t' > t$ or all lines are replaced with G^{A} if $t > t'$, along with an overall '$-$' sign for the full diagram.

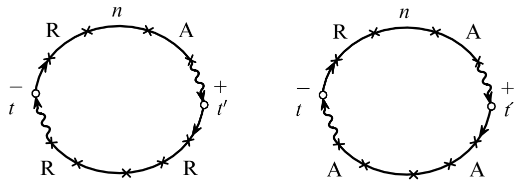

Figure 35. The only possible diagram types for $G^<_{ii}$.

A similar analysis yields selection rules on the pseudoparticle loop for the function G^{--}_{ii}. In what follows, we are interested in the function $G^{\mathrm{R}}_{ii} = G^{--}_{ii} - G^<_{ii}$, which defines the electron spectral density. Therefore, leaving the function G^{--}_{ii} aside, we show in Fig. 36 what kind of diagrams define the function G^{R}_{ii}.

The general diagram rules are as follows.

(1) Only one closed pseudoparticle loop can appear in each diagram for any site. This fundamental difference from the standard diagram technique prevents using the standard Dyson equation.

(2) Only one pseudoparticle function $G^<$ can appear in each loop. This function is replaced with the renormalized occupation numbers n_0, b_0, or d_0 in (338).

(3) Only R and A parts in all other pseudoparticle functions ('$--$', '$++$') are retained. On a line with a single function $G^<$, all functions located 'before' it (initially connecting the '$-$' vertices) are replaced with G^{R}. Functions

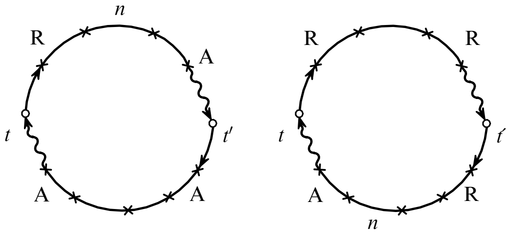

Figure 36. Diagrams for G^{R}_{ii}.

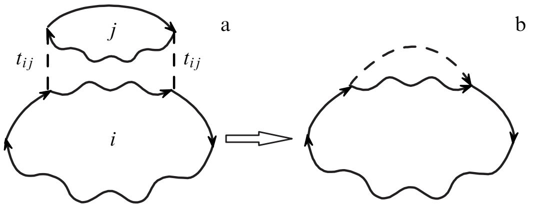

Figure 37. (a) Example of a first-order diagram for the electron on-site Green's function. (b) The same diagram in terms of the 'external electron line' $\mathcal{G}_{\mathrm{el}}^{0\alpha\beta}(\omega) = \sum_j t_{ij}\, G_{jj}^{0\alpha\beta}(\omega)\, t_{ji}$.

located 'after' it (connecting the '+' vertices) are replaced with $-G^{\mathrm{A}}$.

(4) The electron Green's functions carry the Keldysh index '−' in those vertices where they are adjacent to the pseudoparticle function G^{R}, and the index '+' if they are adjacent to the pseudoparticle function G^{A}.

(5) Oscillating factors $\exp(-\mathrm{i}\lambda_i t)$ originally contained in pseudoparticle Green's functions cancel in any vertex and should be omitted.

In the Hubbard model, electron Green's function (346) represented as a sum of two loops in Fig. 34 gives the zeroth-order approximation. We construct the perturbation series in interaction Hamiltonian (335), i.e., in the intersite hopping t_{ij}. First-order diagrams contain two pseudoparticle loops for neighboring sites connected by two hopping vertices t_{ij}. One of these diagrams is shown in Fig. 37a. Such diagrams can be regarded as the beginning of a series that renormalizes a given pseudoparticle line. It is convenient to introduce an 'external electron line' (Fig. 37b) for the on-site Green's function:

$$\mathcal{G}_{\mathrm{el}}^{0\alpha\beta}(\omega) = \sum_j t_{ij}\, G_{jj}^{0\alpha\beta}(\omega)\, t_{ji}\,. \tag{349}$$

Diagrams with renormalized pseudoparticle lines contain secular divergences and turn out to be more significant than the vertex diagrams shown in Fig. 38. The secular divergences are related to the general NDT properties: passing from occupation numbers in the original noninteracting system to the correct occupation numbers in the interacting system looks like the appearance of secular divergences in calculating the functions $G^{<}$ in the perturbation theory. In this case, we speak about variations of pseudoparticle occupation numbers. Such a behavior of first-order terms shows that in order to obtain physically relevant results within the pseudoparticle method, we should have consistent equations similar to the Dyson equation. First-order calculations in the perturbation theory can make sense only in some special problems (e.g., the Kondo problem).

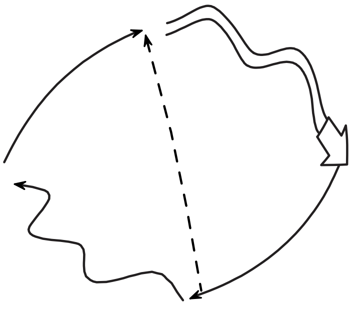

Figure 38. Example of the first-order vertex correction.

The simplest self-consistent procedure of this type, which allows summing a diagram series, was proposed in [100].

The on-site electron Green's function without vertex corrections is defined by the same two-loop diagrams shown in Fig. 34 but with renormalized upper and bottom pseudoparticle lines. By virtue of the pseudoparticle method, one of these lines contains only retarded (advanced) pseudoparticle functions. We call this line the retarded or advanced pseudoparticle (PP) Green's function for brevity. A line containing a pseudoparticle occupation number is called the 'lesser' pseudoparticle function. We should understand that the name 'pseudoparticle Green's function' is applied to a particular diagram series for which we can construct the Dyson equation, but the sum of these diagrams is not a physical particle Green's function.

Summing all the diagrams with insertions like the one shown in Fig. 37, we obtain the usual Dyson equation for the retarded PP Green's function:

$$\begin{aligned} N_\sigma^{\mathrm{R}}(\omega) &= N_\sigma^{0\mathrm{R}}(\omega) + N_\sigma^{0\mathrm{R}}(\omega)\Sigma_{N\sigma}^{\mathrm{R}}(\omega)N_\sigma^{\mathrm{R}}(\omega)\,,\\ B_\sigma^{\mathrm{R}}(\omega) &= B^{0\mathrm{R}}(\omega) + B^{0\mathrm{R}}(\omega)\Sigma_B^{\mathrm{R}}(\omega)B^{\mathrm{R}}(\omega)\,,\\ D_\sigma^{\mathrm{R}}(\omega) &= D^{0\mathrm{R}}(\omega) + D^{0\mathrm{R}}(\omega)\Sigma_D^{\mathrm{R}}(\omega)D^{\mathrm{R}}(\omega)\,. \end{aligned} \tag{350}$$

Here, N, B, and D denote the respective functions for a (single-occupied site) pseudofermion, empty-site pseudoboson, and double-occupied site pseudoboson. The zeroth-order Green's functions N^0, B^0, and D^0 are given by (344) and (345).

The simplest approximation for the self-energy parts Σ^{R} is given by

$$\begin{aligned} \Sigma_{N\sigma}^{\mathrm{R}}(\omega) &= \mathrm{i}\sum_\sigma \int \frac{\mathrm{d}\omega_1}{2\pi}\,\big[\mathcal{G}_\sigma^{\mathrm{el}>}(\omega_1)B^{\mathrm{R}}(\omega-\omega_1)\\ &\qquad + \mathcal{G}_{-\sigma}^{\mathrm{el}<}(\omega_1)D^{\mathrm{R}}(\omega+\omega_1)\big]\,,\\ \Sigma_B^{\mathrm{R}}(\omega) &= \mathrm{i}\sum_\sigma \int \frac{\mathrm{d}\omega_1}{2\pi}\,\mathcal{G}_\sigma^{\mathrm{el}<}(\omega_1)N_\sigma^{\mathrm{R}}(\omega+\omega_1)\,,\\ \Sigma_D^{\mathrm{R}}(\omega) &= \mathrm{i}\sum_\sigma \int \frac{\mathrm{d}\omega_1}{2\pi}\,\mathcal{G}_{-\sigma}^{\mathrm{el}>}(\omega_1)N_\sigma^{\mathrm{R}}(\omega-\omega_1)\,, \end{aligned} \tag{351}$$

where the 'external electron line' $\mathcal{G}_\sigma^{<(>)}$, Eqn (349), in the k, ω representation is

$$\mathcal{G}_\sigma^{<(>)}(\omega) = \sum_k \varepsilon_k^2\, G_{\mathrm{el}\sigma}^{<(>)}(\omega, k)\,. \tag{352}$$

The electron Green's function satisfies the general relations

$$G_{\mathrm{el}\sigma}^{<}(\omega, k) = -2\mathrm{i}\, n(\omega)\, \mathrm{Im}\, G_{\mathrm{el}\sigma}^{\mathrm{R}}(\omega, k)\,, \tag{353}$$

$$G_{\mathrm{el}\sigma}^{>}(\omega, k) = -2\mathrm{i}\big(n(\omega) - 1\big)\, \mathrm{Im}\, G_{\mathrm{el}\sigma}^{\mathrm{R}}(\omega, k)\,, \tag{354}$$

where $n(\omega)$ is the Fermi distribution. For the Anderson model, the retarded electron Green's function $G_{\mathrm{el}\sigma}^{\mathrm{R}}$ is simply the Green's function for band electrons, while for the Hubbard model, it must be determined self-consistently.

Taking self-energy parts in form (351) implies that we sum only 'nested' series of diagrams shown in Fig. 39. In this approximation, we consider electron interaction on a given site (using the pseudoparticle method) and replace complicated correlated electron motion over other sites by the sum of uncorrelated processes: hopping from the site, free motion, and hopping back to the site. The electron propagation is

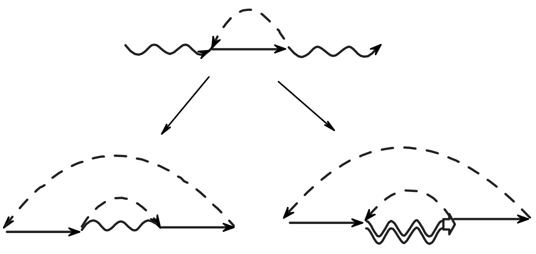

Figure 39. Example of self-energy parts used in the approximation. Dashed lines denote 'external electron line' (349).

described by an average electron Green's function, which is to be determined self-consistently by means of the on-site electron Green's function found within the pseudoparticle method. The ideology is similar to the dynamical mean-field theory (DMFT) [101], although the approach itself and the basic equations are quite different.

We note again that although the Dyson equation for the selected diagram series has the usual form, it cannot be considered an equation for real particles. The retarded self-energy parts are incomplete compared to the case of real particles. They do not contain terms with the PP function $G^<$, i.e., there are no terms with PP occupation numbers. For a given function $G^{\mathrm{R}}_{\mathrm{el}\sigma}$, system of equations (350), (351) is complete and allows finding all PP retarded and advanced functions in a consistent way.

Using the same approximation for the irreducible parts, we can also write the Dyson equation for lines with one pseudoparticle occupation number:

$$\begin{aligned}
N^<_\sigma(\omega) &= N^{\mathrm{R}}_\sigma(\omega)\big[\Sigma^<_{N\sigma}(\omega) + (N_0^{\mathrm{R}})^{-1} N^{0<}_\sigma(\omega)(N_0^{\mathrm{A}})^{-1}\big] N^{\mathrm{A}}_\sigma(\omega)\,,\\
B^<(\omega) &= B^{\mathrm{R}}(\omega)\big[\Sigma^<_B(\omega) + (B_0^{\mathrm{R}})^{-1} B^{0<}(\omega)(B_0^{\mathrm{A}})^{-1}\big] B^{\mathrm{A}}(\omega)\,,\\
D^<(\omega) &= D^{\mathrm{R}}(\omega)\big[\Sigma^<_D(\omega) + (D_0^{\mathrm{R}})^{-1} D^{0<}(\omega)(D_0^{\mathrm{A}})^{-1}\big] D^{\mathrm{A}}(\omega)\,,
\end{aligned} \tag{355}$$

where the irreducible parts are given by

$$\begin{aligned}
\Sigma^<_{N\sigma}(\omega) &= \mathrm{i}\int \frac{\mathrm{d}\omega_1}{2\pi}\,\big[\mathcal{G}^{\mathrm{el}<}_\sigma(\omega_1) B^<(\omega-\omega_1)\\
&\quad + \mathcal{G}^{\mathrm{el}>}_{-\sigma}(\omega_1) D^<(\omega+\omega_1)\big]\,,\\
\Sigma^<_B(\omega) &= \mathrm{i}\sum_\sigma \int \frac{\mathrm{d}\omega_1}{2\pi}\,\mathcal{G}^{\mathrm{el}>}_\sigma(\omega_1) N^<(\omega+\omega_1)\,,\\
\Sigma^<_D(\omega) &= \mathrm{i}\sum_\sigma \int \frac{\mathrm{d}\omega_1}{2\pi}\,\mathcal{G}^{\mathrm{el}<}_{-\sigma}(\omega_1) N^<_\sigma(\omega-\omega_1)\,.
\end{aligned} \tag{356}$$

System of equations (355), (356) is also complete because the PP retarded and advanced Green's functions have already been found. Therefore, all the 'lesser' PP functions can be self-consistently calculated from these equations.

Having found all the renormalized PP Green's functions, we can calculate the on-site electron Green's function from the same diagrams as in the case of the zeroth-order Green's function, but using the 'total' pseudoparticle lines

$$\begin{aligned}
&G^{\mathrm{R\,el}}_{ii\sigma}(\omega)\\
&= \mathrm{i}\int \frac{\mathrm{d}\omega_1}{2\pi}\,\big[B^<(\omega_1) N^{\mathrm{R}}_\sigma(\omega+\omega_1) + B^{\mathrm{A}}(\omega_1) N^<_\sigma(\omega+\omega_1)\\
&\quad - N^<_{-\sigma}(\omega_1) D^{\mathrm{R}}(\omega+\omega_1) - N^{\mathrm{A}}_{-\sigma}(\omega_1) D^<(\omega+\omega_1)\big]\,.
\end{aligned} \tag{357}$$

In the simplest approximation, the band-electron Green's function contained in the 'external electron line' of PP diagrams is related to the on-site function by the usual formula

$$G^{\mathrm{R}}_{\mathrm{el}\sigma}(\omega,k) = \frac{1}{(G^{\mathrm{R\,el}}_{ii\sigma})^{-1}(\omega) - \varepsilon_k}\,. \tag{358}$$

Thus, given the electron Green's function, we can find renormalized PP lines that determine the on-site electron Green's function. In turn, the on-site function determines the electron band function that appears in irreducible parts of PP functions. In this way, we develop a self-consistent method for calculating the electron Green's function.

Using the self-consistent method, we observe differences from the usual equations for Green's functions of real particles. The objects called PP Green's functions are just sums of particular diagrams, and their properties are not necessarily the same as for the real-particle Green's functions. In particular, their spectral weight is not automatically normalized, contrary to the real particle case. The self-consistent method gives the shape of the spectral function but not its absolute value. Therefore, we require that the electron Green's function be normalized as

$$-\frac{1}{\pi}\int \mathrm{d}\omega \sum_k \mathrm{Im}\, G^{\mathrm{R}}_{\mathrm{el}\sigma}(\omega,k) = 1\,.$$

Despite the simplicity of our approximations, this approach yields a quite reasonable shape of the density of electron states and its behavior with increasing the Coulomb repulsion. It is very important that the PP occupation numbers in the self-consistent approach are determined by the model parameters only. Irrespective of the changes in the initial values n_0, b_0, and d_0 during the self-consistent procedure, all the 'lesser' PP functions converge to the same value. In other words, they are eventually independent of the initial distribution function, as it should be in nonperturbative NDT calculations.

In what follows, we present results of calculations for the two-dimensional Hubbard model on a square lattice. Figure 40 shows the case of a half-filled electron band ($\mu = \varepsilon + U/2$). A dielectric gap begins to form when the Coulomb repulsion is comparable to the bandwidth. With a further increase in Coulomb repulsion, the Hubbard two-subband structure with a well-defined gap becomes more apparent. We note that in this approach, there is no artificial central peak in the density of states that appears in the DMFT [95]. The relative value of the 'lesser' PP functions allows estimating the ratio between the numbers of differently occupied sites. Figure 40 shows that most sites are single-occupied in the half-filling case. The fraction of empty and double-occupied sites is negligible.

If the electron concentration is less than 1/2, the lower subband becomes larger. It follows that the self-consistently found relation between states with different site occupations begins to change. There is a growing fraction of empty sites and almost no double-occupied sites (Fig. 41). Conversely, when the electron concentration increases, the upper subband becomes larger, the fraction of double-occupied sites increases, and the number of empty sites decreases. The behavior is monotonic and physically relevant.

Although the 'lesser' PP functions are not real-particle Green's functions, their relative value gives physically mean-

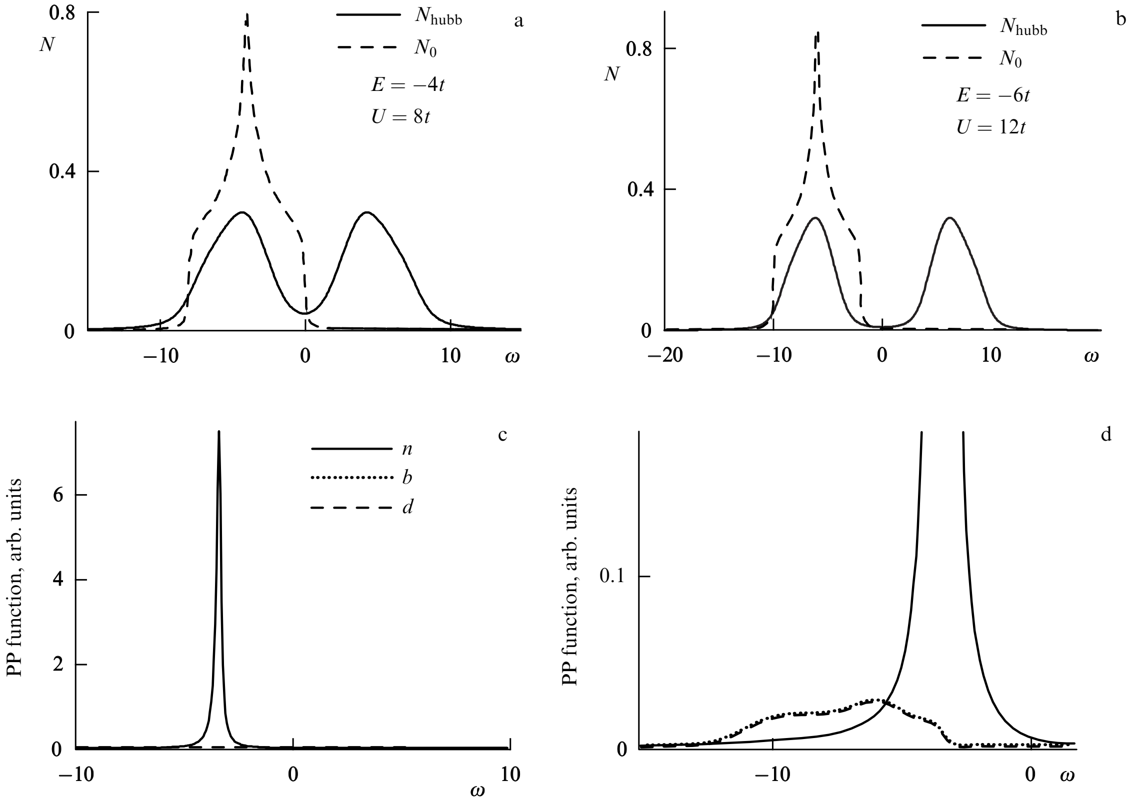

Figure 40. (a, b) Density of electron states (solid line) in the half-filling case for two different values of the Coulomb repulsion U. Density of states for the band with no interaction is shown (dashed line), U is measured in units of the intersite hopping t_{ij}. (c, d) PP 'lesser' functions for $U = 12t$. They determine the relative weight of empty sites (dotted line), single-occupied sites (solid line), and double-occupied sites (dashed line). (d) Enlarged part of (c). It is seen that a small fraction of empty and double-occupied sites also exists in the half-filling case.

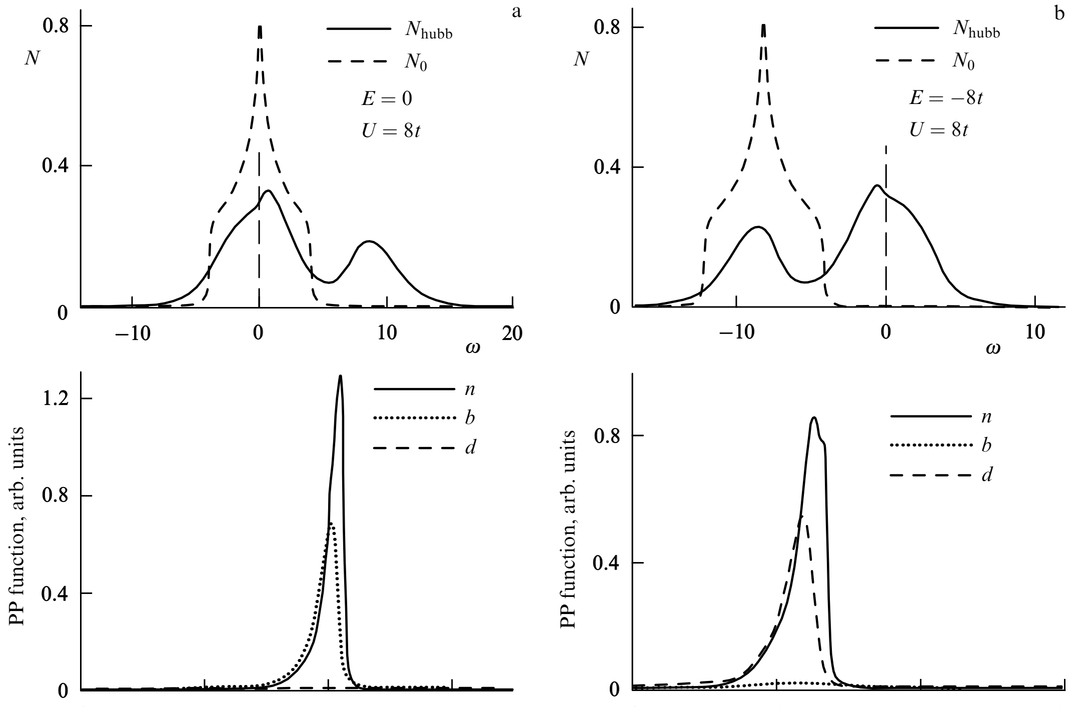

Figure 41. Density of electron states (solid line) for intermediate concentrations (upper row): concentration is (a) less than 1/2, (b) greater than 1/2. The chemical potential position corresponds to zero at the abscissa (vertical line). Lower row: corresponding relative fractions of differently occupied sites. Dotted line — relative weight of empty sites, solid line — single-occupied, dashed line — double-occupied.

ingful fractions of empty, single-occupied, and double-occupied sites. The main advantage of using the NDT in the pseudoparticle method is that it can work with real-time expressions. Therefore, similar calculations can be easily generalized to nonequilibrium and unsteady effects in Hubbard systems, Kondo systems, etc.

12. Other applications

12.1 Disordered systems

The NDT has also, and in some sense unexpectedly, found application in the theory of disordered electron systems. It turns out that the NDT can be used in the study of equilibrium characteristics of such systems, even though it is apparently not needed there. The NDT solves the following problem. To calculate the characteristics of a disordered system, we average over random disorder, not only over quantum states. The average of an operator $\hat{A}$ is given by the double averaging

$$\bar{A} = \left\langle \frac{\mathrm{Sp}\left\{\exp\left[-(H+V)/T\right]\hat{A}\right\}}{\mathrm{Sp}\left\{\exp\left[-(H+V)/T\right]\right\}} \right\rangle_{\mathrm{disorder}} . \tag{359}$$

The perturbation Hamiltonian $\hat{V}$ contains a random potential $u(r)$. It is usually assumed that the disorder is Gaussian with the correlation function

$$\left\langle u(r)u(r')\right\rangle = g(r-r') . \tag{360}$$

Because the random potential of impurities is included in the density matrix ρ, the numerator and the denominator in (359) cannot be averaged separately. In terms of diagrams, electron scattering on the impurity potential is described by the usual diagrams in Fig. 2, where the random impurity potential is denoted by a cross. Regarding the random potential of impurities as a Gaussian random quantity, we find that when averaging over disorder, the vertices in diagrams are joined pairwise by the random potential correlation function. In the temperature technique, the sum of all loops corresponds to the denominator in (359) and cancels disconnected parts in the diagram expansion of the numerator. But now, when the whole expression (359) is averaged over disorder, formerly disconnected diagrams are related to other diagrams of the correlation function (Fig. 42). Thus, formerly disconnected parts are not factored, and the diagram technique immediately becomes more complicated.

The use of the NDT solves the problem (of averaging the denominator in thermodynamic averages) because the sum of disconnected loops is then zero, and hence there are no diagrams similar to those shown in Fig. 42.

The application of the NDT to localization was considered in [102]. In that paper, in addition to a diagram analysis, the so-called nonlinear sigma model was derived within the NDT formulation. The functional integral method based on the NDT nonlinear sigma model is currently most widely used in this field (it is usually called the Keldysh nonlinear sigma model for short).

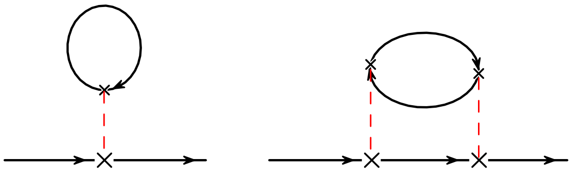

Figure 42. After averaging over disorder; initially disconnected loops are linked with other parts of the diagrams by the potential correlation function (dashed line).

The functional integral formulation of the NDT is considered in many articles (see [30, 103]). A detailed discussion of the NDT and localization can be found in [104, 105]. The long-standing problem of the mutual influence of Coulomb interaction and localization has also been considered within the Keldysh nonlinear sigma model approach. The renormalization-group equations were found in [106] by means of a diagram analysis that clarified the original result of Finkelstein [107]. Recent work [108] generalized these results to different types of interaction in the framework of the Keldysh nonlinear sigma model.

12.2 Particle physics and cosmology

The Feynman diagram technique appeared in quantum field theory and was apparently successful in solving most of the problems in that area. But it turned out that the NDT can be applied not only in condensed matter physics but also in field theory and elementary particle physics, in areas such as scattering processes at high temperatures and densities of elementary particles and multi-particle production in strong interactions. New challenges arise in describing the early Universe, the intermediate stages of heavy-ion collisions, and stellar processes, including neutron stars.

In order to apply the NDT in elementary particle physics, the method was extended to relativistic quantum field theory [34, 103, 109, 110]. Field theory operates in terms of functional integrals, which are beyond the scope of this review. In addition to the papers cited above, a summary of the NDT formulated by means of the functional integration method can be found, e.g., in [30, 104, 105]. The only difference from the conventional functional integrals is that because average (28) contains two types of operators with times on either the upper or lower part of the Keldysh contour, the functional integrals also contain a double set of integration field variables. Recently, using a relativistic formulation of the NDT, for example, new results were found in such an old subject as pair production in strong fields [111].

Many interesting applications of the NDT can be found in cosmology. Baryon production and possible reasons for the baryon asymmetry are discussed in [112] using the quantum kinetic equation obtained by the NDT methods. In relativistic theory, a time-dependent metric is a fluctuation in the field space. Conventional field theory is formulated in flat space, while the quantum evolution in curved space is generally unknown. The time evolution, even starting from the 'vacuum' state, can produce instabilities due to particle creation. The instability related to rapid particle production in de Sitter scalar field theory was discussed in [113]. The NDT has also been used in quantum gravity [114].

13. Conclusion

In conclusion, we focus on the areas where the NDT (the Keldysh diagram technique) can be applied, and whether it has advantages over other methods in solving various problems.

1. *Relaxation processes and semiclassical kinetic equations.*

Here, we can directly build a chain of equations for correlators using the Heisenberg equations. These equations are essentially quantum, and the only question is to decouple higher correlation functions in order to obtain a closed system of equations. The semiclassical kinetic equations can also be obtained by other methods; however, the NDT provides a simple and clear way to derive them. Moreover, the NDT allows systematically calculating the collision term in all orders in interactions.

2. *Response functions, time correlators, and fluctuations in equilibrium systems.*

The Matsubara (temperature) diagram technique and the Eliashberg analytic continuation method are successfully applied to the study of the properties of equilibrium systems or their small perturbations by external fields. Of course, the NDT can also solve such problems (sometimes by doing simpler calculations), but without a distinct advantage. We note that the problem of calculating time correlation functions for equilibrium systems is often confused with the NDT itself, with a single term 'real-time Green's functions' (RTGF) being used for both. However, if the NDT automatically also gives all time correlation functions in an equilibrium system, the RTGF methods elaborated in [16, 29] are not suitable for calculating characteristics of nonequilibrium systems.

3. *Nonequilibrium states with particle and heat fluxes in the intermediate system between two* (*or more*) *thermal reservoirs.*

This subject is very wide. Here, we find tunnel junctions, ballistic junctions, microcontacts between different materials, a variety of thermal effects in micro- and nanostructures, etc. It is in this area where the NDT is perhaps most widely used. Indeed, strictly speaking, except when the usual semiclassical kinetic equation is applicable, the NDT is beyond competition in this field. If the system contains two (or more) different thermal reservoirs, the temperature diagram technique cannot be constructed in principle. A strongly nonequilibrium state arises in the intermediate system that cannot be described by the Gibbs distribution. The fact that this strong disequilibrium is sometimes 'not felt' in simple noninteracting cases and the result can be obtained in the temperature technique is to some extent accidental.

4. *Nonequilibrium states in strong external fields.*

This is the case of such a strong interaction that using response functions is meaningless because the system goes into a state very far from equilibrium. For example, we mention the problem of interaction between high-intensity light and semiconductors, describing lasing in semiconductor structures (including cascade lasers). Although under certain conditions we can use simpler approximate approaches (e.g., kinetic balance equations), in many cases, the NDT is in a class by itself.

We can presently add cosmology and multiparticle nuclear reactions to this category.

Thus, it is not surprising that the NDT has a wide range of applications: the use of the NDT is natural wherever the problem of the evolution of an initial quantum many-body state can be posed.

Indeed, the use of the NDT is now natural for many authors: the Web of Science in 2015 indicates about 200 papers citing [1], while Google Scholar in 2015 finds more than 500 papers using the Keldysh technique. But — "Carthage must be destroyed" — we would like to conclude the review by repeating the following idea once more. Because the beginning of the active use of the NDT (not counting sporadic articles in various fields) was separated from its inception by decades, and because there are just a few people who really read the original 1960s papers, a number of enduring myths have appeared. In particular, the NDT is often referred to as the technique (or the method) of Kadanoff–Baym–Schwinger–Keldysh. Of course, the work by Kadanoff and Baym [29] and Schwinger [22] was very important. Among others (for example, the paper by Konstantinov and Perel' [18]), they clarified matters using the field theory methods in many-body problems. This work can be regarded as the prehistory of the NDT. As to the computational technique — a universal machinery that 'automated' calculations in nonequilibrium many-body systems — such a formulation was first proposed only in [1]. Therefore, it is natural that the NDT history starts from this work.

14. Appendix. Wick's theorem for the nonequilibrium diagram technique and initial correlations

Usually, Wick's theorem in condensed matter theory is the statement that the average of a T-ordered product of particle creation and annihilation operators is the sum of all possible products of pairwise averages of T-ordered pairs of these operators. In fact, the statement has two parts. The theorem originally proved by Wick [27] gives a decomposition of the T-ordered product of operators into the sum of operator products, but with N-ordering instead of T-ordering. The second step is to show that by averaging the above operator equation, we obtain the correct relation between the average of the product of operators and the product of all possible pairwise averages.

Wick's theorem as an operator reordering method can be directly used in the NDT case. The most important element in Wick's theorem is the notion of 'contraction' of two operators. Usually, this quantity is defined as the difference between the T-ordered and N-ordered pair of operators:

$$\overbrace{\hat{a}_1(t_1)\hat{a}_2^+(t_2)} = T\big(\hat{a}_1(t_1)\hat{a}_2^+(t_2)\big) - N\big(\hat{a}_1(t_1)\hat{a}_2^+(t_2)\big)\,. \tag{361}$$

(Normal ordering rearranges any creation operators to the left of all annihilation operators; the sign is reversed if two Fermi operators are transposed):

$$N(\hat{a}\hat{a}^+) = \mp\hat{a}^+\hat{a}\,.$$

The contraction of two operators is not zero only when the creation and annihilation operators belong to the same state (due to their noncommutativity). The contraction of any other pair is zero. Using the explicit form of operators in the interaction representation,

$$\hat{a}^+(t_k) = \exp\left(\mathrm{i}\varepsilon t_k\right)\hat{a}^+\,, \qquad \hat{a}(t_k) = \exp\left(-\mathrm{i}\varepsilon t_k\right)\hat{a}\,, \tag{362}$$

we find that the contraction of two operators is a simple function:

$$\overbrace{\hat{a}_1(t_1)\hat{a}_2^+(t_2)} = \theta(t_1 - t_2)\exp\left[-\mathrm{i}\varepsilon(t_1 - t_2)\right]. \tag{363}$$

The notion of contraction can be naturally extended to the NDT case. Here, the contraction of two operators is defined as the difference between their T_C-ordered product along the Keldysh contour and the normal product. We can easily find that

$$\overbrace{\hat a_1(t_1^\alpha)\hat a_2^+(t_2^\beta)} = T_C\big(\hat a_1(t_1)\hat a_2^+(t_2)\big) - N\big(\hat a_1(t_1)\hat a_2^+(t_2)\big)$$
$$= \theta_C(t_1^\alpha - t_2^\beta)\exp\left[-\mathrm{i}\varepsilon(t_1 - t_2)\right], \qquad (364)$$

where θ_C is a function with values 0 or 1 depending on which time is 'after' the other in terms of their location on the Keldysh contour:

$$\theta_C(t_1^\alpha - t_2^\beta) = \begin{cases} \theta(t_1^- - t_2^-)\,, \\ \theta(t_1^- - t_2^+) = 0\,, \\ \theta(t_1^+ - t_2^-) = 1\,, \\ \theta(t_2^+ - t_1^+)\,. \end{cases}$$

Considering operator products in the interaction representation, we can explicitly factor all exponentials containing the time dependence of any creation and annihilation operators (362). No matter how we rearrange the operators, the whole expression is always multiplied by the product of the exponentials of each operator. Therefore, we omit the overall numerical factor and consider transpositions of Schrödinger operators only. Moreover, we label the operators in order to control their positions when ordering them with respect to their time arguments. The most general form of the operator Wick's theorem for any (creation or annihilation) operators and states in the T-product is as follows:

$$T(\hat a_1\hat a_2\hat a_3\ldots\hat a_n) = N(\hat a_1\hat a_2\hat a_3\ldots\hat a_n) + N(\overbrace{a_1a_2}\,\hat a_3\ldots\hat a_n)$$
$$+ N(\overbrace{a_1a_2a_3}\,a_4\ldots\hat a_n) + \ldots + N(\overbrace{a_1a_2}\,\overbrace{a_3a_4}\,a_5\ldots\hat a_n) + \ldots$$
$$+ N(\overbrace{a_1a_2}\,\overbrace{a_3a_4}\ldots\overbrace{a_{n-1}a_n})\,. \qquad (365)$$

In the first term in the right-hand side, all operators are ordered normally; hence, there is a sum of terms in which one pair of operators is contracted (i.e., replaced by a numerical function), while other operators are normally ordered. Then, two pairs of operators are contracted and the rest are normally ordered, etc. When contracting a given number of operator pairs, we have to consider all possible ways to choose a number of pairs from the initial set of operators. In the fermionic case, the anticommutativity gives rise to an additional rule: when contracting operators, we have to rearrange them in pairs and then count the number of necessary transpositions. If the number is odd, then such terms in (365) have a minus sign. (For simplicity, we omitted the signs in (365).) Because Wick's theorem is essentially a way to systematically rearrange neighboring operators to pass from T-ordering to the normal ordering, the proof of (365) is the same if the T-product is understood as the T_C-ordering along the Keldysh contour, and the contraction of two operators is replaced by generalized expression (364).

If the initial density matrix corresponds to a noninteracting system, it is clear that operators related to different one-particle states are averaged independently. Therefore, it remains to see what happens when both sides of operator relation (365) are averaged over the initial density matrix and any operator $\hat a$ is either a creation or an annihilation operator in a given state. Moreover, it is clear that only those averages can be nonvanishing that contain equal numbers of creation and annihilation operators. In what follows, we work out the example of four operators. It shows the general principle of how the average of a large number of terms in the right-hand side of (365) is rearranged into T-ordered pairs of operators. Averaging all operators in the right-hand side of (365) over the initial density matrix in the bosonic case, we obtain the result

$$\big\langle T_C\, a(t^\alpha)a^+(t_3^\beta)a^+(t_1^\gamma)a(t_2^\delta)\big\rangle$$
$$= 2n^2$$
$$+ n\theta_C(t^\alpha - t_1^\gamma) + n\theta_C(t_2^\delta - t_1^\gamma) + n\theta_C(t^\alpha - t_3^\beta)$$
$$+ n\theta_C(t_2^\delta - t_3^\beta) + \theta_C(t^\alpha - t_3^\beta)\theta_C(t_2^\delta - t_1^\gamma)$$
$$+ \theta_C(t^\alpha - t_1^\gamma)\theta_C(t_2^\delta - t_3^\beta)$$
$$= \big[\theta_C(t^\alpha - t_3^\beta) + n\big]\big[\theta_C(t_2^\delta - t_1^\gamma) + n\big]$$
$$+ \big[\theta_C(t^\alpha - t_1^\gamma) + n\big]\big[\theta_C(t_2^\delta - t_3^\beta) + n\big]\,, \qquad (366)$$

where the resulting combinations $[\theta_C(t^\alpha - t_1^\beta) - n]$ are exactly the Keldysh Green's functions $G^{\alpha\beta}$ in (37) (up to a factor of 'i'). In other words, the T-ordered average is factored into the product of T-ordered pairs of operators.

In the case of averaging over the Gibbs density matrix, bosonic operators have the property

$$\big\langle (a^+)^k (a)^k \big\rangle = k!\,n^k\,, \qquad n = \langle a^+ a\rangle\,. \qquad (367)$$

It follows that by averaging any $2m$ bosonic operators (m creation and m annihilation operators), we obtain the following structure in the right-hand side of Wick's theorem:

$$\sum_{k=0}^{m} k!\,n^k \sum_{P(m-k)} \prod \theta_C(t_i - t_j)\,, \qquad (368)$$

where the symbol $\sum_{P(m-k)}$ means that we have to sum over all possible choices of $m-k$ pairs of times from the original $2m$ time arguments in the product of $m-k$ theta functions. On the other hand, the sum is exactly equal to the product

$$\sum_{P(m)} \prod \big[\theta_C(t_i - t_j) + n\big]\,, \qquad (369)$$

i.e., to the sum of all possible products of one-particle Green's functions.

In the case of four fermionic operators, we find

$$\big\langle T_C\, a(t^\alpha)a^+(t_3^\beta)a^+(t_1^\gamma)a(t_2^\delta)\big\rangle$$
$$= 0$$
$$- n\theta_C(t^\alpha - t_1^\gamma) + n\theta_C(t_2^\delta - t_1^\gamma) + n\theta_C(t^\alpha - t_3^\beta)$$
$$- n\theta_C(t_2^\delta - t_3^\beta) - \theta_C(t^\alpha - t_3^\beta)\theta_C(t_2^\delta - t_1^\gamma)$$
$$+ \theta_C(t^\alpha - t_1^\gamma)\theta_C(t_2^\delta - t_3^\beta)\,. \qquad (370)$$

For fermions, terms involving a^k with $k > 1$ are absent; hence, $\langle \hat a^+\hat a^+\hat a\hat a\rangle = 0$. The zero is explicitly left in the equation. Writing this term as $(n^2 - n^2)$, we can again represent expression (370) as a product of one-particle Green's functions:

$$\big\langle T_C\, a(t^\alpha)a^+(t_3^\beta)a^+(t_1^\gamma)a(t_2^\delta)\big\rangle$$
$$= -\big[\theta_C(t^\alpha - t_3^\beta) - n\big]\big[\theta_C(t_2^\delta - t_1^\gamma) - n\big]$$
$$+ \big[\theta_C(t^\alpha - t_1^\gamma) - n\big]\big[\theta_C(t_2^\delta - t_3^\beta) - n\big]\,. \qquad (371)$$

A change of sign for an odd permutation of fermionic operators automatically results in the sum of products of m Green's functions, which is similar to that for bosons,

$$\sum_{P(m-k)} (-1)^P \prod \left[\theta_C(t_i - t_j) - n\right] , \tag{372}$$

containing, albeit formally, terms with n^k for $k \geqslant 2$. However, for each such term, there is exactly the same term with the opposite sign. Therefore, in the fermionic case, the average of a T-ordered product can also be represented as the sum of T-products of pairwise averages.

Using the algebraic derivation of Wick's theorem, we can easily generalize the NDT to the case of initial correlations between particles in different states. Originally, this generalization was formulated by Hall [25]. Later, Kukharenko and Tikhodeev [26] showed how to build kinetic equations for a system with initial correlations. Using the operator form of Wick's theorem (365), which remains valid in the presence of correlations, we can easily see that the difference between a system with initial correlations and a noninteracting system is only that the average of the N-ordered product does not factor into the product of particle occupation numbers in individual states. Indeed, the initial correlations imply that for two different states '1' and '2',

$$\langle \hat a_1^+ \hat a_2^+ \hat a_2 \hat a_1 \rangle \neq n_1 n_2 . \tag{373}$$

There may also be ternary and higher-order correlations. In the noninteracting case, the absence of correlations made it possible to average operators belonging to different states independently. Now, when we average operator equation (365), correlation functions arise that do not allow the standard analysis starting with this equation to be applied for each particular state. Averages of normal-ordered operators do not factor into products of one-particle occupation numbers. Such averages form correlation blocks, considered now to be additional elements of the diagram technique. For example, if the system involves only two-particle correlations, it is convenient to introduce the correlation function of the form

$$K(1,\,2) = \langle \hat a_1^+ \hat a_2^+ \hat a_2 \hat a_1 \rangle - n_1 n_2 . \tag{374}$$

Hence, any two pairs of points previously connected by two separate one-particle lines can now be connected by the correlation block $K(1,2)$ (Fig. 43). Moreover, because correlation blocks arise from normal-ordered sets of operators, they are the same for diagrams with any positions of indices '$-, +$' at the ends. It follows that to any usual diagram containing two Green's functions of the first and second states, we have to add the same diagram but with the correlation block $K(1,2)$ connecting the same points. The figure can also be interpreted as follows. In the presence of correlations, we draw the usual diagrams and then connect two Green's functions of correlated states by two transverse lines to form a single block,

$$G_{11}^{\alpha\beta}(t,t_1)G_{22}^{\gamma\delta}(t_2,t_3) \to K(1,2)\exp\left[-\mathrm{i}\varepsilon_1(t-t_1)\right]\exp\left[-\mathrm{i}\varepsilon_1(t_2-t_3)\right] , \tag{375}$$

for any Keldysh indices α, β, γ, and δ.

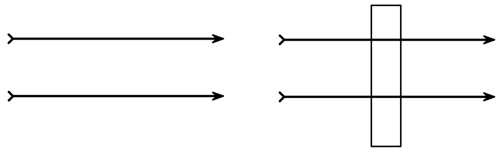

Figure 43. Pairwise correlation block replacing two independent lines of Green's functions of individual particles.

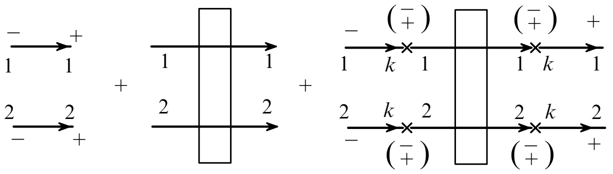

Figure 44. Diagrams corresponding to the pair correlation function $K_{12}(t)$. The correlation block defining initial pair correlations of two-electron states is in the middle.

Specific diagram rules for higher-order correlation blocks depend on how we define higher correlation functions (for example, if higher correlators cannot be factored into simpler correlators, then any diagram contains just one correlation block of a fixed order). Because a correlation block is a matrix in which all elements are equal to 1, a diagram vanishes if it has a part connected to others only by correlation blocks. This is similar to the vanishing sum of closed loops in the NDT.

It was shown in [26] that there are secular divergences in diagram rows containing correlation blocks. It follows that instead of integral equations, we have to use kinetic ones, which give time variations of initial correlations. We note that similarly to the occupation numbers, the correlation functions eventually forget about initial values; they are determined only by interaction and external fields acting on the system.

We demonstrate the technique with correlations with a simple example. We consider a system with two correlated electrons in two different states denoted by '1' and '2' (states with different spins at the same level, states with different angular momentum in an atom or a quantum dot, etc.) and 'connect' these states to a thermostat using the tunneling transitions matrix elements T_{1k} and T_{2k}. It follows that any electron can escape from the initial state [see tunneling Hamiltonian (310)]. To find time variations of the initial correlation, we calculate the pair function of two electrons $\Gamma_{12}^{<}(t,t') = -\mathrm{i}\langle a_1^+(t')a_2^+(t')a_2(t)a_1(t)\rangle$, which at equal times yields the correlator $K_{12}(t) = \mathrm{i}\Gamma_{12}^{<}(t,t)$. Diagrams for the pair function are shown in Fig. 44.

Four edge Green's functions are converted to R and A due to the summation over the '±' indices in the vertices adjacent to the correlation block. For example,

$$T_{1k}(G_{1k}^{--} - G_{1k}^{-+}) = T_{1k}G_{1k}^{\mathrm{R}} . \tag{376}$$

Therefore, the analytic expression corresponding to the diagram in Fig. 44 is given by

$$\begin{aligned}\Gamma_{12}^{<}(t,t') &= \mathrm{i}G_{11}^{<}(t,t')G_{22}^{<}(t,t')\\ &\quad - \mathrm{i}K_{12}(0)\exp\left[-\mathrm{i}(\varepsilon_1+\varepsilon_2)(t-t')\right]\\ &\quad + T_{1k}^2T_{2k}^2\int_0^{\infty}\mathrm{d}t_1\,\mathrm{d}t_2\,\mathrm{d}t_3\,\mathrm{d}t_4\sum_{k,k'k'',k'''}G_{1k}^{\mathrm{R}}(t,t_1)G_{2k'}^{\mathrm{R}}(t,t_2)\\ &\quad \times\exp\left(-\mathrm{i}\varepsilon_1t_1-\mathrm{i}\varepsilon_2t_2\right)K_{12}(0)\exp\left(\mathrm{i}\varepsilon_1t_3+\mathrm{i}\varepsilon_2t_4\right)\\ &\quad \times G_{k''1}^{\mathrm{A}}(t_3,t')G_{k'''2}^{\mathrm{A}}(t_4,t') .\end{aligned} \tag{377}$$

The Dyson equation for single-particle functions, which is typical for a tunneling system, is

$$G^{\mathrm{R}}_{1k}(t,t') = T_{1k}\int_0^{\infty} \mathrm{d}t_1\, G^{0\mathrm{R}}_{11}(t,t_1)G^{0\mathrm{R}}_{k}(t_1,t')$$

$$+\,T^2_{1k}\int_0^{\infty} \mathrm{d}t_1\,\mathrm{d}t_2 \sum_{k'} G^{0\mathrm{R}}_{11}(t,t_1)G^{0\mathrm{R}}_{k'}(t_1,t_2)G^{\mathrm{R}}_{1k}(t_2,t')\,. \quad (378)$$

After simple calculations of $K_{12}(t) = \mathrm{i}\Gamma^{<}_{12}(t,t) + G^{0<}_1 G^{0<}_2$, we find

$$K_{12}(t) = K_{12}(0)\left[1 - \left(1 - \exp\left(-\gamma_1 t\right)\right)^2\left(1 - \exp\left(-\gamma_2 t\right)\right)^2\right], \quad (379)$$

where $\gamma_{1,2} = \pi T^2_{(1k,\,2k)}\nu_k$ are the usual tunneling transition rates.

We see that the initial correlations decay exponentially whenever there is particle exchange with the thermostat. This independence from the initial correlation is a quite general phenomenon, and this technique is therefore needed, in fact, only to describe transient processes.

References

1. Keldysh L V *Sov. Phys. JETP* **20** 1018 (1965); *Zh. Eksp. Teor. Fiz.* **47** 1515 (1964)
2. Éliashberg G M *Sov. Phys. JETP* **14** 886 (1962); *Zh. Eksp. Teor. Fiz.* **41** 1241 (1961); *Sov. Phys. JETP* **15** 1151 (1962); *Zh. Eksp. Teor. Fiz.* **42** 1658 (1962)
3. Caroli C et al. *J. Phys. C Solid State Phys.* **4** 916 (1971)
4. Caroli C et al. *J. Phys. C Solid State Phys.* **4** 2598 (1971)
5. Caroli C et al. *J. Phys. C Solid State Phys.* **5** 21 (1972)
6. Meir Y, Wingreen N S *Phys. Rev. Lett.* **68** 2512 (1992)
7. Haug H, Jauho A-P *Quantum Kinetics in Transport and Optics of Semiconductors* (Berlin: Springer, 1996)
8. Feynman R P *Phys. Rev.* **76** 769 (1949)
9. Dyson F J *Phys. Rev.* **75** 1736 (1949)
10. Ivanenko D D (Ed.) *Noveishee Razvitie Kvantovoi Elektrodinamiki. Sbornik Statei* (The Modern Development of Quantum Electrodynamics. Collection of Articles) (Moscow: IL, 1954) pp. 161, 205
11. Matsubara T *Prog. Theor. Phys.* **14** 351 (1955)
12. Abrikosov A A, Gor'kov L P, Dzyaloshinskii I E *Sov. Phys. JETP* **9** 636 (1959); *Zh. Eksp. Teor. Fiz.* **36** 900 (1959)
13. Fradkin E S *Sov. Phys. JETP* **9** 912 (1958); *Zh. Eksp. Teor. Fiz.* **36** 1286 (1959); *Nucl. Phys.* **12** 465 (1959)
14. Dzyaloshinskii I E *Sov. Phys. JETP* **15** 778 (1962); *Zh. Eksp. Teor. Fiz.* **42** 1126 (1962)
15. Gor'kov L P, Eliashberg G M *Sov. Phys. JETP* **27** 328 (1968); *Zh. Eksp. Teor. Fiz.* **54** 612 (1968)
16. Mills R, Preprint (1962)
17. Keldysh L V, in *Progress in Nonequilibrium Green's Functions. Proc. of the Conf. Kadanoff – Baym Equations: Progress and Perspectives for Many-Body Physics, Rostock, Germany, 20 – 24 September 1999* (Ed. M Bonitz) (Singapore: World Scientific, 2003) p. 4
18. Konstantinov O V, Perel' V I *Sov. Phys. JETP* **12** 142 (1961); *Zh. Eksp. Teor. Fiz.* **39** 197 (1960)
19. Gor'kov L P *Sov. Phys. JETP* **7** 505 (1958); *Zh. Eksp. Teor. Fiz.* **34** 735 (1958); Abrikosov A A, Gor'kov L P, Khalatnikov I M *Sov. Phys. JETP* **8** 182 (1959); *Zh. Eksp. Teor. Fiz.* **35** 265 (1958); Landau L D *Sov. Phys. JETP* **7** 182 (1958); *Zh. Eksp. Teor. Fiz.* **34** 262 (1958); Migdal A B *Sov. Phys. JETP* **5** 333 (1957); *Zh. Eksp. Teor. Fiz.* **32** 399 (1957); *Sov. Phys. JETP* **7** 996 (1958); *Zh. Eksp. Teor. Fiz.* **35** 1438 (1958); Galitskii V M, Migdal A B *Sov. Phys. JETP* **7** 96 (1958); *Zh. Eksp. Teor. Fiz.* **34** 139 (1957); Galitskii V M *Sov. Phys. JETP* **7** 104 (1958); *Zh. Eksp. Teor. Fiz.* **34** 151 (1957); Beliaev S T *Sov. Phys. JETP* **7** 289 (1958); *Zh. Eksp. Teor. Fiz.* **34** 417 (1958); *Sov. Phys. JETP* **7** 299 (1958); *Zh. Eksp. Teor. Fiz.* **34** 433 (1958)
20. Kirzhnits D A *Field Theoretical Methods in Many-Body Systems* (Oxford: Pergamon Press, 1967); Translated from Russian: *Polevye Metody Teorii Mnogikh Chastits* (Moscow: Gosatomizdat, 1963)
21. Abrikosov A A, Gorkov L P, Dzyaloshinski I E *Methods of Quantum Field Theory in Statistical Physics* (New York: Dover Publ., 1975); Translated from Russian: *Metody Kvantovoi Teorii Polya v Statisticheskoi Fizike* (Moscow: Fizmatgiz, 1962)
22. Schwinger J *J. Math. Phys.* **2** 407 (1961)
23. Craig R A *J. Math. Phys.* **9** 605 (1968)
24. Mills R *Propagators for Many-Particle Systems. An Elementary Treatment* (New York: Gordon and Breach, 1969)
25. Hall A G *J. Phys. A Math. Gen.* **8** 214 (1975); *Physica A* **80** 369 (1975)
26. Kukharenko Yu A, Tikhodeev S G *Sov. Phys. JETP* **56** 831 (1982); *Zh. Eksp. Teor. Fiz.* **83** 1444 (1982)
27. Wick G C *Phys. Rev.* **80** 268 (1950)
28. Lifshitz E M, Pitaevskii L P *Physical Kinetics* (Oxford: Pergamon Press, 1981); Translated from Russian: *Fizicheskaya Kinetika* (Moscow: Fizmatlit, 2002)
29. Kadanoff L P, Baym G *Quantum Statistical Mechanics. Green's Function Methods in Equilibrium and Nonequilibrium Problems* (New York: W.A. Benjamin, 1962); Translated into Russian: *Kvantovaya Statisticheskaya Mekhanika. Metody Funktsii Grina v Teorii Ravnovesnykh i Neravnovesnykh Protsessov* (Moscow: Mir, 1964)
30. Schuster H G, Vieira V R *Phys. Rev. B* **34** 189 (1986)
31. Moyal J E *Proc. Camb. Phil. Soc.* **45** 99 (1949)
32. Klimontovich Yu L, Silin V P *Sov. Phys. Usp.* **3** 84 (1960); *Usp. Fiz. Nauk* **70** 247 (1960)
33. Kubo R *J. Phys. Soc. Jpn.* **12** 570 (1957)
34. Niemi A J, Semenoff G W *Ann. Physics* **152** 105 (1984); *Nucl. Phys. B* **230** 181 (1984)
35. Matsumoto H, Nakano Y, Unezawa H *J. Math. Phys.* **25** 3076 (1984)
36. Dugaev V K, Khmel'nitskii D E *Sov. Phys. JETP* **63** 1097 (1986); *Zh. Eksp. Teor. Fiz.* **90** 1871 (1986)
37. Umezawa H, Matsumoto H, Tachiki M *Thermo Field Dynamics and Condensed States* (Amsterdam: North-Holland, 1982)
38. Vieira V R, Pimentel I R *Phys. Rev. B* **39** 7196 (1989)
39. Rammer J, Smith H *Rev. Mod. Phys.* **58** 323 (1986)
40. Bogoliubov N N, Tolmachev V V, Shirkov D V *A New Method in the Theory of Superconductivity* (New York: Consultants Bureau, 1959); Translated from Russian: *Novyi Metod v Teorii Sverkhprovodimosti* (Moscow: Izd. AN SSSR, 1958)
41. Anderson P W *Phys. Rev.* **112** 1900 (1958)
42. Schrieffer J R *Theory of Superconductivity* (New York: W.A. Benjamin, 1964); Translated into Russian: *Teoriya Sverkhprovodimosti* (Moscow: Nauka, 1970)
43. Arseev P I, Loiko S O, Fedorov N K *Phys. Usp.* **49** 1 (2006); *Usp. Fiz. Nauk* **176** 3 (2006)
44. Ambegaokar V, Kadanoff L P *Nuovo Cimento* **22** 914 (1961)
45. Jauho A-P, Wingreen N S, Meir Y *Phys. Rev. B* **50** 5528 (1994)
46. Büttiker M *Phys. Rev. B* **46** 12485 (1992)
47. Blanter Y M, Büttiker M *Phys. Rep.* **336** 1 (2000)
48. Nazarov Y V (Ed.) *Quantum Noise in Mesoscopic Physics* (Dordrecht: Kluwer Acad. Publ., 2003)
49. Haupt F, Novotný T, Belzig W *Phys. Rev. B* **82** 165441 (2010)
50. Novotný T, Haupt F, Belzig W *Phys. Rev. B* **84** 113107 (2011)
51. Zhu J-X, Balatsky A V *Phys. Rev. B* **67** 165326 (2003)
52. Galperin M, Nitzan A, Ratner M A *Phys. Rev. B* **74** 075326 (2006)
53. Conley J W, Mahan G D *Phys. Rev.* **161** 681 (1967)
54. Viljas J K et al. *Phys. Rev. B* **72** 245415 (2005)
55. Yu L H et al. *Phys. Rev. Lett.* **93** 266802 (2004)
56. Chen Z-Z, Lü R, Zhu B *Phys. Rev. B* **71** 165324 (2005)
57. Tikhodeev S G, Ueba H *Phys. Rev. B* **70** 125414 (2004)
58. Ueba H, Mii T, Tikhodeev S G *Surf. Sci.* **601** 5220 (2007)
59. Arseyev P I, Maslova N S *JETP Lett.* **82** 297 (2005); *Pis'ma Zh. Eksp. Teor. Fiz.* **82** 331 (2005)
60. Arseev P I, Maslova N S *JETP Lett.* **85** 251 (2007); *Pis'ma Zh. Eksp. Teor. Fiz.* **85** 304 (2007)
61. Arseev P I, Maslova N S *Phys. Usp.* **53** 1151 (2010); *Usp. Fiz. Nauk* **180** 1197 (2010)
62. Shchadilova Y E et al. *Phys. Rev. B* **89** 165418 (2014)

63. Arseyev P I, Maslova N S *JETP Lett.* **84** 93 (2006); *Pis'ma Zh. Eksp. Teor. Fiz.***84** 99 (2006)
64. Rocha A R et al. *Phys. Rev. B* **73** 085414 (2006)
65. Brandbyge M et al. *Phys. Rev. B* **65** 165401 (2002)
66. Montgomery M J et al. *J. Phys. Condens. Matter* **15** 731 (2003)
67. Starostin A N, Chesnokov M A *JETP* **97** 1219 (2003); *Zh. Eksp. Teor. Fiz.* **124** 1367 (2003)
68. Bergeret F S, Verso A, Volkov A F *Phys. Rev. B* **86** 214516 (2012)
69. Bergeret F S, Giazotto F *Phys. Rev. B* **88** 014515 (2013)
70. Chen W, Clerk A A *Phys. Rev. B* **86** 125443 (2012)
71. Zhou L-L et al. *Phys. Rev. B* **83** 195303 (2011)
72. Crépieux A et al. *Phys. Rev. B* **83** 153417 (2011)
73. Kaasbjerg K, Nitzan A *Phys. Rev. Lett.* **114** 126803 (2015)
74. Komnik A, Gogolin A O *Phys. Rev. B* **66** 035407 (2002)
75. Gutman D B, Gefen Y, Mirlin A D *Phys. Rev. B* **81** 085436 (2010)
76. Protopopov I V, Gutman D B, Mirlin A D *Phys. Rev. Lett.* **110** 216404 (2013)
77. Dinh S N, Bagrets D A, Mirlin A D *Phys. Rev. B* **88** 245405 (2013)
78. Lutchyn R M, Skrabacz J H *Phys. Rev. B* **88** 024511 (2013)
79. Gamboa Saraví R E, Naón C M, Schaposnik F A *J. Stat. Mech.* P09034 (2014); arXiv:1406.4578
80. Ivanov A L, Keldysh L V *Sov. Phys. JETP* **57** 234 (1983); *Zh. Eksp. Teor. Fiz.* **84** 404 (1982)
81. Schmitt-Rink S, Chemla D S, Haug H *Phys. Rev. B* **37** 941 (1988)
82. Jauho A P, Johnsen K *Phys. Rev. Lett.* **76** 4576 (1996)
83. Popov Yu M *Tr. Fiz. Inst. Akad. Nauk SSSR* **31** 3 (1965)
84. Galitskii V M, Elesin V F *Rezonansnoe Vzaimodeistvie Elektromagnitnykh Polei s Poluprovodnikami* (The Resonant Interaction of Electromagnetic Fields with Semiconductors) (Moscow: Energoatomizdat, 1986)
85. El Sayed K et al. *Phys. Rev. B* **49** 7337 (1994)
86. Vu Q T, Haug H, Keldysh L V *Solid State Commun.* **115** 63 (2000)
87. Wacker A, Jauho A-P *Phys. Rev. Lett.* **80** 369 (1998)
88. Wacker A et al. *Phys. Rev. Lett.* **83** 836 (1999)
89. Wacker A *Phys. Rev. B* **66** 085326 (2002)
90. Banit F et al. *Appl. Phys. Lett.* **86** 041108 (2005)
91. de Leeuw A-W, Stoof H T C, Duine R A *Phys. Rev. A* **88** 033829 (2013)
92. Abrikosov A A *Physics* **2** (1) 5 (1965)
93. Barnes S E *J. Phys. F Met. Phys.* **6** 1375 (1976)
94. Coleman P *Phys. Rev. B* **29** 3035 (1984)
95. Kotliar G et al. *Rev. Mod. Phys.* **78** 865 (2006)
96. Goldin Y, Avishai Y *Phys. Rev. B* **61** 16750 (2000)
97. Paaske J, Rosch A, Wölfle P *Phys. Rev. B* **69** 155330 (2004)
98. Paaske J et al. *Phys. Rev. B* **70** 155301 (2004)
99. Arseev P I, Maslova N S, Rubtsov A N *Novye Diagrammnye Metody Sovremennykh Teoreticheskikh Issledovanii Sil'nokorrelirovannykh Elektronnykh System* (New Diagrammatic Methods of Modern Theoretical Research of Strongly Correlated Electron Systems) (Moscow: Fizicheskii Fakul'tet MGU im. M.V. Lomonosova, 2011)
100. Arseyev P I, Maslova N S *JETP Lett.* **100** 197 (2014); *Pis'ma Zh. Eksp. Teor. Fiz.* **100** 218 (2014)
101. Georges A et al. *Rev. Mod. Phys.* **68** 13 (1996)
102. Horbach M L, Schön G *Physica A* **167** 93 (1990); *Ann. Physik* **505** 51 (1993)
103. Kobes R L, Semenoff G W, Weiss N *Z. Phys. C* **29** 371 (1985)
104. Kamenev A, Andreev A *Phys. Rev. B* **60** 2218 (1999)
105. Kamenev A, Levchenko A *Adv. Phys.* **58** 197 (2009)
106. Chamon C, Ludwig A W W, Nayak Ch *Phys. Rev. B* **60** 2239 (1999)
107. Finkel'shtein A M *Sov. Phys. JETP* **57** 97 (1983); *Zh. Eksp. Teor. Fiz.* **84** 168 (1983)
108. Schwiete G, Finkel'stein A M *Phys. Rev. B* **89** 075437 (2014)
109. Semenoff G W, Umezava H *Nucl. Phys. B* **220** 196 (1983)
110. Lutz M, Kunihiro T *Z. Phys. C* **49** 123 (1991)
111. Akhmedov E T, Astrakhantsev N, Popov F K *JHEP* (09) 071 (2014); arXiv:1405.5285
112. Konstandin T *Phys. Usp.* **56** 747 (2013); *Usp. Fiz. Nauk* **183** 785 (2013)
113. Akhmedov E T *Phys. Rev. D* **87** 044049 (2013)
114. Barvinsky A O *Phys. Rev. D* **85** 104018 (2012)